Title	Elastic and Dielectric Properties of LiTaO_3 and LiNbO_3 Crystals
Author(s)	Tomeno, Izumi
Citation	大阪大学, 1987, 博士論文
Version Type	VoR
URL	https://hdl.handle.net/11094/2428
rights	
Note	

Elastic and Dielectric Properties

of $LiTaO_3$ and $LiNbO_3$ Crystals

Izumi TOMENO

Toshiba Research and Development
Center, Toshiba Corporation

February 1987

Contents

Synopsis

Elastic constants C_{11}, C_{33}, C_{44} and $C_{66}=(C_{11}-C_{12})/2$ in single-domain (SD) and multi-domain (MD) LiTaO$_3$ and LiNbO$_3$ crystals have been measured over the temperature range from 300 to above 980 K using the ultrasonic phase-comparison method. Dielectric susceptibilities χ_{33} and conductivities σ_{33} in ferroelectric (FE) and paraelectric (PE) phases, and χ_{11} and σ_{11} up to 1200 K have been determined in the frequency range between 10 kHz and 13 MHz using the impedance analyzer.

The phase-comparison method was improved so that automatic velocity measurements could be made at temperatures up to 1200 K. A series of grooves was cut around the lateral surface of the fused-silica buffer rod to scatter unnecessary reflections. Silver paste was used as the bond between the rod and the sample over the wide temperature range.

Effective elastic constant C'_{ii} (i=1,4 and 6) for the MD LiTaO$_3$ crystal is higher than constant-field elastic constant C^E_{ii} for the SD crystal, while C'_{33} for the MD LiTaO$_3$ and LiNbO$_3$ crystals is equal to C^E_{33}, which is lower than constant-polarization elastic constant C^P_{33} for the SD crystals. These results are ascribed to the piezoelectric effect. Constant-stress susceptibility χ^X_{mm} is obtained from the value at frequencies up to 1.5 MHz, while constant-strain susceptibility χ^x_{mm} is obtained from the values at 10 and 13 MHz.

The elastic-constant difference $C^P_{ii}-C^E_{ii}$ and the inverse-susceptibility difference $(\chi^x_{mm})^{-1}-(\chi^X_{mm})^{-1}$ are interpreted

consistently, based on the interaction between strain x and polarization P. Electrostrictive interaction qxP^2 is inadequate to explain the temperature dependence of $C_{ii}^P - C_{ii}^E$ and $(\chi_{mm}^x)^{-1} - (\chi_{mm}^X)^{-1}$. Higher-order interaction rxP^4 contributes to $C_{33}^P - C_{33}^E$ and $(\chi_{33}^x)^{-1} - (\chi_{33}^X)^{-1}$. The contribution of rxP^4 may result from the anharmonicity in soft phonon.

Constant-stress susceptibilities χ_{33}^X in the FE and PE phases of $LiTaO_3$ and $LiNbO_3$ obey the Curie-Weiss behavior. The results for χ_{33} indicate that these crystals undergo nearly second-order phase transition at Curie temperature T_C of 880 K and 1410 K, respectively.

Both χ_{33} and σ_{33} in $LiTaO_3$ show a marked dispersion over the wide temperature range, including T_C. The elastic-constant difference $C_{33}^P - C_{33}^E$ for $LiTaO_3$ exhibits drastic change between 780 K and T_C, which is attributed to the dispersion of χ_{33} at high temperatures. Susceptibility χ_{33} in the PE phase of $LiNbO_3$ exhibits the dispersion in the frequency range from 1 MHz to 13 MHz, although its difference due to frequency change is far less than that for $LiTaO_3$. A comparison of these observations with the light-scattering results suggests that the soft mode couples with the low-frequency relaxation process near T_C. The dielectric dispersion may arise from the motion of Li ions or vacancies. The results for C_{ii} and χ_{mm} suggest that the phase transition in $LiTaO_3$ and $LiNbO_3$ has an intermediate character, between displacive and order-disorder categories.

§1 Introduction

Lithium tantalate ($LiTaO_3$) and lithium niobate ($LiNbO_3$) are known to possess unique piezoelectric, electro-optic and non-linear optical properties.[1] These isomorphic materials are applicable as large single crystals and are currently exploited for surface acoustic wave (SAW) devices.[2]

Lithium tantalate and lithium niobate undergo only a single structural phase transition, from the low-temperature ferro-electric (FE) phase to the high-temperature paraelectric (PE) phase at Curie temperature T_C of 880 K and 1410 K, respectively. The FE phase has a crystal structure with the R3c space group symmetry and the PE phase with the centrosymmetric space group $R\bar{3}c$. The crystal structure and optical properties of these materials have been studied extensively to elucidate the mechanism of the phase transition. In particular, the existence of soft-phonon modes in $LiTaO_3$ and $LiNbO_3$ has been discussed on the analogy of the situation in the perovskites.[1,3-5] It has been established that the ferroelectric phase transitions in perovskites are associated with an instability of the crystal against a transverse optic mode, whose frequency varies as $(T-T_C)^{0.5}$.[1,6-8] Compared with perovskites, there is still considerable uncertainty concerning the characters of the phase transition in $LiTaO_3$ and $LiNbO_3$. This may be primarily owing to considerably high Curie temperatures, which induce technical difficulties in the experimental investigation.

In 1966, Abrahams et al.[9-12] carried out a series of investigations on the room temperature crystal structure of $LiTaO_3$ and

LiNbO$_3$, both by x-ray and neutron diffraction. As shown in Fig. 1(a), it consists of a sequence of distorted oxygen octahedra joined by their faces along the polar trigonal axis. In the FE phase, the distorted octahedra contain, in sequence, Ta or Nb atoms, vacancies and Li atoms. At room temperature, the Ta or Nb atom is displaced along the polar axis from the center of its octahedron and the Li atom is displaced along the polar axis from the shared face. Moreover, Abrahams et al.[13] performed x-ray diffraction measurement on polycrystalline LiNbO$_3$, up to 1473 K, and found that the Nb atoms approach the center of the octahedra with increasing temperature. Thus, they proposed the PE crystal structure in which the Li atoms move into the nearest oxygen layers and the Nb atoms are located at the center of adjacent oxygen layers, as shown in Fig.1(d).

In 1967, Barker and Loudon[3] investigated the optical phonons in LiNbO$_3$ by measurements of Raman scattering and infrared reflection. They interpreted that the phase transition in LiNbO$_3$ is driven by the instability of an A$_1$ mode, based on the group theory analysis and the crystal structure determinations.[9-13] Johnston and Kaminow[4] studied the Raman spectra in LiTaO$_3$ and LiNbO$_3$ as a function of temperature up to 1100 K. They observed that the frequency of this A$_1$ mode varies approximately as $(T_C-T)^{0.5}$ over the wide temperature range. In view of these results, the phase transition in the two crystals is regarded as the displacive category.

In 1973, Abrahams et al.[14] made neutron scattering

measurements on single-crystal $LiTaO_3$, both in FE and PE phases. From the neutron results, they deduced that Li atoms above T_C occupy two equivalent positions, on either side of the oxygen plane with equal probability, as indicated in Fig.1(b). Below T_C, the Li atom position was found to remain practically invariant as a function of temperature. Samuelsen and Grande[15] studied the temperature dependence of elastic neutron scattering from two reflections in $LiTaO_3$ below T_C and have explained the spontaneous polarization in terms of the gradual ordering of Li atoms as the temperature decreases. Chowdhury et al.[16] investigated the phonon dispersion curves in $LiNbO_3$ by inelastic neutron scattering. They reported that there is no evidence of the softening of the A_1 mode at temperatures up to $0.6T_C$. Thus, the neutron scattering results support the concept that the phase transition in $LiTaO_3$ and $LiNbO_3$ has the order-disorder character involving the Li atoms.

Recently, the soft-mode behavior was re-examined by light scattering measurements.[17-21] In the case of $LiTaO_3$, Penna et al.[17,18] reported the diffusive central mode in the Raman spectra and anomalous polarition dispersion curve. They suggested that the dynamical domain fluctuations occur below T_C in $LiTaO_3$. Muller et al.[19] deduced the temperature dependence of soft-mode frequency in $LiTaO_3$ from infrared reflectivity data and found that soft-mode frequency remains finite in the vicinity of T_C. They interpreted the results as the crossover from displacive to order-disorder character. In 1985, Okamoto et al.[20]

measured the Raman spectra in $LiNbO_3$ and found that the soft mode becomes overdamped and couples with the relaxation process at temperatures far lower than T_C. A similar conclusion has been obtained from the Raman spectra in $LiTaO_3$ by Zhang and Scott.[21]

Elastic anomalies, associated with structural phase transitions, have been examined by the acoustic-resonance at the kHz range, ultrasonic velocity measurements at the MHz range and Brillouin-scattering at the GHz range. These techniques yield constant-field values of elastic compliance S_{ij}^E or stiffness c_{ij}^E for piezoelectric materials, because the order parameter can follow their elastic strain. Constant-polarization elastic-constant c_{ij}^P represents the elastic response at high frequencies, when the order parameter is unable to follow the strain. Yamada et al.[22] determined the constant-field elastic compliance S_{ij}^E in $LiTaO_3$ as a function of temperature up to T_C using the acoustic-resonance technique. They did not observe anomalous temperature dependence of S_{ij}^E associated with the phase transition. Avakyants and Kiselev[23] measured c_{11}^E and c_{33}^P of $LiTaO_3$ up to 973 K using Brillouin scattering. They failed to identify the phase transition from the anomalies in sound velocities near T_C, presumably because the experimental error of 1 % was too large. On the other hand, the elastic-property data on $LiNbO_3$ were limited in the temperature range far lower than T_C. Yamada et al.[24] observed that S_{ij}^E in $LiNbO_3$ increases linearly with increasing temperature up to 473 K. The extension of elastic-constant measurement to temperatures as high as possible was needed in order to

explain the elastic behavior in relation to the phase transition.

Dielectric constants ε_{ii} in piezoelectric materials can be measured under two different conditions. Constant-stress dielectric constant ε_{ii}^X is determined at frequencies of the order of 100 kHz, where the strain can follow the electric fields. Constant-strain dielectric constant ε_{ii}^x is obtained at frequencies of the order of 10 MHz, where the strain is unable to follow the fields. Glass[25] and Yamada et al.[22] reported the temperature dependence of constant-stress dielectric constant ε_{33}^X in both FE and PE phases of LiTaO$_3$. The low-frequency dielectric data indicated that the phase transition in LiTaO$_3$ is of the second order. Recently, Prieto et al.[26] measured the frequency dependence of dielectric constant ε_{33} in the PE phase of LiTaO$_3$ up to 20 kHz and concluded that defects contribute to the low-frequency dielectric dispersion. In the case of LiNbO$_3$, dielectric-constant measurements were limited in the temperature range below T_C. Nassau et al.[27] measured ε_{ii} in LiNbO$_3$ at 100 kHz as a function of temperature up to 1220 K. Ohmachi et al.[28] reported the dielectric constants in LiNbO$_3$ at 9 GHz up to 573 K. In order to clarify the phase-transition mechanism, it appears desirable to determine both constant-stress and constant-strain dielectric constants in LiTaO$_3$ and LiNbO$_3$ over a wide temperature range, including the Curie temperature.

The interaction between acoustic and optic soft modes gives rise to both elastic-constant difference $C_{ij}^P - C_{ij}^E$ and inverse-dielectric-susceptibility difference $(\chi_{ii}^x)^{-1} - (\chi_{ii}^X)^{-1}$.[29-31] The

interaction is expressed in terms of powers of strain x and order parameter P. In $LiTaO_3$ and $LiNbO_3$, the piezoelectric coupling of the form axP is forbidden by symmetry in the PE phase. The lowest-order interaction in the PE phase of these crystals is then the electrostrictive coupling of the form qxP^2. In the absence of the polarization fluctuation effects, both elastic constant and dielectric susceptibility are frequency independent in the PE phase. In the FE phase, the piezoelectric interaction is induced by the spontaneous polarization P_S along the Z axis. Temperature dependence of $C_{ij}^P - C_{ij}^E$ and $(\chi_{ii}^x)^{-1} - (\chi_{ii}^X)^{-1}$ in the FE phase is expected to be explained on the basis of Landau's phenomenological theory.[29-31]

The connection between the constant-strain susceptibility and the soft-mode frequency is predicted by the Lyddane-Sachs-Teller relationship.[6] It is, therefore, highly desirable to investigate the susceptibility χ_{ii}^x in both phases of $LiTaO_3$ and $LiNbO_3$.

In order-disorder ferroelectrics, dielectric dispersion near T_C occurs at low frequencies and is described by the Debye relaxation. In displacive ferroelectrics, the dielectric dispersion is observed at infrared frequencies and is described by the damped harmonic oscillator. Based on the Raman results reported by Johnston and Kaminow[4], dielectric susceptibility χ_{33} in the PE phase of $LiTaO_3$ and $LiNbO_3$ is expected to be independent of frequency, up to the MHz region.

The present paper [32-36] gives the experimental results for elastic constants C_{11}^E, C_{33}^P, C_{44}^E and $C_{66}^E = (C_{11}^E - C_{12}^E)/2$ in single domain (SD) LiTaO$_3$ and LiNbO$_3$ crystals and corresponding effective constants $C_{ii}^!$ in multidomain (MD) crystals in the temperature range from 300 to above 980 K, using the ultrasonic phase-comparison method. Furthermore, dielectric susceptibilities χ_{33} and conductivities σ_{33}, both in FE and PE phases, and χ_{11} and σ_{11} up to 1200 K are presented in the frequency range between 10 kHz and 13 MHz, using the impedance analyzer. Full knowledge regarding the temperature dependence of elastic and dielectric constants is needed for an understanding of the phase-transition mechanism. The present study has been undertaken in the hope of obtaining the information concerning the coupling between optic and acoustic phonons, the dielectric constants connected with optic phonons, and the dielectric dispersion.

The experimental procedures and results are described in §2 and §3, respectively. In §4, the phenomenological expressions for $C_{ii}^P - C_{ii}^E$ and $(\chi_{ii}^X)^{-1} - (\chi_{ii}^X)^{-1}$ in these crystals are derived from the interaction, including the electrostrictive and the higher-order coupling. In §5, the experimental results are analyzed, using the equations given in §4. In §5, the temperature dependene of inverse susceptibility $(\chi_{33}^X)^{-1}$ is discussed in relation to soft-mode frequency, determined by the light-scattering measurements. In addition, the observed dielectric dispersion is compared with the soft-mode behavior. The conclusion reached in this study is presented in §6.

§2 Experimental procedures

2-1 Sample preparation

Curie temperatures and lattice parameters for $LiTaO_3$ and $LiNbO_3$ were reported to change as a function of the melt composition from which they are grown.[37,38] As is clear in the phase diagram shown in Fig.2, the $LiNbO_3$ crystal, solidified from the raw materials with the stoichiometric composition, deviates significantly from the stoichiometry.[37] This means that crystals, grown from stoichiometric composition, have inhomogeneous composition along the direction of the crystal growth.[38] Similar behavior was observed for $LiTaO_3$ crystal. Therefore, samples used for the present investigation were cut from $LiTaO_3$ and $LiNbO_3$ crystals with congruent melt compositions. The congruent melt composition is approximately 49 mole % Li_2O for $LiTaO_3$ and 48.6 % for $LiNbO_3$. Both crystals, grown by the Czochralski technique, are now extensively used as SAW device materials. The melting point is 1923 K for $LiTaO_3$ and 1526 K for $LiNbO_3$. Because of the higher melting point, $LiTaO_3$ crystals should be grown in a Pt-Rh crucible, which inevitably causes contamination by Rh impurities for about 100 ppm concentration. It was checked that the Rh impurity exerts no influence on elastic constant and dielectric constant in $LiTaO_3$. The high optical-quality $LiNbO_3$ crystal was made with a Pt crucible.

Single domain (SD) crystals were obtained by field-cooling as-grown crystals with an applied electric field of 5V/cm along the c axis through T_C, whereas multidomain (MD) crystals were

made by cooling without an electric field.

Both SD and MD crystal samples for elastic-constant measurements were formed into cylinders 7 mm in length and 25 mm in diameter, in which the cylinder axes agree with one of the principal crystal axes.

The SD samples for dielectric-constant measurements were shaped into plates, 16 to 25 mm^2 in area and 1.0 to 1.2 mm in thickness. The SD $LiNbO_3$ samples were coated with platinum electrodes on the large faces perpendicular to either Y or Z axis. The electrodes were made of fritless platinum paste, fired at 1000 K in the initial warm-up. The $LiTaO_3$ sample with platinum electrodes on large Z faces was transformed into the SD state after the firing. The MD $LiTaO_3$ sample with platinum electrodes on the Y surface, was used for measuring ε_{11} above T_C, while the SD $LiTaO_3$ sample, with gold electrodes, was prepared for measuring ε_{11} below T_C. Gold electrodes were vapor deposited in a vacuum, and then covered with gold paste, fired at 800 K. Capacitance measurements on the thicker sample yielded the same ε_{ii} value in the entire temperature range. The measured data were not affected by the boundary between electrodes and crystal.

2-2 Elastic-constant measurements

(1) Ultrasonic apparatus

Elastic constants were deduced from sound-velocity measurements. Sound velocities were determined at around 20 MHz, using the ultrasonic phase-comparison method invented by McSkimin.[39] The phase-comparison method was improved so that automatic measurements could be made at temperatures up to 1200 K. The detection system and a microcomputer were introduced for the automation. High-temperature measurements were achieved by using silver paste as the bond between the buffer rod and the sample.

Figure 3 shows an apparatus block-diagram. The gated amplifier fed the more than 150 V peak to peak burst to the quartz transducer. Longitudinal and transverse ultrasonic waves were, respectively, generated by chromium-gold plated X- and Y-cut quartz transducers, 15 mm in diameter. The transducer was bonded to the end of the buffer rod with salol (phenyl salicylate) and cooled to room temperature by blowing nitrogen gas during high temperature measurements, as illustrated in Fig.3. This simple cooling system makes it possible to maintain the temperature sufficiently low. The fused-silica buffer rod, 25 mm in diameter and 200 mm in length , was used for ultrasonic interference with multiple reflections and for thermal insulation of the transducer from the hot zone in the furnace. The difference in thermal expansion, between the rod and the sample, created the difficulty in obtaining the data over a wide temperature range. The buffer rod with a taper at the end showed an advantage in measurements at high temperatures. The rod with the taper was designed to

prevent distorting the echo pattern for a shear wave. A small portion of the pulses was reflected at the lateral surface of the rod, due to the diffraction effect, although a large portion reached the end of the rod. Reflection at the smooth lateral surface of the rod gave rise to ultrasonic delay, which is not distinguished from the sample echo. Thus, a series of grooves, 1 mm in depth, was cut around the lateral surface of the rod to scatter the unnecessary reflections.

The sample was bonded with the buffer rod using silver paste (Shouei Chemical Inc. H4040A, H4244) or organic adhesive (Aron Alpha). Silver paste, fired at 853 K on initial warm-up, was used to obtain the data on the SD $LiTaO_3$ and $LiNbO_3$ crystals in the range from 470 K to above 1000 K. In the case of the MD $LiTaO_3$, the sample was cooled or heated slowly after the paste was fired at above T_C. Ultrasonic velocities, propagated along one of the principal axes in $LiTaO_3$, were measured above 973 K. Ultrasonic velocities along the X or Y axis in $LiNbO_3$ were determined up to about 1200 K, while velocities along the Z axis in $LiNbO_3$ were determined up to about 1000 K. Because of bond breakdown or high attenuation in acoustic waves, shear echoes from the $LiNbO_3$ sample disappeared at the higher temperatures. The organic adhesive was exploited for longitudinal-velocity measurements below 473 K. Shear velocities, between 373 and 473 K, were not measured, because no suitable acoustic-bond was found in this temperature range.

The sample was mounted in a nickel block for good thermal stabilization. The temperature difference across the sample was

less than 0.1 K at 900 K. Temperature measurements were made using a platinum-rhodium thermocouple, which was in contact at the taper position of the buffer rod. For measurements on $LiTaO_3$ crystals, the temperature change rate was 0.2 K/min near T_c, while the 0.5 K/min rate was used in the other temperature range. For measurements on $LiNbO_3$ crystals, the rate of 0.5 K/min was adopted in the entire temperature range.

Echoes received by the transducer were converted to digital output by the A/D converter. If the burst width is longer than the one round trip time through the sample, interference between echoes occurs. The typical overlapped echo amplitude is shown in Fig.4 as a function of frequency. The amplitude exhibits minima periodically at frequency f_n, on the condition that there is an integer n of wavelength in twice the sample thickness 2L. Thus, ultrasonic velocity V is written as

$$V = 2L(f_n - f_{n-1}). \qquad (2.1)$$

The microcomputer (Hewlett-Packard 9816) measured the temperature, ajusted the synthesizer frequency for minimum signal, and then accumulated the elastic-constant data. Although the change in the sound velocity was detected at an accuracy of 0.01%, the absolute value of the velocity might have systematic error of less than 0.5 %, which originated from the phase shift in the paste or adhesive layer.

(2) Elastic-constants calculation

The Voigt notation[40] is adopted here to simplify writing the second-rank stress and strain tensors, the third-rank piezoelectric tensor and the fourth-rank elastic constant tensor. In piezoelectric materials, stress X_i (i=1,2,3,4,5,6) and electric displacement D_k (k=1,2,3) are described in terms of strain x_i and electric field E_k. The equations of state, govering a piezoelectric crystal, are given by

$$X_i = \sum_{j=1}^{6} C_{ij}^E x_j - \sum_{k=1}^{3} e_{ki} E_k, \qquad (2.2)$$

$$D_k = \sum_{j=1}^{6} e_{kj} x_j + \sum_{l=1}^{3} \varepsilon_{lk}^x E_l, \qquad (2.3)$$

where e_{ij} denotes the piezoelectric constant.

The phase transition from the low-temperature FE phase to the high-temperature PE phase in $LiTaO_3$ and $LiNbO_3$ is accompanied by the structural change from the non-centrosymmetric space group R3c to the centrosymmetric space group $R\bar{3}c$. For crystals belonging to either R3c or $R\bar{3}c$ symmetry group, elastic constant C_{ij} and dielectric constant ε_{ii} are written as[40]

$$C_{ij} = \begin{pmatrix} C_{11} & C_{12} & C_{13} & C_{14} & 0 & 0 \\ C_{12} & C_{11} & C_{13} & -C_{14} & 0 & 0 \\ C_{13} & C_{13} & C_{33} & 0 & 0 & 0 \\ C_{14} & -C_{14} & 0 & C_{44} & 0 & 0 \\ 0 & 0 & 0 & 0 & C_{44} & C_{14} \\ 0 & 0 & 0 & 0 & C_{14} & C_{66} \end{pmatrix} \qquad (2.4)$$

$$\varepsilon_{ii} = \begin{pmatrix} \varepsilon_{11} & 0 & 0 \\ 0 & \varepsilon_{11} & 0 \\ 0 & 0 & \varepsilon_{33} \end{pmatrix} \qquad (2.5)$$

For convenience, C_{66} is defined by

$$C_{66} = (C_{11} - C_{12})/2. \qquad (2.6)$$

Below T_C, piezoelectric constant e_{ij} is given by

$$e_{ij} = \begin{pmatrix} 0 & 0 & 0 & 0 & e_{15} & -e_{22} \\ -e_{22} & e_{22} & 0 & e_{15} & 0 & 0 \\ e_{31} & e_{31} & e_{33} & 0 & 0 & 0 \end{pmatrix} \qquad (2.7)$$

From eqs.(2.2)-(2.7) and the condition $D_i=0$, elastic-constant differences $C_{ij}^P - C_{ij}^E$ are expressed as

$$C_{11}^P - C_{11}^E = e_{22}^2/\varepsilon_{11}^x + e_{31}^2/\varepsilon_{33}^x, \qquad (2.8)$$

$$C_{33}^P - C_{33}^E = e_{33}^2/\varepsilon_{33}^x, \qquad (2.9)$$

$$C_{44}^P - C_{44}^E = e_{15}^2/\varepsilon_{11}^x, \qquad (2.10)$$

$$C_{66}^P - C_{66}^E = e_{22}^2/\varepsilon_{11}^x. \qquad (2.11)$$

In the PE phase, C_{ij}^P is equivalent to C_{ij}^E, because the crystals are non-piezoelectric above T_C.

Ultrasonic waves, transmitted in the SD crystal, are approximately regarded as plane wave, because the acoustic wavelength is considerably small, compared with the sample dimensions and with the transducer diameter. The acoustic plane wave gives rise to electrostatic fields, due to piezoelectric coupling. In addition, an acoustic plane wave in a piezoelectric crystal may couple with an electromagnetic wave. Hutson and White,[41] and Kyame[42] pointed out that plane wave solutions for the piezoelectric material satisfy both equations of state and Maxwell's equations. In practice, the dispersion of an acoustic wave, caused by the coupling to the electromagnetic wave, is negligibly small, compared with that caused by the coupling to the electrostatic field. This is based on the fact that the light velocity is far higher than the sound velocity. The plane-wave assumption means that the transverse components of piezoelectric polarization induce alternating charges only at the lateral surface of the SD sample. Thus, transverse components exert very little influence on the acoustic velocity. In contrast to this, the longitudinal component of piezoelectric polarization creates charges in the crystal. Consequently, the longitudinal electrostatic field, due to the piezoelectric coupling, has a marked effect on the acoustic velocity.

Table I shows the relationship between acoustic modes and elastic constants in the SD and MD crystals. Ultrasonic velocity measurements along the principal axes yield elastic constants C_{11}, C_{33}, C_{44} and $C_{66}=(C_{11}-C_{12})/2$. Effective constant C_{33} for

the SD crystal is identical to C_{33}^P , because the longitudinal acoustic wave along the z axis produces the longitudinal electrostatic field. With the exception of C_{33}, effective constants C_{ii} in the SD crystal are equal to C_{ii}^E, because piezoelectric constants e_{11}, e_{34} and e_{26} are zero. An explanation of effective constants in the MD crystal is given in §5.

2-3 Dielectric-constant measurements

Dielectric constant ε_{33} along the Z axis and ε_{11} along the Y axis were determined at several frequencies, between 10 kHz and 13 MHz, using a YHP impedance analyzer model 4192A. The sample was mounted on a large Ni crucible in the furnace and connected by 10 cm parallel Pt lead-in wires with the YHP standard test cable. The microcomputer was connected with the impedance analyzer, and the digital voltmeter recording the temperature of the sample. The ε_{ii} and σ_{ii} data were accumulated with the microcomputer.

Dielectric constant ε_{ii} and conductivity σ_{ii} at angular frequency ω were obtained from the equations,

$$\varepsilon_{ii} = \frac{t(C_{ii}^{ap}-C_0)}{\varepsilon_0 S\{1+\omega^2 L_0(C_{ii}^{ap}-C_0)\}} \quad , \qquad (2.12)$$

$$\sigma_{ii} = \frac{tG_{ii}^{ap}}{S}(1-\omega^2 L_0 C_{ii})^2, \qquad (2.13)$$

where C_{ii}^{ap} and G_{ii}^{ap} are the apparent values of capacitance and conductance, respectively, L_0 is the residual inductance, C_0 is the stray capacitance, S is the area of electrodes and t is the sample length. Equations (2.12) and (2.13) are valid, when $\omega^2 L_0 C_{ii}$ is smaller than 1. Since a typical L_0 value was 0.1 μH, ε_{33} at 13 MHz was determined in the range up to about 8×10^3. Measurements on ε_{11} and σ_{11} were carried out in the temperature range up to 1200 K, where $\tan\delta$ was lower than 20.

§3 Results

3-1 Elastic constants in $LiTaO_3$

Temperature dependence of elastic constants in $LiTaO_3$ crystal is shown in Fig.5. The open and closed circles refer to room temperature values for C_{ii}^P and C_{33}^E, taken from the results reported by Yamada al.[22] and by Warner et al.[43], respectively. The variations in $C_{ii}^!$ near T_C are presented in Fig.6. The values of effective elastic constants $C_{ii}^!$ (i=1, 4 and 6) for the MD crystal lie between the values of C_{ii}^P and C_{ii}^E, respectively. On the other hand, $C_{33}^!$ for the MD crystal is approximately equal to C_{33}^E at room temperature. At Curie temperature T_C, the values for $C_{ii}^!$ in the MD crystal agree with those for C_{ii}^E in the SD crystal. Curie temperature in $LiTaO_3$ crystals, used in this work, is found to vary from 873 to 883 K.

In the FE phase, both C_{11}^E and $C_{11}^!$ exhibit nonlinear temperature dependence, while, in the PE phase, C_{11}^P shows the linear temperature dependence up to the highest observed temperature. Shear elastic constants C_{44}^E and $C_{44}^!$ decrease slowly with increasing temperature up to 370 K and then increases up to T_C. These decrease again above T_C, exhibiting a cusp at T_C. Variation in $C_{44}^!$ above 670 K is small, compared with that in C_{44}^E. Similar behavior is found for shear elastic constants C_{66}^E and $C_{66}^!$ in the entire temperature range. In addition, C_{66}^E shows a jump at T_C, where the shear wave attenuation is large. No abrupt change is observed for $C_{66}^!$ for the MD crystal. Longitudinal elastic constant C_{33}^P shows the linear temperature dependence with the same

slopes on either side of T_C, except for a small dip around T_C. In contrast to C_{33}^P in the FE phase, C_{33}' decreases drastically with decreasing temperature below T_C. It once shows a minimum near 820 K and then increases linearly with a further decrease in the temperature below 770 K.

3-2 Elastic constants in LiNbO$_3$

Temperature dependence of elastic constants in LiNbO$_3$ crystal is shown in Fig.7. The C_{11}' values for the MD crystal are slightly higher than those for C_{11}^E for the SD crystal. On the other hand, C_{33}' for the MD crystal is nearly equal to C_{33}^E at room temperature, taken from the results of Warner et al.[43] Due to the large attenuation of shear ultrasonic waves in the MD crystal, elastic constants C_{44}' and C_{66}' were not obtained.

As shown in Fig.7, both C_{11}^E and C_{11}' decrease linearly with increasing temperature, up to 1223 K (0.86 T_C). Furthermore, both C_{33}^P and C_{33}' exhibit linear temperature dependence, up to 980 K. The elastic-constant difference $C_{33}^P - C_{33}'$ in LiNbO$_3$ is found to be practically independent of temperature. In contrast to C_{11}^E and C_{33}', shear elastic constants C_{44}^E and C_{66}^E deviate from the linear relation at high temperatures. Elastic constant C_{44}^E decreases linearly with increasing temperature, up to 450 K. Constant C_{44}^E deviates from linear decrease, exhibits a minimun at about 840 K and then increases slowly up to 1040 K. Elastic constant C_{66}^E decreases linearly with increasing temperature up to 500 K, shows nonlinear behavior between 500 and 1100 K and then becomes practically independent of temperatures up to 1190 K.

3-3 Dielectric constants in $LiTaO_3$

Figure 8 indicates dielectric constants ε_{11} and ε_{33} in $LiTaO_3$ as a function of temperature. Except for the high temperature range, the measured values ε_{ii} up to 1.5 MHz represent the constant-stress dielectric constants ε_{ii}^X, while the values at 10 and 13 MHz represent the constant-strain dielectric constants ε_{ii}^x.

At room temperature, dielectric-constant difference $\varepsilon_{11}^X - \varepsilon_{11}^x$ in $LiTaO_3$ is small compared with that in $LiNbO_3$, as indicated in Tables II and III. Both free and clamped dielectric constant ε_{11} increase gradually with increasing temperature. They exhibit a maximum at T_C and then decrease slowly in the PE phase. Dielectric dispersion, perpendicular to z axis, is observed in the PE phase, where the crystal is centrosymmetric.

Dielectric-constant difference $\varepsilon_{33}^X - \varepsilon_{33}^x$ in $LiTaO_3$ at room temperature is much less than $\varepsilon_{11}^X - \varepsilon_{11}^x$. The relationship $(\varepsilon_{33}^X - \varepsilon_{33}^x) << (\varepsilon_{11}^X - \varepsilon_{11}^x)$ is also found in $LiNbO_3$ at temperatures far lower than T_C. Note that there is a significant dispersion in ε_{33} over the wide temperature range, including the Curie temperature.

The inverse dielectric susceptibility χ_{33}^{-1} is plotted in Fig.9 as a function of temperature. The lowest-frequency inverse susceptibility $(\chi_{33}^X)^{-1}$ in the PE phase clearly obeys the Curie-Weiss behavior:

$$(\chi_{33}^X)^{-1} = (T-T_C)/C^+, \qquad T > T_C \qquad (3.1)$$

where C^+ is the Curie constant above T_C. As indicated in Fig.9, $(\chi_{33}^X)^{-1}$ in the FE phase shows the linear temperature dependence and is described by a modified Curie-Weiss relation:

$$(\chi_{33}^X)^{-1}=(T_C-T)/C^-, \qquad T<T_C \qquad (3.2)$$

where C^- is the Curie constant below T_C. Note that the experimental results in both FE and PE phases can be expressed by the same Curie temperature T_C. Curie temperature T_C in the LiTaO$_3$ sample used for dielectric measurements is 868 K and agrees with the value with the congruent melt composition reported by Barns and Carruthers.[38] The slope for $(\chi_{33}^X)^{-1}$ at 10 kHz in the PE phase yields a Curie constant $C^+=1.43\times10^5$, which is in good agreement with the value reported by Yamada et al.[22] and by Glass.[25] The ratio of the Curie constants C^+/C^- for LiTaO$_3$ at 10 kHz is 2.7 and agrees well with that for LiNbO$_3$, although the C^+ value for LiNbO$_3$ is a half as large as that for LiTaO$_3$. According to the Landau-Devonshire theory,[1] these ratios clearly indiciate that both LiTaO$_3$ and LiNbO$_3$ undergo a nearly second-order phase transition.

High-frequency inverse susceptibility χ_{33}^{-1} in the PE phase decreases linearly with decreasing temperature, deviates from linearity and then becomes practically constant with temperature in the neighborhood of T_C. In the range between 950 and 1200 K, the slope for 100 kHz is equal to the slopes for high frequencies. Compared with χ_{33}^{-1} up to 100 kHz, high-frequency inverse susceptibility χ_{33}^{-1} in the PE phase exhibits remarkable deviations

from linearity in the neighborhood of T_C. In the FE phase, $(\chi_{33}^x)^{-1}$ at 10 MHz is expressed as

$$(\chi_{33}^x)^{-1} = (T_0 - T)/C^\top, \qquad T < T_C \qquad (3.3)$$

where $C^\top$ is the modified Curie constant below T_C. The temperature T_0, at which $(\chi_{33}^x)^{-1}$ extrapolates to zero, is higher than T_C.

As shown in Fig.10, conductivity σ_{33} along the z axis exhibits a maximum at T_C. In addition, σ_{33} shows significant dispersion over the wide temperature range between 700 and 1200 K. Conductivity σ_{33} increases with increasing frequency. As indicated in Fig.10(b), variations of σ_{11} with frequency near T_C are far less than those of σ_{33}. Conductivity σ_{11} increases with increasing temperature, up to 1150 K. Lowest-frequency conductivity σ_{33} shows similar temperature dependence, with the exception of the anomalous part associated with the phase transition.

3-4 Dielectric constants in LiNbO$_3$

Figure 11 shows dielectric constants ε_{11}, ε_{33} and the loss tan δ in LiNbO$_3$ as a function of temperature. Because of the electric resonance, dielectric constant ε_{33} values at 10 and 13 MHz were not determined near T_C. As indicated in Table III, room temperature values for ε_{ii} at 10 and 13 MHz are in goood agreement with the data obtained in the GHz region.[28,44] Thus, ε_{ii} values at 10 and 13 MHz are regarded as clamped dielectric

constants ε_{ii}^{X}. The ε_{ii} value at 100 kHz is practically equal to ε_{ii} at 10 kHz, except for the high temperature region, where the loss tan δ at 10 kHz is large. In addition, ε_{33} at 1 MHz agrees well with ε_{33} values at 10 and 100 kHz, as long as tan δ values at 10 kHz and 100 kHz are small. Therefore, the ε_{11} values, up to 100 kHz, and ε_{33} values, up to 1 MHz, with a small tan δ denote free dielectric constants ε_{11}^{X} and ε_{33}^{X}, respectively.

Clamped dielectric constant ε_{11}^{X} is approximately a half as large as the free dielectric constant ε_{11}^{X}, as shown in Fig.11(a). Both free and clamped dielectric constants ε_{11} increase gradually with increasing temperature. In contrast to ε_{11}, there is a difference between clamped dielectric constant ε_{33}^{X} and free di-electric constant ε_{33}^{X}. Although, in the FE phase, the ε_{33} value at 13 MHz is in agreement with the ε_{33} value at 10 MHz, in the PE phase, ε_{33} at 13 MHz is lower than ε_{33} at 10 MHz, as shown in Fig.11(c). Above T_C, dielectric constant ε_{33} decreases with increasing frequency, from 1 MHz to 13 MHz.

Figure 12 shows inverse dielectric susceptibility χ_{33}^{-1} vs. temperature relationship. Inverse susceptibility χ_{33}^{-1} near T_C, in both FE and PE phases, obeys a Curie-Weiss law described by eqs.(3.1) and (3.2). Curie temperature T_C for the LiNbO$_3$ sample is 1410 K and agrees with the value with the congruent melt com-position reported by Bergman et al.[45] and by Carruthers et al.[37] The slope for χ_{33}^{-1} at 1 MHz in the PE phase yields a Curie con-stant $C^+ = 2.7 \times 10^5$ K, which is a typical value for the displacive phase transitions. The ratio of Curie constants C^+/C^- for 1

MHz is about 2.6. This indicates that $LiNbO_3$ undergoes a nearly second-order phase transition. Below T_C, the slope $(d\chi_{33}^{-1}/dT)$ for 10 MHz is steeper than that for 1 MHz, while, above T_C, the slopes for 10 MHz and 13 MHz are parallel with that for 1 MHz. Deviations from the Curie-Weiss behavior were observed in both phases, far from T_C.

Conductivity σ_{33} along the Z axis is plotted in Fig.13 as a function of temperature. Near T_C, σ_{33} values at 10 and 13 MHz were not obtained, due to the electric resonance. Anomalous conductivity change, related with the phase transition, was observed near T_C. With the exception of the anomalous part, σ_{33} increases with increasing temperature. Conductivity σ_{11} along the Y axis shows similar temperature dependence, up to 1200 K.

Figure 14 shows ε_{33} and χ_{33}^{-1} in $LiTaO_3$ and $LiNbO_3$ as a function of reduced temperature T/T_C. In view of eq.(3.1), Fig.14 shows that the C^{+}/T_C value for $LiTaO_3$ is nearly equal to that for $LiNbO_3$.

§4 Phenomenological treatment

4-1 Differences in elastic-constant and inverse-susceptibility

An interpretation of the elastic and dielectric properties in $LiNbO_3$ and $LiTaO_3$ requires the phenomenological expression of free energy with respect to strain and the order parameter. The primary order parameter in these crystals is regarded as spontaneous polarization along Z axis. For convenience, the suffixes are dropped out to represent the tensors of coupling constants between strain x and polarization P. Since piezoelectric coupling term axP is forbidden by symmetry above T_C, the lowest-order interaction in the PE phase of these crystals is the electrostrictive coupling of the form qxP^2. In addition, higher-order coupling of the form rxP^4 is taken into account, to interpret the temperature dependences of $C_{ii}^P - C_{ii}^E$ and $(\chi_{ii}^x)^{-1} - (\chi_{ii}^X)^{-1}$, consistently. The coupling, expressed as hx^2P^2, may give rise to variation in elastic constant C_{ii}^P proportional to the square of P_s. However, C_{ii}^P values in $LiTaO_3$ and $LiNbO_3$ exhibit no anomalies associated with hx^2P^2: For $LiTaO_3$, C_{33}^P shows the linear temperature dependence with the same slopes on either side of T_C, as indicated in Fig.5. For $LiNbO_3$, C_{33}^P decreases linearly with increasing temperature up to 1070 K, as indicated in Fig.7. Thus, coupling hx^2P^2 is excluded from this analysis. Using the Voigt notation, electrostrictive constant q_{ij} for these crystals is expressed as[40]

$$q_{ij} = \begin{pmatrix} q_{11} & q_{12} & q_{13} & q_{14} & 0 & 0 \\ q_{12} & q_{11} & q_{13} & -q_{14} & 0 & 0 \\ q_{13} & q_{13} & q_{33} & 0 & 0 & 0 \\ q_{14} & -q_{14} & 0 & q_{44} & 0 & 0 \\ 0 & 0 & 0 & 0 & q_{44} & q_{14} \\ 0 & 0 & 0 & 0 & q_{14} & q_{66} \end{pmatrix} \qquad (4.1)$$

The form of the higher-order coupling constant r_{ijk} is given in ref.46. Since spontaneous polarization P_s arises along the z axis below T_C, it is reasonable to neglect higher-order terms with respect to P_1 and P_2. Interaction energy $F_C(x_i, P_m)$ for $LiTaO_3$ and $LiNbO_3$ is then written as

$$F_C(x_i, P_m) = q_{33}x_3P_3^2 + q_{13}(x_1+x_2)P_3^2 + q_{14}\{(x_1-x_2)P_2+x_6P_1\}P_3$$

$$+q_{44}(x_4P_2+x_5P_1)P_3$$

$$+\{r_{133}(x_1+x_2)+r_{333}x_3\}P_3^4+\{r_{134}(x_1-x_2)+r_{344}x_4\}P_2P_3^3$$

$$+(r_{344}x_5+r_{356}x_6)P_1P_3^3. \qquad (4.2)$$

According to Slonczewski and Thomas,[30] c_{ij}^E is related with c_{ij}^P by

$$c_{ij}^E = c_{ij}^P - \sum_k \frac{\partial^2 F_C}{\partial x_i \partial P_k} \chi_{kk}^x \frac{\partial^2 F_C}{\partial P_k \partial x_j} \qquad (4.3)$$

The inverse susceptibility $(\chi_{kk}^X)^{-1}$ at constant stress is given by

$$(\chi_{kk}^X)^{-1} = (\chi_{kk}^x)^{-1} - \sum_{i,j} \frac{\partial^2 F_C}{\partial P_k \partial x_i} s_{ij}^P \frac{\partial^2 F_C}{\partial x_j \partial P_k} . \qquad (4.4)$$

Here, elastic compliance s_{ij}^P is equal to the inverse of c_{ij}^P.

In the FE phase, spontaneous polarization P_s along the Z axis generates piezoelectric coupling $a_{mi}x_iP_m$, which is dominant over the electrostrictive and higher-order coupling. Using the relation $a_{mi} = (\partial^2 F_C / \partial x_i \partial P_m)$, a_{mi} values in $LiTaO_3$ and $LiNbO_3$ are written as

$$a_{22} = -(q_{14} + r_{134}P_s^2)P_s, \qquad (4.5)$$

$$a_{33} = 2(q_{33} + 2r_{333}P_s^2)P_s, \qquad (4.6)$$

$$a_{15} = (q_{44} + r_{344}P_s^2)P_s, \qquad (4.7)$$

$$a_{31} = 2(q_{13} + 2r_{133}P_s^2)P_s. \qquad (4.8)$$

Consequently, elastic-constant difference $c_{ii}^P - c_{ii}^E$ and inverse-susceptibility difference $(\chi_{ii}^x)^{-1} - (\chi_{ii}^X)^{-1}$ are expressed as

$$c_{11}^P - c_{11}^E = (q_{14} + r_{134}P_s^2)^2 P_s^2 \chi_{11}^x + 4(q_{13} + 2r_{133}P_s^2)P_s^2 \chi_{33}^x, \qquad (4.9)$$

$$c_{33}^P - c_{33}^E = 4(q_{33} + 2r_{333}P_s^2)^2 P_s^2 \chi_{33}^x, \qquad (4.10)$$

$$c_{44}^P - c_{44}^E = (q_{44} + r_{344}P_s^2)^2 P_s^2 \chi_{11}^x, \qquad (4.11)$$

$$c_{66}^P - c_{66}^E = (q_{14} + r_{134}P_s^2)^2 P_s^2 \chi_{11}^x, \qquad (4.12)$$

$$(\chi_{11}^{x})^{-1} - (\chi_{11}^{X})^{-1} = 2(q_{14} + r_{134}P_s^2)^2 P_s^2 (S_{11}^P - S_{12}^P)$$

$$+ (q_{44} + r_{134}P_s^2)^2 P_s^2 S_{44}^P$$

$$+ 4(q_{14} + r_{134}P_s^2)(q_{44} + r_{344}P_s^2)P_s^2 S_{14}^P , \qquad (4.13)$$

$$(\chi_{33}^{x})^{-1} - (\chi_{33}^{X})^{-1} = 4(q_{33} + 2r_{333}P_s^2)^2 P_s^2 S_{33}^P$$

$$+ 8(q_{13} + 2r_{133}P_s^2)^2 P_s^2 (S_{11}^P + S_{12}^P)$$

$$+ 16(q_{33} + 2r_{333}P_s^2)(q_{13} + 2r_{133}P_s^2)S_{13}^P . \qquad (4.14)$$

In this analysis, four assumptions are made: (1) Coefficients q_{ij} and r_{ijk} are temperature independent. (2) Elastic constants c_{11}^P, c_{44}^P and c_{66}^P decrease linearly with increasing temperature. (3) For LiNbO$_3$ the slope dc_{ii}^P/dT (i=1, 4 and 6) is equal to the slope dc_{ii}^E/dT in the range between 300 and 450 K. (4) In eqs. (4.13) and (4.14), variation of S_{ij}^P with temperature is negligibly small, compared with that of P_s^2.

With the exception of c_{33}^P, elastic constant c_{ii}^P at constant polarization cannot be directly determined by ultrasonic methods. Room temperature values for c_{11}^P, c_{44}^P and c_{66}^P are calculated from eqs.(4.3)-(4.8), using corresponding elastic constants c_{ii}^E and dielectric susceptibilities χ_{ii}^x obtained by the present work, and piezoelectric constants a_{mi} reported by Warner et al.[43] or by Yamada et al.[22] The results are presented in Tables Ⅳ and Ⅴ.

The temperature dependence of elastic constants c_{ij}^P arises from the variation in the lattice potential energy, due to anharmonicity. According to Leibfried and Ludwig,[47] the temperature

dependence of C_{ij}^P is expressed reasonably as

$$C_{ij}^P = \bar{C}_{ij}^P \{1 - D_{ij} F(T/\theta)\}, \qquad (4.15)$$

where $\bar{C}_{ij}^P$ refers to C_{ij}^P at 0 K, D_{ij} depends on the lattice anharmonicity, θ is the Debye temperature and

$$F(T/\theta) = 3(T/\theta)^4 \int_0^{T/\theta} x^3 (e^x - 1) dx. \qquad (4.16)$$

Glass and Lines[48] reported that Debye temperature θ values are 450 K for $LiTaO_3$ and 560 K for $LiNbO_3$. Thus, C_{ii}^P for these crystals is expected to show approximately the linear decrease in the observed temperature range. The experimental results for C_{33}^P are consistent with the expectation, as indicated in Figs.5(b) and 7(b).

In the FE phase of $LiTaO_3$, temperature coefficients for C_{ii}^P (i=1, 4 and 6) are determined from the calculated values of C_{ii}^P at room temperature and the measured values of C_{ii}^P at T_C. In $LiNbO_3$, slopes for C_{44}^P and C_{66}^P are assumed to be equal to those for C_{44}^{ex} and C_{66}^{ex}, which were obtained by linearly extrapolating C_{44}^E and C_{66}^E in the range between 300 and 450 K to higher temperatures, as shown in Fig.7. On the basis of the experimental results for C_{33}^P, S_{33}^P is expected to increase linearly with increasing temperature. According to Yamada et al.[22,24], the relative temperature derivatives $(S_{ii}^E)^{-1}(dS_{ii}^E/dT)$ in these crystals are of the order of 2×10^{-4} K^{-1}. Thus, it appears reasonable to neglect the temperature dependence of S_{ij}^P in eqs.(4.13) and (4.14).

As indicated in Tables IV and V , the a_{31} values for LiTaO$_3$ and LiNbO$_3$ are small, compared with the other a_{mi} values at room temperature. According to eq. (4.8), the low a_{31} value leads to small q_{13} and r_{133}. In the absence of q_{13} and r_{ijk}, eqs.(4.9)-(4.14) predict the following relationships: (1) Elastic-constant differences $c_{11}^P - c_{11}^E$, $c_{44}^P - c_{44}^E$ and $c_{66}^P - c_{66}^E$ vary as $P_s^2 \chi_{11}^x$, while $c_{33}^P - c_{33}^E$ varies as $P_s^2 \chi_{33}^x$. (2) Inverse-susceptibility differences $(\chi_{11}^x)^{-1} - (\chi_{11}^X)^{-1}$ and $(\chi_{33}^x)^{-1} - (\chi_{33}^X)^{-1}$ are proportional to P_s^2.

4-2 Dielectric susceptibility

The dielectric susceptibility is derived from an expression of the lattice free energy $F(x_m, P_i)$ involving strain x and polarization P_i. For LiTaO$_3$ and LiNbO$_3$, elastic constant and dielectric tensors are given by eqs.(2.4) and (2.5), respectively. Thus, the free energy $F(x_m, P_i)$ for two crystals is written as

$$F(x_m, P_i) = F_m(x_m) + F_0(P_i) + F_C(x_m, P_i), \qquad (4.17)$$

$$F_m(x_m) = \frac{1}{2} c_{11}^P (x_1^2 + x_2^2) + \frac{1}{2} c_{33}^P x_3^2 + \frac{1}{2} c_{44}^P (x_4^2 + x_5^2) + \frac{1}{2} c_{66}^P x_6^2 + c_{12}^P x_1 x_2$$

$$+ c_{13}^P (x_1 + x_2) x_3 + c_{14}^P (x_1 - x_2) x_4 + c_{14}^P x_5 x_6, \qquad (4.18)$$

$$F_0(P_i) = \frac{1}{2} (\varepsilon_0 \chi_{11})^{-1} (P_1^2 + P_2^2) + \frac{1}{2} (\varepsilon_0 \chi_{33})^{-1} P_3^2 + \frac{1}{4} A P_3^4. \qquad (4.19)$$

Here, $F_m(x_m)$ refers to the elastic strain energy and $F_0(P_i)$ represents the Landau free energy expansion, with respect to the polarization alone. For simplicity, terms higher than P_3^6 are

dropped in eq.(4.19) and coefficient A is assumed to be a constant. Free interaction energy $F_C(x_m, P_i)$ is given by eq.(4.2).

Spontaneous values for strain x_{ms} and polarization P_s are obtained by setting stress X_m and electric field E_3 equal to zero:

$$X_m = \left| \frac{\partial F(x_m, P_i)}{\partial x_m} \right|_{P} = 0 \ , \tag{4.20}$$

$$E_3 = \left| \frac{\partial F(x_m, P_i)}{\partial P_3} \right|_{x} = 0 \ . \tag{4.21}$$

In the FE phase, spontaneous strains x_{1s}, x_{2s}, x_{3s} appear along the principal axes, while the values for shear strain x_{4s}, x_{5s} and x_{6s} are zero. When q_{13} and r_{133} are neglected, the spontaneous strains x_{ms} values are expressed as

$$x_{1s} = x_{2s} = P_s^2 (q_{33} + r_{333} P_s^2) C_{13}^P / \Delta C, \tag{4.22}$$

$$x_{3s} = - P_s^2 (q_{33} + r_{333} P_s^2)(C_{11}^P + C_{12}^P) / \Delta C, \tag{4.23}$$

where $\Delta C = C_{33}^P (C_{11}^P + C_{12}^P) - 2(C_{13}^P)^2$. $\tag{4.24}$

The ratio of spontaneous strains x_{3s}/x_{1s} below T_C is then given by

$$\frac{x_{3s}}{x_{1s}} = - \frac{C_{11}^P + C_{12}^P}{C_{13}^P} \ . \tag{4.25}$$

In the absence of r_{333}, values of x_{1s}, x_{2s}, x_{3s} are expected to be proportional to P_s^2.

Inverse susceptibility $(\chi_{33}^x)^{-1}$ at constant strain is given by

$$(\chi_{33}^x)^{-1} = \left| \frac{\partial E_3}{\partial P_3} \right| x \; , \tag{4.26}$$

From eq.(4.21), inverse susceptibility $(\chi_{33}^x)^{-1}$ is approximately written as

$$(\chi_{33}^x)^{-1} = \chi_{33}^{-1}, \qquad T > T_C \tag{4.27}$$

$$(\chi_{33}^x)^{-1} = -2\chi_{33}^{-1} + 4P_s^2 q_{33}(q_{33} + r_{333}P_s^2)(C_{11}^P + C_{12}^P)/\Delta C, \qquad T < T_C. \tag{4.28}$$

According to the Landau-Devonshire theory, inverse susceptibility χ_{33}^{-1} in eq.(4.19) is assumed to vary as $(T - T_C)$. Thus, it follows that the ratio of the Curie constants C^+/C^- is approximately -2. The second term in eq.(4.28), derived from the interaction between strain and polarization, is smaller than the inverse-susceptibility difference $(\chi_{33}^x)^{-1} - (\chi_{33}^X)^{-1}$, given by eq.(4.14).

§5 Discussion

5-1 Elastic constants

(1) Effective elastic constants for the MD crystals

At room temperature, observed C'_{33} values for the MD LiTaO$_3$ and LiNbO$_3$ crystals are practically equal to the calculated C^E_{33} values, as indicated in Figs.5(b) and 7(b). The longitudinal ultrasonic wave, propagated along the Z axis in the MD crystal, cannot induce the effective longitudinal electric field, because the average P_s value is small and because the sign of the induced charge depends on the domain orientation. The longitudinal ultrasonic strain x_3 cannot generate the transverse field, because transverse piezoelectric components e_{31} and e_{32} are zero. Thus, C'_{33} for the MD crystal is assumed to be identical to C^E_{33} over the entire temperature range.

In the presence of tranverse components of e_{ij}, an ultrasonic wave, transmitted in the MD crystal, induces a transverse electric field, whose direction depends on domain orientation. Consequently, ultrasonic velocity v'_i (i=1, 4 and 6) for the MD crystal yields effective elastic constant C'_{ii} higher than corresponding constant-field elastic constant C^E_{ii} for the SD crystal.

The piezoelectric constant e_{31} in two crystals is negligibly small, compared with e_{22}. Substitution of $e_{31}=0$ into eqs.(2.8) and (2.11) leads to the agreement between $C^P_{11}+C^P_{12}$ and $C^E_{11}+C^E_{12}$ in the FE phase. As shown in Fig.15, elastic constants $C'_{11}+C'_{12}$, obtained from C'_{11} and C'_{66} in the MD LiTaO$_3$ crystal, are in good agreement with $C^E_{11}+C^E_{12}$ in the SD crystal. Furthermore, the

difference $C'_{44} - C^E_{44}$ in $LiTaO_3$ is approximately proportinal to $C^P_{44} - C^E_{44}$ over the wide temperature range, as shown in Fig.16. Therefore, these results support the interpretation that the elastic-constant difference between SD and MD crystal arises from the piezoelectric effect.

The ultrasonic shear wave attenuation in the MD $LiNbO_3$ crystal is significantly higher than that in the MD $LiTaO_3$. The wavelength of the shear modes in these crystals is of the order of 0.2 mm at 20 MHz. By referring to the result of Miyazawa and Iwasaki[49], the ferroelectric domain size in $LiNbO_3$ crystal is presumed to be comparable with the ultrasonic wavelength. In contrast to this, the domain size in $LiTaO_3$ is reported to be less than 0.001 mm.[49] Consequently, the higher attenuation of shear waves in the MD $LiNbO_3$ crystal is ascribed to scattering by ferroelectric domains.

(2) Elastic constants in $LiTaO_3$

Figure 17 shows elastic-constant difference $C^P_{ii} - C^E_{ii}$ in $LiTaO_3$ vs. temperature relation. Note that the relative values for $C^P_{11} - C^E_{11}$ are in good agreement with those for $C^P_{44} - C^E_{44}$ and $C^P_{66} - C^E_{66}$ over the entire temperature range. According to eqs.(4.9)-(4.12), the agreement requires that coefficients q_{13} and r_{133} are zero and that the ratio r_{344}/q_{44} is equal to r_{134}/q_{14}. In contrast to $C^P_{ii} - C^E_{ii}$ (i=1, 4 and 6), $C^P_{33} - C^E_{33}$ in $LiTaO_3$ decreases slowly with increasing temperature up to 770 K and shows a marked change between 770 K and T_C.

Figure 18 shows the temperature dependence of $(C_{ii}^P - C_{ii}^E)/\chi_{mm}^x$ for LiTaO$_3$, deduced from the elastic-constant and dielectric measurements. Relative values for $(C_{11}^P - C_{11}^E)/\chi_{11}^x$ and $(C_{44}^P - C_{44}^E)/\chi_{11}^x$ are lower than those for P_s^2, taken from the pyroelectric measurement reported by Glass.[25] In view of eqs.(4.9) and (4.11) with $q_{13}=0$, the deviation from P_s^2 is attributed to higher-order coupling terms. As indicated in Fig.16, relative values for $(C_{33}^P - C_{33}^E)/\chi_{33}^x$ are lower than those for $(C_{11}^P - C_{11}^E)/\chi_{11}^x$ and $(C_{44}^P - C_{44}^E)/\chi_{11}^x$. This is due to the contribution of higher-order coupling $r_{333}x_3P_3^2$ to $C_{33}^P - C_{33}^E$ over the wide temperature range.

The significance of higher-order interaction $r_{333} x_3 P_3^4$ in $C_{33}^P - C_{33}^E$ appears compatible with the observation of spontaneous strain x_{is} in LiTaO$_3$ reported by Yamada et al.[22] They revealed that a linear relationship between x_{3s} and P_s^2 is not valid at temperatures far lower than T_C and that higher-order term P_s^4 contributes largely to the results for x_{is}. The temperature dependence of x_{1s} and x_{3s} is accounted for by eqs.(4.22)-(4.24). According to eq.(4.25), the spontaneous strain ratio x_{3s}/x_{1s} is expected to be temperature independent. The ratio $x_{3s}/x_{1s}=-3.5$, obtained from the C_{ij}^P data, seems to be consistent with the results reported by Yamada et al.[22]

Both $(C_{33}^P - C_{33}^E)/\chi_{33}^x$ and P_s^2 vary approximately as (T_C-T) in the vicinity of T_C, as indicated in Fig 18(b). Equation (4.10) predicts that $C_{33}^P - C_{33}^E$ is temperature independent in the neighborhood of T_C, on the assumption that the relation $\chi_{33}^x \propto (T_C-T)^{-1}$ and

$P_s^2 \propto (T_C - T)$ is valid and that the higher term $2r_{333} P_s^2$ is negligibly small, compared with q_{33}. As indicated in Fig.9(b), χ_{33}^x at 10 MHz deviates significantly from the Curie-Weiss law near T_C. The temperature dependence of $(\chi_{33}^x)^{-1}$ is expressed by eq.(3.3). From the relation $P_s^2 \propto (T_C - T)$ and eq.(3.3), elastic-constant difference $c_{33}^P - c_{33}^E$ near T_C is given by

$$c_{33}^P - c_{33}^E = A \frac{T_C - T}{T_0 - T} , \qquad (5.1)$$

where A is a constant. The solid curve in Fig.17(b) is obtained from eq.(5.1) with $A = 6.1 \times 10^9$ N/m^2, $T_C = 875$ K and $T_0 = 888$ K. The good agreement indicates that the drastic change in $c_{33}^P - c_{33}^E$ between 800 K and T_C is attributed to the anomalous behavior of χ_{33}^x at high temperatures.

As shown in Fig.6, c_{33}^P exhibits a small dip around T_C. In addition, shear elastic constants c_{44}^P and c_{66}^P in the PE phase deviate from the linear temperature behavior as T_C is approached from above. These results may be explained by the electostrictive interaction, which connects the two polarization fluctuations $\delta P(\vec{q}) \delta P(-\vec{q})$ of nearly opposite wave-vector $\vec{q}$ with the ultrasonic strain.[29,50]

(3) Elastic constants in LiNbO$_3$

Figure 19 shows elastic constant differences $c_{ii}^P - c_{ii}^E$ (i=3, 4 and 6) in LiNbO$_3$ as a function of temperature. Both $c_{44}^P - c_{44}^E$ and $c_{66}^P - c_{66}^E$ decrease gradually with increasing temperature, while $c_{33}^P - c_{33}^E$ is independent of temperature. Linear decrease in c_{11}^E implies that $c_{11}^P - c_{11}^E$ decreases slowly with increasing temperature. As indicated in Figs.17 and 19, the agreement between $c_{44}^P - c_{44}^E$ and between $c_{66}^P - c_{66}^E$ is recognized for both LiNbO$_3$ and LiTaO$_3$.

Figure 20 indicates relative values for $(c_{33}^P - c_{33}^E)/\chi_{33}^x$ and $(c_{44}^P - c_{44}^E)/\chi_{11}^x$ obtained by the present work and those for P_s^2, taken from unpublished pyroelectric measurement reported by Glass.[51] In the absence of higher-order coupling rxP^4, eqs. (4.10)-(4.12) predict that the quantities $(c_{33}^P - c_{33}^E)/\chi_{33}^x$, $(c_{44}^P - c_{44}^E)/\chi_{11}^x$ and $(c_{66}^P - c_{66}^E)/\chi_{11}^x$ are proportional to P_s^2. There are, however, considerable discrepancies between $(c_{ii}^P - c_{ii}^E)/\chi_{mm}^x$ and P_s^2, as indicated in Fig.20. Elastic-constant differences $c_{33}^P - c_{33}^E$, $c_{44}^P - c_{44}^E$ and $c_{66}^P - c_{66}^E$ should be affected by higher-order interaction rxP^4. For LiNbO$_3$, values of $(c_{33}^P - c_{33}^E)/\chi_{33}^x$ are considerably lower than those of $(c_{44}^P - c_{44}^E)/\chi_{11}^x$ and $(c_{66}^P - c_{66}^E)/\chi_{11}^x$ at high temperatures. The same behavior is also observed for LiTaO$_3$, as shown in Fig.18. These results indicate that the higher-order coupling rxP^4 has the most profound influence on $c_{33}^P - c_{33}^E$ in LiTaO$_3$ and LiNbO$_3$.

It is of interest to compare elastic constants in LiNbO$_3$ with those in LiTaO$_3$. Figure 21 shows $c_{ii}^P - c_{ii}^E$ in these crystals

as a function of reduced temperature T/T_C. With the exception of the range near T_C, $C_{33}^P - C_{33}^E$ values in these crystals are practically temperature independent. On the other hand, there is a marked difference in $C_{ii}^P - C_{ii}^E$ (i=4 and 6) vs. reduced temperature relations between these materials. These observations are interpreted as the difference in variation of P_S with temperature between these crystals. Spontaneous polarization P_S for $LiNbO_3$ decreases slowly with increasing temperature, compared with the case of $LiTaO_3$.[25,51]

5-2 Dielectric susceptibility

(1) Comparison with the phenomenological expression

The values for inverse-dielectric-susceptibility difference $(\chi_{mm}^x)^{-1}-(\chi_{mm}^X)^{-1}$ in $LiTaO_3$ and $LiNbO_3$ are plotted as a function of temperature in Fig.18 and Fig.20, respectively. In the case of $LiNbO_3$, difference $(\chi_{33}^x)^{-1}-(\chi_{33}^X)^{-1}$ decreases almost linearly with increasing temperature, while the difference $(\chi_{11}^x)^{-1}-(\chi_{11}^X)^{-1}$ shows remarkable nonlinear temperature dependence. For $LiTaO_3$, the distinction is also recognized between $(\chi_{33}^x)^{-1}-(\chi_{33}^X)^{-1}$ and $(\chi_{11}^x)^{-1}-(\chi_{11}^X)^{-1}$. Since, in $LiNbO_3$, the relative values for $(\chi_{mm}^x)^{-1}-(\chi_{mm}^X)^{-1}$ near T_C are lower than those for P_s^2, the higher order interaction rxP^4 contributes significantly to the inverse-susceptibility difference. The higher r_{333} value can account for the distinct difference between $(\chi_{11}^x)^{-1}-(\chi_{11}^X)^{-1}$ and $(\chi_{33}^x)^{-1}-(\chi_{33}^X)^{-1}$. As indicated in Fig.20, relative values of $(\chi_{33}^x)^{-1}-(\chi_{33}^X)^{-1}$ for $LiNbO_3$ agree well with those of $(C_{44}^P-C_{44}^E)/\chi_{11}^x$, while the values of $(\chi_{33}^x)^{-1}-(\chi_{33}^X)^{-1}$ agree with those of $(C_{33}^P-C_{33}^E)/\chi_{33}^x$. This correspondence is also found for $LiTaO_3$, except for near T_C, as shown in Fig.18. Following eqs. (4.9)-(4.14), the temperature dependence of inverse-susceptibility difference $(\chi_{mm}^x)^{-1}-(\chi_{mm}^X)^{-1}$ is compatible with that of the elastic-constant difference $C_{ii}^P-C_{ii}^E$.

(2) Comparison with the soft mode

For LiTaO$_3$ and LiNbO$_3$, the connection between the constant-strain (clamped) dielectric constants and optical phonon frequencies is described by the generalized Lyddane-Sachs-Teller (LST) relation,[52]

$$\frac{\varepsilon_{11}^{x}}{\varepsilon_{11}(\infty)} = \prod_{i} \frac{\omega_{iLO}^{2}}{\omega_{iTO}^{2}} , \qquad\qquad (5.2)$$

$$\frac{\varepsilon_{33}^{x}}{\varepsilon_{33}(\infty)} = \prod_{j} \frac{\omega_{jLO}^{2}}{\omega_{jTO}^{2}} , \qquad\qquad (5.3)$$

where ω_{iLO} and ω_{iTO} refer to the longitudinal and transverse optical-phonon frequencies; i and j denote the various sets of E and A$_1$ modes, respectively, and $\varepsilon_{ii}(\infty)$ is the dielectric constant in the optical frequency region. As indicated in Tables II and III, room temperature clamped dielectric constants ε_{11}^{x} and ε_{33}^{x}, determined by this work, are in good agreement with the values for ε_{11} and ε_{33}, estimated from infrared reflection spectra[3,5] and from Raman scattering.[53] Clamped dielectric constant ε_{11}^{x} in LiNbO$_3$ increases slightly with increasing temperature, as shown in Fig. 11(a). According to the Raman results for LiNbO$_3$[3,53], the low-frequency E mode with large oscillator strength shows a gradual decrease with increasing temperature, while the other E modes remain approximately constant. Thus, variation in ε_{11}^{x} for LiNbO$_3$ corresponds to the shift in the E mode with temperature. The increase in ε_{11}^{x} for LiTaO$_3$ may also be due to the shift in the low-frequency E mode. Johnston and Kaminow[4] found that only one A$_1$ mode decreases considerably with increasing temperature, in marked

-42-

contrast to the other optical modes. Due to mixing with the E modes, they had difficulty in following the A_1 mode at high temperatures. They concluded that the intensity-weighted mean frequency $\bar{\omega}$ of the soft-mode structure in these crystals varies as $(T_C - T)^{0.5}$ in the temperature range up to 1200 K. As indicated in Figs.22 and 23, the quantity $\bar{\omega}^2$ is proportional to the inverse susceptibility $(\chi_{33}^x)^{-1}$ over a wide temperature range. Consequently, temperature dependence of $\bar{\omega}^2$ and $(\chi_{33}^x)^{-1}$ can be accounted for in terms of LST relation given by eq.(5.3), on the assumption that $\varepsilon_{33}(\infty)$ is temperature independent. Thus, the results reported by Johnston and Kaminow[4] seemed to be in favor of the soft-mode phase transition in LiTaO$_3$ and LiNbO$_3$, with the exception of the temperature range near T_C.

Recently, Raman spectra in LiTaO$_3$ and LiNbO$_3$ were reexamined by Zhang and Scott[21], and by Okamoto et al.[20], respectively. According to their results, the soft A_1 mode is overdamped and coupled with the relaxation process at high temperatures. They analyzed the Raman data using a response function $G(\omega)$,[54-56]

$$G(\omega) = (\omega_\infty^2 - \omega^2 - i\gamma\omega - \frac{\delta^2}{1 - i\omega\tau})^{-1}, \qquad (5.4)$$

where δ and τ denote the strength and characteristic time, respectively, the relaxation process coupled to the soft mode, and γ is the damping constant for the soft phonon. In eq.(5.4), ω_∞ represents the soft-mode frequency, deduced from the Raman experiments. The inverse clamped dielectric susceptibility $(\chi_{33}^x)^{-1}$ is expected to be proportional to squared soft-mode frequency ω_0^2, where $\omega_0^2 = \omega_\infty^2 - \delta^2$. Figures 22 and 23 indicate, however,

that the relative values for $(\chi^x_{33})^{-1}$ deviate significantly from those for $\omega^2_\infty - \delta^2$ at high temperatures. The reason for this discrepancy may be attributed to the underestimation for the δ^2 values near T_C. They pointed out that parameter δ^2 is ambiguous, compared with effective coupling parameter $\delta^2 \tau$.[20,21] Thus, comparison with $(\chi^x_{33})^{-1}$ implies that the coupling term δ^2 for these crystals increases considerably with increasing temperature.

Müller at al.[19] deduced soft-mode frequency in LiTaO$_3$ from infrared reflectivity data and found that its frequency remains finite at T_C. The coupling term δ^2 in eq.(5.4) may contribute to the finite value for squared soft-mode frequency ω^2_0.

(3) Dielectric dispersion

For LiTaO$_3$, both dielectric constant ε_{33} and conductivity σ_{33} a marked dispersion over the wide temperature range,including T_C, as indicated in Figs. 8 and 10. In the PE phase of LiNbO$_3$, ε_{33} varies with frequency from 1 MHz to 13 MHz, as shown in Fig.11 (c). Note in Fig.9(b) that for LiTaO$_3$ the difference in χ^{-1}_{33} between 10 kHz and 13 MHz is approximately independent of temperature above 950 K. Similarly, for LiNbO$_3$ the difference in χ^{-1}_{33} between 1 MHz and 13 MHz is nearly constant in the range between 1435 and 1495 K.

Frequency-dependent conductivity $\sigma(\omega)$ is connected directly with the imaginary part of dielectric constant ε''. From the Maxwell equation, $\sigma_{ii}(\omega)$ is described as

$$\sigma_{ii}(\omega) = \varepsilon_0 \varepsilon_{ii}'' \omega. \qquad (5.5)$$

Results for σ_{11} and σ_{33} in LiTaO$_3$ are presented in Fig.10. In marked contrast to σ_{33}, σ_{11} is practically frequency independent, up to 13 MHz. For these crystals, frequency-independent conductivities σ_{11} increase with increasing temperature. This implies that LiTaO$_3$ and LiNbO$_3$ have a semiconductive character at high temperatures. Figure 24 indicates the imaginary part of dielectric constant ε_{33}'' in LiTaO$_3$, obtained from the anomalous part of σ_{33}. At T_C, ε_{33}'' increases with increasing frequency. Above 1000 K, ε_{33}'' becomes small and variation in ε_{33}'' with frequency disappears. In contrast to ε_{33}'', the real part ε_{33}' has frequency dependence up to 1200 K. Figure 25 shows the Cole-Cole plot obtained from imaginary part ε_{33}'' vs. real part ε_{33}' at 880 K for LiTaO$_3$. It has been appreciated that the dielectric response in the order-disorder character ferroelectrics is given by a Debye relaxation equation,

$$\varepsilon = \varepsilon' + i\varepsilon'' = \varepsilon(\infty) + \frac{A}{1+i\omega\tau} , \qquad (5.6)$$

where A is a constant. The Debye form with a single relaxation time τ is based on the model of a dipole with two equivalent positions acting under the influence of an average local field. For LiTaO$_3$, the Cole-Cole plot in the frequency range up to 13 MHz cannot be described by eq.(5.6). Consequently, the present results for ε_{33} deny the possibility that the phase-transition mechanism in LiTaO$_3$ is of a pure order-disorder character.

In the SD LiTaO$_3$ crystal, Penna et al.[17,18] reported diffusive central mode near T_C and the anomalous polariton dispersion above 660 K. They analyzed the central mode using the Debye relaxation equation and found that the relaxation time near T_C is of the order of 5×10^{-12} sec. Zhang and Scott[21] assigned the broad peak centered at $\omega = 0$ in LiTaO$_3$ near T_C to the A$_1$ soft mode. They reported that damping constant γ in eq.(5.4) increases considerably with increasing temperature and that the relaxation time at T_C is 2.6×10^{-12} sec. However, the dielectric dispersion, observed in the frequency range between 10 kHz and 13 MHz, cannot be fitted by eq.(5.6) with the relaxation time of the order of 10^{-12} sec. Comparison of these results implies that the dielectric dispersion in LiTaO$_3$ is characterized by multiple relaxation times.

Penna et al.[18] attributed the anomalous polariton dispersion to domain fluctuation below T_C. As indicated in Figs.5 and 6, elastic-constant measurements clarify the distinction between the SD and the MD state just below T_C. Furthermore, dielectric dispersion exists in the PE phase of LiTaO$_3$. Consequently, the domain fluctuation model appears incompatible with the elastic-constant and dielectric-constant data.

Dielectric dispersion, associated with the soft phonon, is expected to be found at infrared frequencies. Thus, the dispersion observed for these crystals is imcompatible with the under-damped soft-mode behavior presented by Johnston and Kaminow.[4] According to Lines,[57] an anharmonic potential is responsible for

order-disorder character in Li ion distribution in these crystals. The lowest-order electrostrictive interaction between strain and polarization is inadequate to interpret temperature dependence of $c^P_{33} - c^E_{33}$ and $(\chi^x_{33})^{-1} - (\chi^X_{33})^{-1}$. Therefore, the dielectric dispersion and the significance of higher-order interaction may be interpreted in terms of the anharmonicity in soft-mode phonon.

Figure 10(a) indicates that the anomaly in σ_{33} for LiTaO$_3$ is associcated with the phase transition, because frequency-dependent conductity σ_{33} exhibits a peak at T_C. The σ_{33} behavior may be related to the defects which become mobile near T_C. Halperin and Varma[58] discussed the influence of defects on susceptibility near a displacive phase transition and showed that the quantity δ^2 in eq.(5.4) is proportional to the defect concentration. They predicted that the difference between the static and dynamic inverse susceptibility, caused by defects, would be practically independent of temperature. As shown in Figs.9 and 12, the results for χ^{-1}_{33} above T_C appear consistent with the above prediction. As illustrated in Fig.2, the change in Curie temperature is related to the deviation from the stoichiometric composition.[37,38] The neutron scattering measurements revealed that Li atoms above T_C occupy two equivalent positions on either side of the oxygen plane.[14,15] Thus, the coupling of soft mode with vacancies or Li ion motion may give rise to the dispersion.

As shown in Figs.9(b) and 12(b), the difference in $(\chi_{33})^{-1}$ with frequency is small in the PE phase of LiNbO$_3$, in marked

contrast to the case of $LiTaO_3$. In view of this, the soft mode in $LiNbO_3$ may couple with the relaxation process weakly compared with the soft phonon in $LiTaO_3$.

Lohnert et al.[59] studied the Mössbauer spectroscopy of ^{181}Ta nucleus in $LiTaO_3$ and pointed out that a charge transfer from neighboring oxygen ions to the central Ta ion increases non-linearly as a function of temperature. The dielectric dispersion may be influenced by change in the electric structure with temperature.

§6 Conclusion

Elastic and dielectric properties of $LiTaO_3$ and $LiNbO_3$ have been investigated over the temperature range from 300 to above 980 K. Both elastic-constant difference $c_{ii}^P - c_{ii}^E$ and inverse-dielectric-susceptibility difference $(\chi_{mm}^x)^{-1} - (\chi_{mm}^X)^{-1}$ have been interpreted consistently, on the basis of the interaction between strain x and polarization P. Electrostrictive interaction qxP^2 is inadequate to explain the temperature dependence of $c_{ii}^P - c_{ii}^E$ and $(\chi_{mm}^x)^{-1} - (\chi_{mm}^X)^{-1}$. Higher-order interaction rxP^4 contributes to both $c_{33}^P - c_{33}^E$ and $(\chi_{33}^x)^{-1} - (\chi_{33}^X)^{-1}$. These results may be attributed to the anharmonicity in soft phonon.

Both susceptibility χ_{33} and conductivity σ_{33} in $LiTaO_3$ exhibit the marked dispersion over the wide temperature range, including T_C. Susceptibility χ_{33} in the PE phase of $LiNbO_3$ shows a slight dispersion. A comparison of the dielectric results with soft-mode frequency suggests that the soft mode couples with the low-frequency relaxation process near T_C. The dielectric dispersion may arise from the motion of Li ions or vacancies. The results for c_{ii} and χ_{mm} imply that the phase transition in $LiTaO_3$ and $LiNbO_3$ has an intermediate character between displacive and order-disorder categories.

References

1) M. E. Lines and A. M. Glass: Principles and Applications of Ferroelectric and Related Materials (Clarendon Press, Oxford, 1977).

2) A. A. Oliner: Topics in Applied Physics 24, Acoustic Surface Wave (Springer, Berlin, 1978).

3) A. S. Barker, Jr. and R. Loudon: Phys. Rev. 158 (1967) 433.

4) W. D. Johnston, Jr. and I. P. Kaminow: Phys. Rev. 168 (1968) 1045.

5) A. S. Barker, Jr., A. A. Ballman and J. A. Ditzenberger: Phys. Rev. B2 (1970) 4233.

6) W. Cochran: Adv. Phys. 9 (1960) 387; Adv. Phys. 18 (1969) 157.

7) G. Shirane: Rev. Mod. Phys. 46 (1974) 437.

8) R. A. Cowley: Adv. Phys. 29 (1980) 1.

9) S. C. Abrahams, J. M. Reddy and J. L. Bernstein: J. Phys. & Chem. Solids 27 (1966) 997.

10) S. C. Abrahams, W. C. Hamilton and J. M. Reddy: J. Phys. & Chem. Solids 27 (1966) 1013.

11) S. C. Abrahams, H. J. Levinston and J. M. Reddy: J. Phys. & Chem. Solids 27 (1966) 1019.

12) S. C. Abrahams and J. L. Bernstein: J. Phys. & Chem. Solids 28 (1967) 1685.

13) S. C. Abrahams, W. C. Hamilton and A. Sequeira: J. Phys. & Chem. Solids 28 (1967) 1693.

14) S. C. Abrahams, E. Buehler, W. C. Hamilton and S. J. Laplaca: J. Phys. & Chem. Solids 34 (1973) 521.

15) E. J. Samuelsen and A. P. Grande: Z. Phys. B24 (1976) 207.

16) M. R. Chowdhury, G. E. Peckham and D. H. Saunderson: J. Phys. C 11 (1978) 1671.

17) A. F. Penna, A. Chaves and S. P. S. Porto: Solid State Commun. 19 (1976) 491.

18) A. F. Penna, S. P. S. Porto and E. Wiener-Avnear: Solid State Commun. 23 (1976) 377.

19) K. A. Müller, Y. Luspin, J. L. Servoin and F. Gervais: J. Physique Lett 43 (1982) L-537

20) Y. Okamoto, P. Wang and J. F. Scott: Phys. Rev. B 32 (1985) 6787.

21) M. Zhang and J. F. Scott: Phys. Rev. B 34 (1986) 1880.

22) T. Yamada, H. Iwasaki and N. Niizeki: Jpn. J. Appl. Phys 8 (1969) 1127.

23) L. P. Avakyants and D. F. Kiselev: Sov. Phys.-Solid State 20 (1978) 611.

24) T. Yamada, N. Niizeki and H. Toyoda: Jpn. J. Appl. Phys. 6 (1967) 151.

25) A. M. Glass: Phys. Rev. 172 (1968) 564.

26) C. Prieto, L. Arizmendi, J. A. Gonzalo F. Jaque and F. Agullo-Lopez: Phys. Rev. B31 (1985) 5483.

27) K. Nassau, H. J. Levinstein and G. M. Loiacono: J. Phys. & Chem. Solids 27 (1966) 989.

28) Y. Ohmachi, K. Sawamoto and H. Toyoda: Jpn. J. Appl. Phys. 6 (1967) 1467.

29) W. Rehwald: Adv. Phys. 22 (1973) 721.

30) J. C. Slonczewski and H. Thomas: Phys. Rev. B 1 (1970) 3599.

31) B. Luthi and W. Rehwald: Topics in Current Physics 23, Structural Phase Transitions I. (Springer, Berlin) p.131.

32) I. Tomeno and H. Hirano: J. Phys. Soc. Jpn. 50 (1981) 1809; J. Phys. Soc. Jpn. 51 (1982) 339.

33) I. Tomeno: J. Phys. Soc. Jpn. 51 (1982) 2891.

34) I. Tomeno and S. Matsumura: J. Phys. Soc. Jpn. 52 (1983) 1515.

35) I. Tomeno and S. Matsumura: Proc. 6th International Meeting on Ferroelectricity, Kobe, 1985, Jpn. J. Appl. Phys. 24 (1985) Suppl. 24-2,p. 679.

36) I. Tomeno and S. Matsumura: J. Phys. Soc. Jpn. 56 (1987) 163.

37) J. R. Carruthers, G. E. Peterson, M. Grasso and P. M. Bridenbough: J. Appl. Phys. 42 (1971) 1846.

38) R. L. Barns and J. R. Carruthers: J. Appl. Cryst. 3 (1970) 395.

39) H. J. McSkimin: IRE Trans. Ultrasonic Eng. 25 (1957) 5.

40) J. F. Nye: Physical Properties of Crystals (Clarendon Press, Oxford, 1957).

41) A. R. Hutson and D. L. White: J. Appl. Phys. 33 (1962) 40.

42) J. J. Kyame:J. Acoust. Soc. Am. 26 (1954) 990.

43) A. W. Warner, M. Onoe and G. A. Coquin: J. Acoust. Soc. Am. 42 (1967) 1223.

44) J. R. Teague, R. R. Rice amd R. Gerson: J. Appl. Phys. 46 (1975) 2864.

45) J. B. Bergman, A. Ashkin, A. A. Ballman, J. M. Dziedzic, H. L. Levinstein and R. G. Smith: Appl. Phys. Lett. 12 (1968) 92.

46) R. F. S. Hearmon:Acta Cryst. 6 (1953) 331.

47) G. Leibfried and W. Ludwig:Solid State Physics, ed. F. Seits and D. Turnbull (Academic, New York, 1961) vol.12, p.275.

48) A. M. Glass and M. E. Lines:Phys. Rev. B13 (1976) 180.

49) S. Miyazawa and H. Iwasaki: Mat. Res. Bull. 13(1978) 511.

50) E. Pytte: Phys. Rev. B1 (1970) 924.

51) A. M. Glass: Unpublished work, cited by J. G. Bergman in Chem. Phys. Lett. 38 (1976) 230. See also ref.1 p.482.

52) W. Cochran and R. A. Cowley: J. Phys. & Chem. Solids 23 (1962) 447.

53) I. P. Kaminow and W. D. Johnston, Jr.: Phys. Rev. 160 (1967) 519.

54) S. M. Shapiro, J. D. Axe, G. Shirane and T. Riste:Phys. Rev. B 6 (1972) 4332.

55) R. A. Cowley and G. J. Coombs: J. Phys. C 6 (1973) 143.

56) N. Lagakos and H. Z. Cummins: Phys. Rev. B 10 (1974) 1063.

57) M. E. Lines: Solid State Commun. 10 (1972) 793.
42 (1967) 1223.

58) B. I. Halperin and C. M. Varma: Phys. Rev. B14 (1976) 4030.

59) M. Lohnert, G. Kaindl, G. Wortmann and D. Salomon: Phys. Rev. Lett. 47 (1981) 194.

Table I. Relationship between acoustic modes and elastic stiffnesses in the SD and MD crystals.

Acoustic mode		Velocity	Elastic stiffness	
Propagation direction	Polarization direction		SD crystal	MD crystal
X	X	v_1	c_{11}^E	c_{11}'
Z	Z	v_3	c_{33}^P	c_{33}'
Z	X or Y	v_4	c_{44}^E	c_{44}'
Y	X	v_6	c_{66}^E	c_{66}'

Table II. Dielectric constant values for $LiTaO_3$ at 293 K.

Capacitance measurements

	Present work				Teague et. al.[44]	
f(Hz)	10 k	100 k	1 M	10M	13 M	1 G
ε_{11}	53.5	53.5		41.7	40.6	40.3
ε_{33}	42.4	42.2	42.0	39.2	38.8	41.4

Infrared reflectivity	Raman scattering
Barker et. al.[5]	Kaminow & Johnston[53]
ε_{11}^{x} 41.5	41
ε_{33}^{x} 37.6	43

Table Ⅲ.　Dielectric constant values for $LiNbO_3$ at 293 K.

Capacitance measurements

	Present work					Teague et. al.[44]	Ohmachi et. al.[28]
f(Hz)	10 k	100 k	1 M	10M	13 M	1 G	9 G
ε_{11}	84.2	84.4	79.1	44.7	45.2	43.9	42.5
ε_{33}	29.2	29.2	29.2	26.1	26.7	23.7	26

	Infrared reflectivity	Raman scattering
	Barker & Loudon[3]	Kaminow & Johnston[53]
ε_{11}^{x}	41.5	44
ε_{33}^{x}	26.0	29

Table IV. Room temperature values for C_{ii}^P, C_{ii}^E, S_{ij}^P and a_{mi} in LiTaO$_3$.

Observed value		Estimated value	
C_{11}^E	2.328×10^{11} N/m^2	C_{11}^P	2.43×10^{11} N/m^2
C_{33}^P	2.839	C_{33}^E	2.73
C_{44}^E	0.941	C_{44}^P	1.15
C_{66}^E	0.931	C_{66}^P	1.04

Yamada et al.[22]			
S_{11}^P	4.68×10^{-12} m^2/N	a_{15}	7.5×10^9 N/C
S_{12}^P	-0.16	a_{22}	5.5
S_{13}^P	-1.17	a_{31}	-0.3
S_{33}^P	4.14	a_{33}	5.6
S_{44}^P	9.0		

Table V. Room temperature values for C_{ii}^P, C_{ii}^E, S_{ij}^P and a_{mi} in LiNbO$_3$.

Observed value		Estimated value	
C_{11}^E	1.987×10^{11} N/m^2	C_{11}^P	2.15×10^{11} N/m^2
C_{33}^P	2.509	C_{33}^E	2.44
C_{44}^E	0.595	C_{44}^P	0.95
C_{66}^E	0.719	C_{66}^P	0.88

Warner et al.[43]			
S_{11}^P	5.20×10^{-12} m^2/N	a_{15}	9.3×10^9 N/C
S_{12}^P	-0.44	a_{22}	6.3
S_{13}^P	-1.45	a_{31}	0.8
S_{33}^P	4.89	a_{33}	4.9
S_{44}^P	10.8		

Figure Captions

Fig. 1 Crystal structure of $LiTaO_3$ and $LiNbO_3$. (a) In FE phase (b) In PE phase. In FE phase (a), the distorted octahedra, composed of oxygen atoms (large circles) contain, in sequence, Ta or Nb atoms (hatched circles), vacancies and Li atoms (cross-hatched circles). In the PE phase of $LiTaO_3$ (b), Ta atoms are located at an octahedron center, and Li atoms occupy two equivalent positions, on either side of the oxygen plane with equal probability. The arrangement of Ta (or Nb) and Li atoms with respect to oxygen planes (solid lines) in FE phase (c) and PE phase (e). (d) Structure of $LiNbO_3$ above T_C proposed by Abrahams et al.[13]

Fig. 2 Phase diagram for the $Li_2O-Nb_2O_5$ system (After Carruthers et. al.[37])

Fig. 3 Apparatus for ultrasonic velocity measurements. The phase-comparison method was improved so that automatic velocity measurement could be made at high temperatures.

Fig. 4 Typical overlapped echo amplitude as a function of fre-quency. Amplitude exhibits minima periodically. Arrows refer to frequencis f_n at which there is an integer n of wavelength in twice the sample thickness.

Fig. 5 Temperature dependence of elastic constants in $LiTaO_3$. Elastic constants for SD crystal are denoted by c^E_{11}, c^P_{33}, c^P_{44} and c^E_{66}, while those for MD crystal are denoted by C'_{11}, C'_{33}, C'_{44} and C'_{66}. Linear temperature dependence for c^P_{11}, c^P_{44} and c^P_{66} (broken lines) is assumed. Open and

closed circles refer to room temperature C_{ii}^P values taken

papers published by Yamada et al.[22] and by Warner et al.[43],

respectively.

Fig. 6 Details of elastic constant vs. temperature relation in C_{ij} for LiTaO$_3$ near T_C.

Fig. 7 Elastic constants as a function of temperature in LiNbO$_3$. Room temperature value for C_{33}^E was obtained from the present results for C_{33}^P and χ_{33}^x, and the a_{33} value by Warner et. al.[43]. C_{44}^{ex} and C_{66}^{ex} were obtained by linearly extrapolating C_{44}^E and C_{66}^E in the range between 300 and 450 K to higher temperatures.

Fig. 8 Temperature dependence of dielectric constants ε_{ii} in LiTaO$_3$. (a) ε_{11} along the Y axis. (b) ε_{33} along the Z axis. (c) Details of ε_{33} near T_C.

Fig. 9 Inverse dielectric susceptibility χ_{33}^{-1} in LiTaO$_3$. (a) χ_{33}^{-1} as a function of temperature up to 1200 K. (b) Details of χ_{33}^{-1} near T_C=868 K. Note that χ_{33}^{-1} shows dispersion in the PE phase.

Fig.10 Temperature dependence of conductivity σ_{ii} in LiTaO$_3$. (a) σ_{33} along the Z axis. (b) σ_{11} and σ_{33} at 10 KHz and 10 MHz.

Fig.11 Temperature dependence of dielectric constants ε_{ii} and loss tan δ in LiNbO$_3$. (a) ε_{11} along the Y axis. (b) ε_{33} along the Z axis. Below T_C, the ε_{33} values at 10 kHz, 100 kHz and 1 MHz represent ε_{33}^X, while the ε_{33} value at 10 MHz represents ε_{33}^x. (c) Details of ε_{33} near T_C. (d) tan δ along the Z axis.

Fig.12 Inverse dielectric susceptibility χ_{33}^{-1} in LiNbO$_3$. (a) χ_{33}^{-1} as a function of temperature up to 1520 K. (b) Details of χ_{33}^{-1} near $T_C=1410$ K. Note that χ_{33}^{-1} shows dispersion in the PE phase.

Fig.13 Temperature dependence of conductivity σ_{33} in LiNbO$_3$. Conductivity σ_{11} is similar in behavior to σ_{33}, up to 1200 K.

Fig.14 Dielectric constats ε_{33} and inverse susceptibilities χ_{33}^{-1} in LiTaO$_3$ and LiNbO$_3$, as a function of reduced temperature T/T_C.

Fig.15 Elastic constants $C_{11}^E+C_{12}^E$ and $C_{11}'+C_{12}'$ in LiTaO$_3$. Data are obtained from $C_{11}^E,C_{66}^E,C_{11}'$ and C_{66}'.

Fig.16 Elastic-constant differences $C_{44}^P-C_{44}^E$ and $C_{44}'-C_{44}^E$ in LiTaO$_3$. Each plot is normalized to unity at 300 K.

Fig.17 Elastic-constant difference $C_{ii}^P-C_{ii}^E$ in LiTaO$_3$. (a) Each plot is normalized to unity at 300 K. (b) Details of $C_{33}^P-C_{33}^E$ near T_C. The solid curve is obtained from eq. (5.1) with the parameters given in the text.

Fig.18 Temperature dependence of $(C_{ii}^P-C_{ii}^E)/\chi_{mm}^x$, $(\chi_{mm}^x)^{-1}-(\chi_{mm}^X)^{-1}$ and P_s^2 for LiTaO$_3$. Each plot is normalized to unity at 300 K (a) or $T-T_C=-200$ K (b). The P_s^2 data are taken from the measurement by Glass.[25]

Fig.19 Elastic-constant difference $C_{ii}^P-C_{ii}^E$ in LiNbO$_3$. Each plot is normalized to unity at 300 K.

Fig.20 Temperature dependence of $(C_{ii}^P-C_{ii}^E)/\chi_{mm}^x$, $(\chi_{mm}^x)^{-1}-(\chi_{mm}^X)^{-1}$ and P_s^2 for LiNbO$_3$. Each plot is normalized to unity at

300 K. The P_S^2 data are taken from the unpublished work by Glass.[51]

Fig.21 Elastic-constant difference in $LiTaO_3$ and $LiNbO_3$ as a function of reduced temperature T/T_C.

Fig.22 Inverse susceptibility and squared soft-mode frequencies for $LiTaO_3$. Each plot is normalized to unity at 300 K. The triangles represent the mean squared soft-mode frequency $\bar{\omega}^2$ determined by Johnston and Kaminow.[4] The The solid and open squares denote ω_∞^2 and $\omega_\infty^2 - \delta^2$, respectively, determined by Zhang and Scott.[21] The solid circles denote squared soft-mode frequency, determined by Müller et al.[19] The open circles refer to the constant-strain inverse susceptibility $(\chi_{33}^x)^{-1}$, obtained by the present work.

Fig.23 Inverse susceptibility and squared soft-mode frequencies for $LiNbO_3$. Each plot is normalized to unity at 300 K. The triangles represent the mean squared soft-mode frequency $\bar{\omega}^2$, determined by Johnston and Kaminow.[4] The solid and open squares denote ω_∞^2 and $\omega_\infty^2 - \delta^2$, respectively, determined by Okamoto et al.[20] The open circles denote the constant-strain inverse susceptibility $(\chi_{33}^x)^{-1}$, obtained by the present work.

Fig.24 Dielectric constant ε_{33}'' in $LiTaO_3$.

Fig.25 Imaginary part vs real part of the dielectric constant as a function of frequency at 880 K in $LiTaO_3$ (Cole-Cole plot).
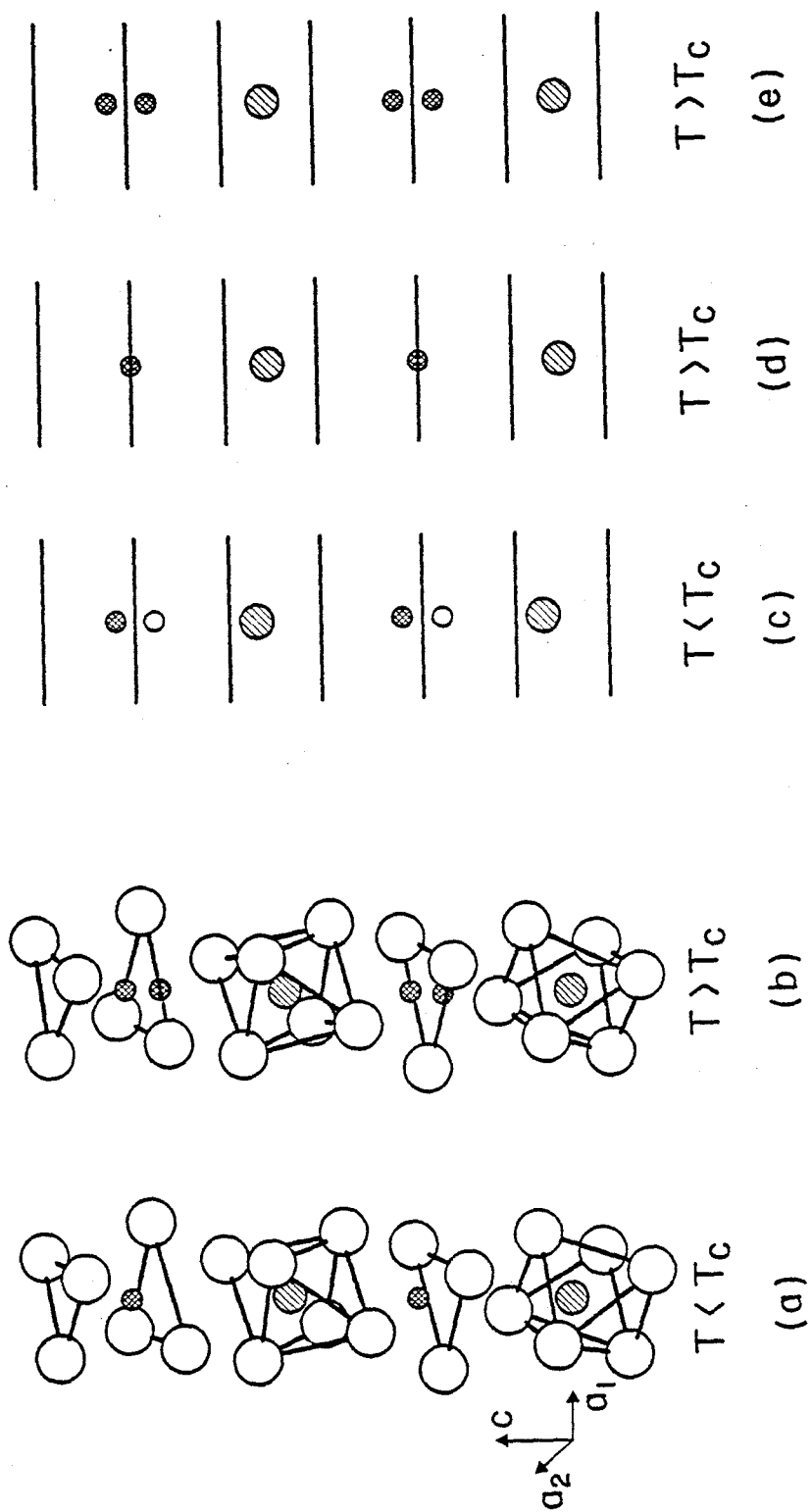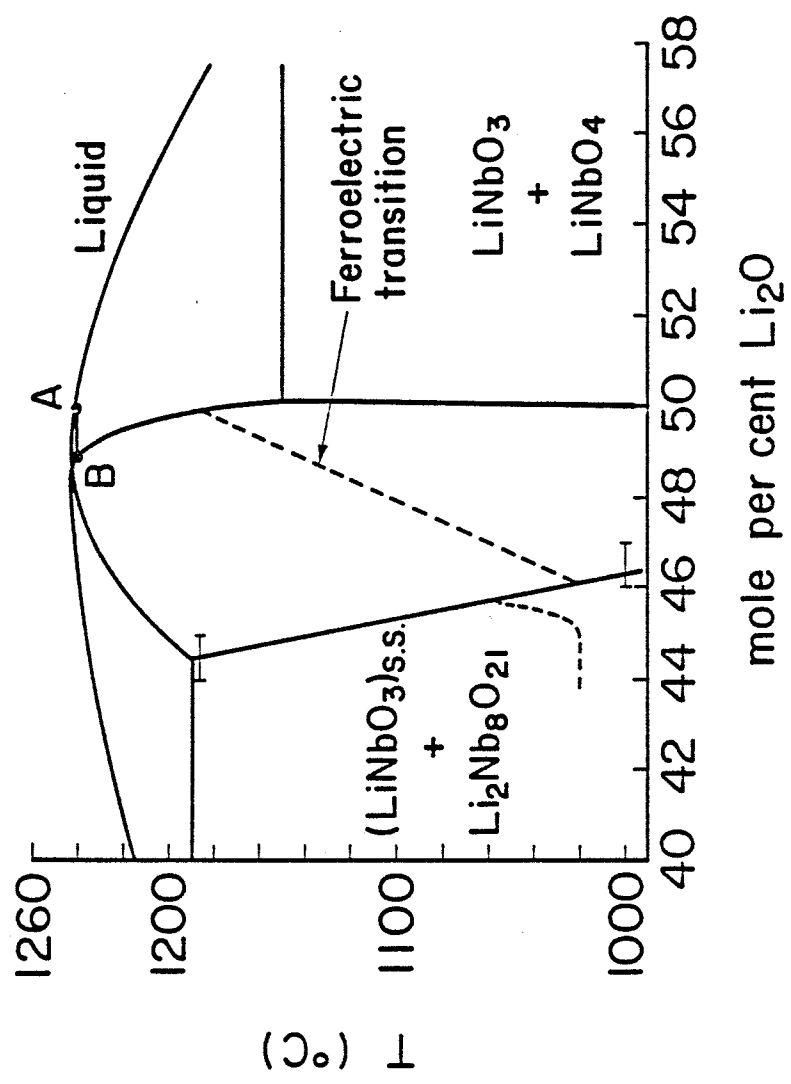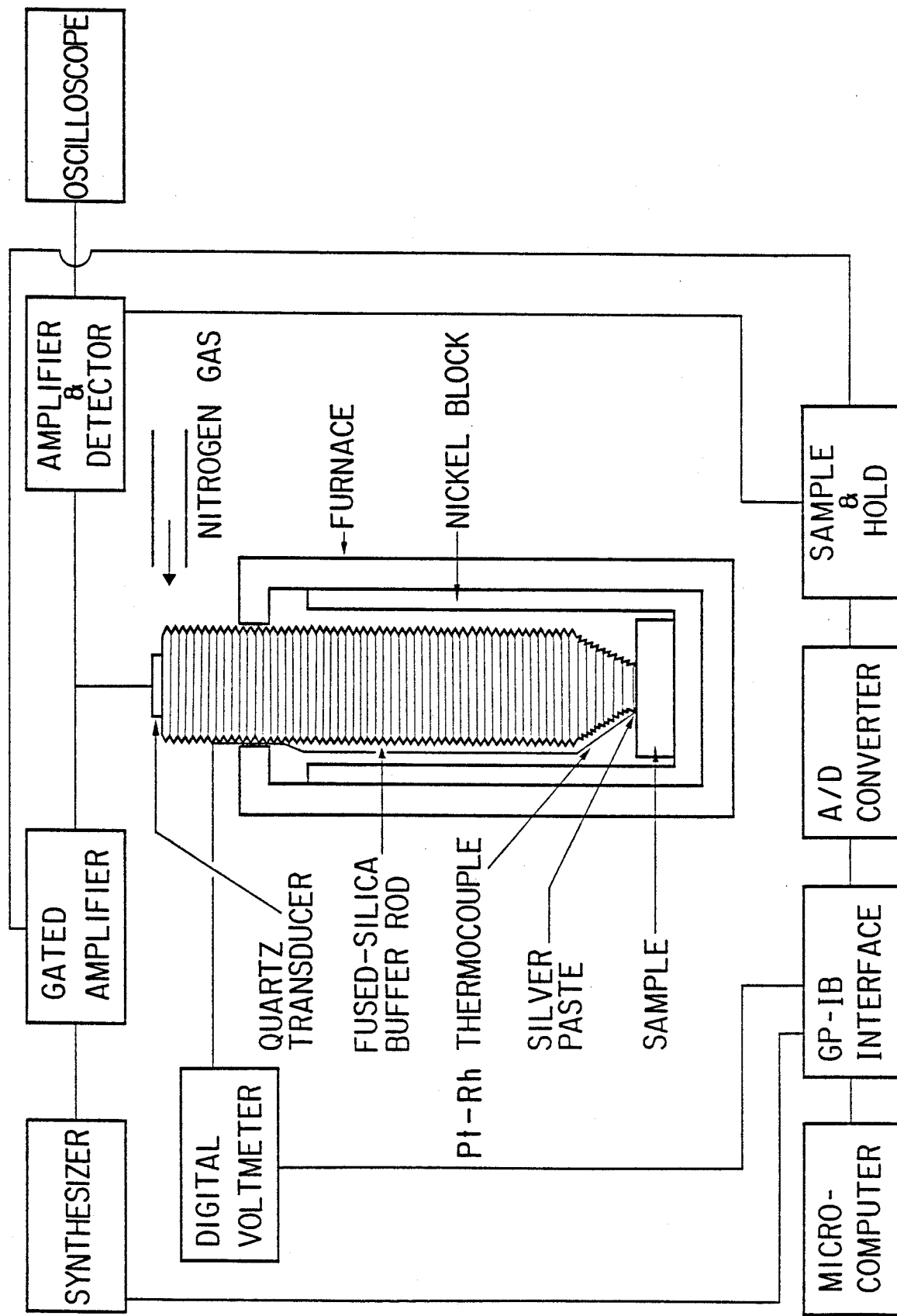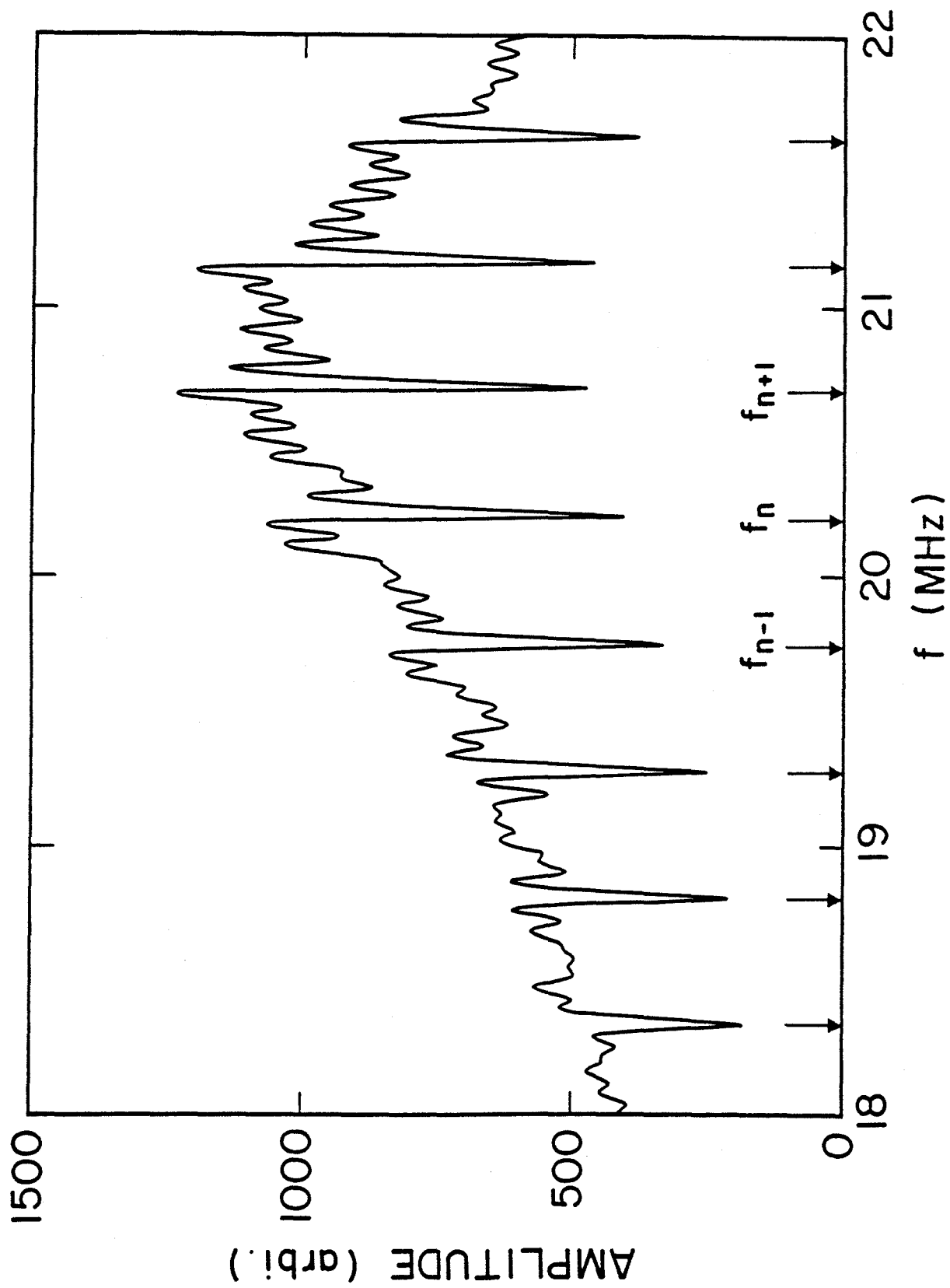
T<Tc   T>Tc   T<Tc   T>Tc   T>Tc
(a)   (b)   (c)   (d)   (e)

Fig. 1

Fig. 2

Fig. 3

Fig. 4
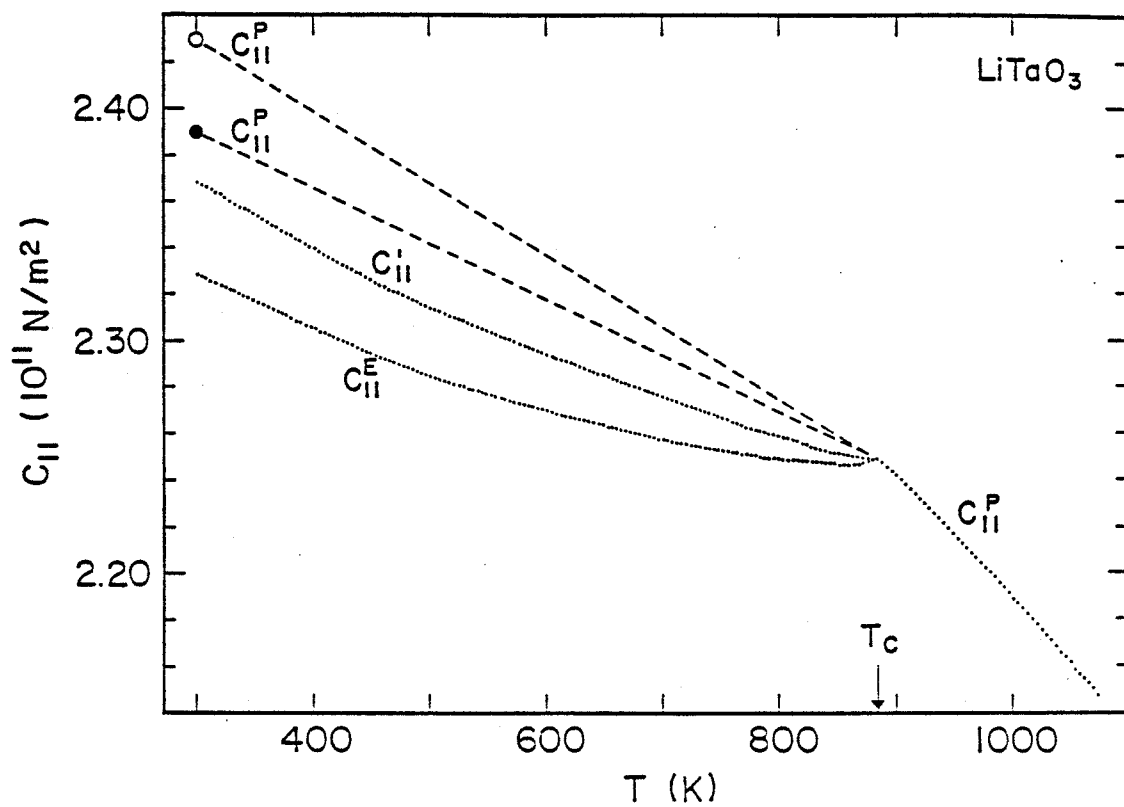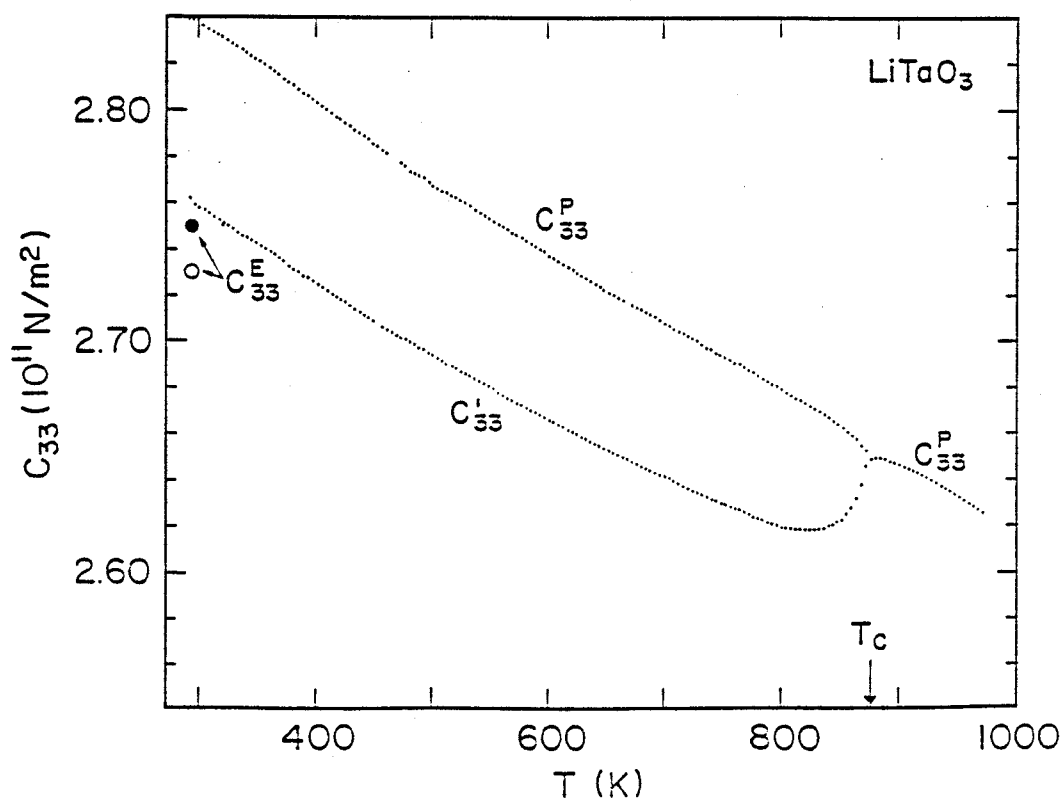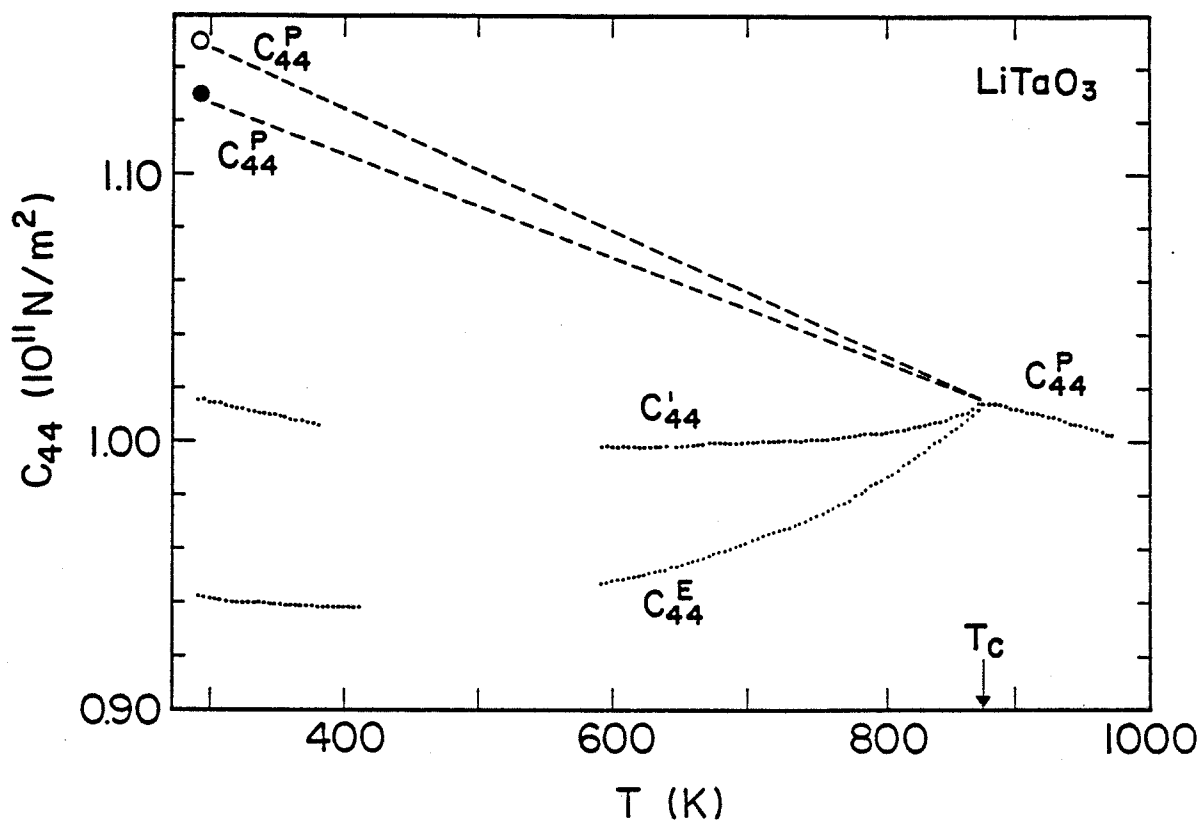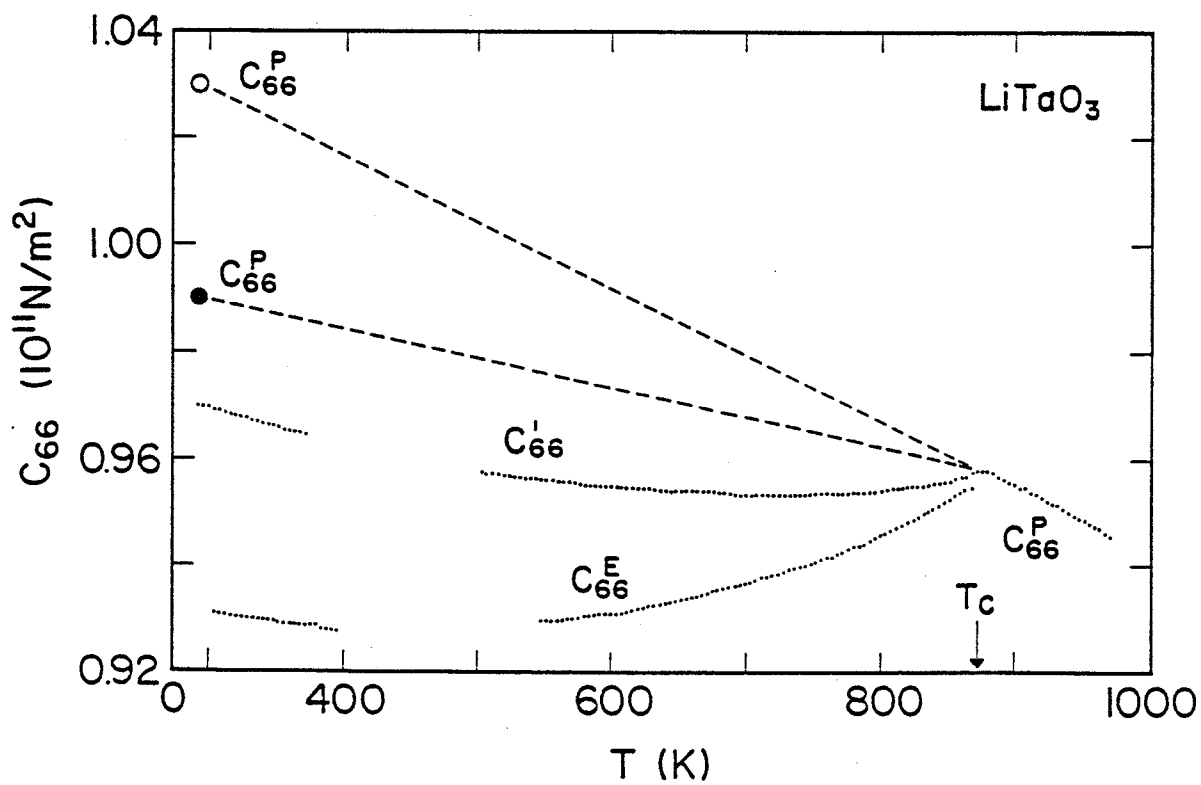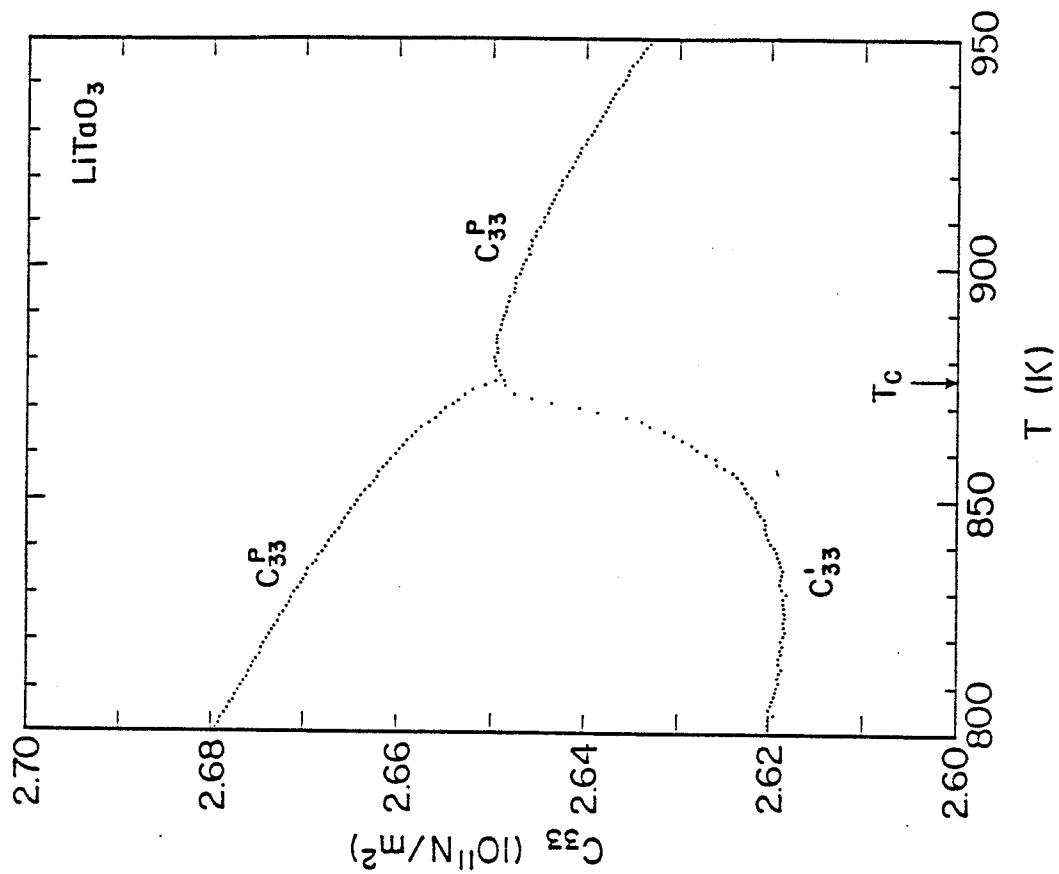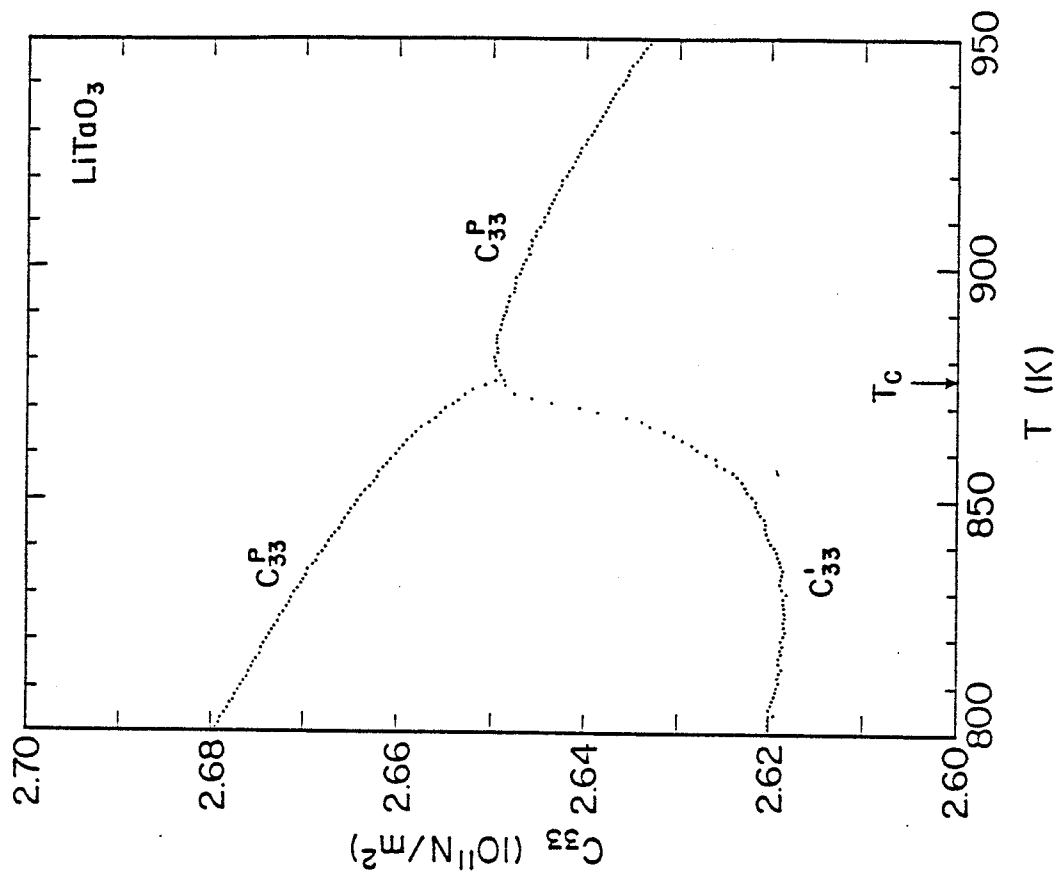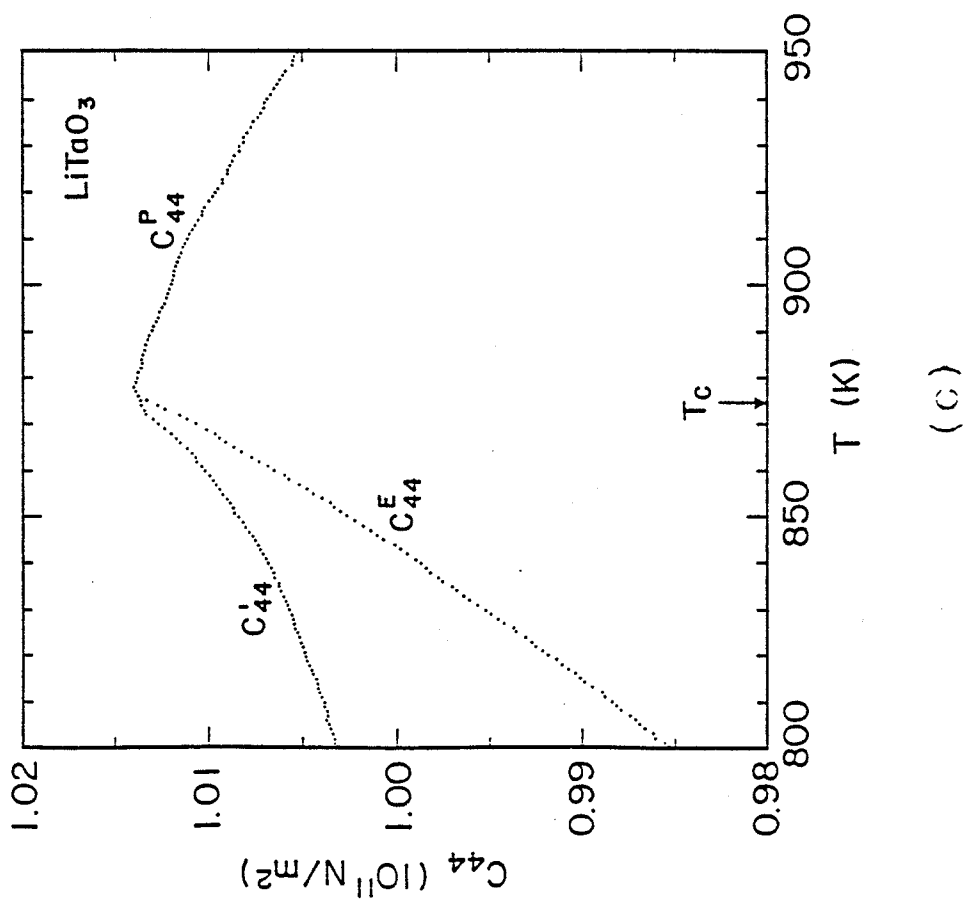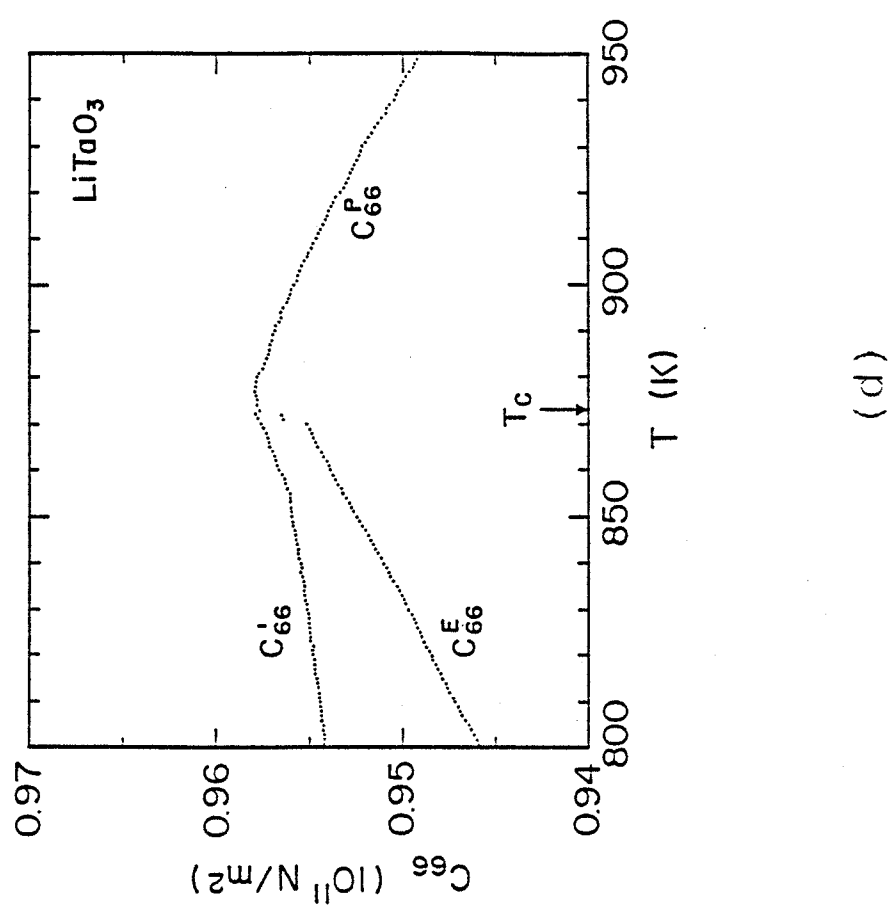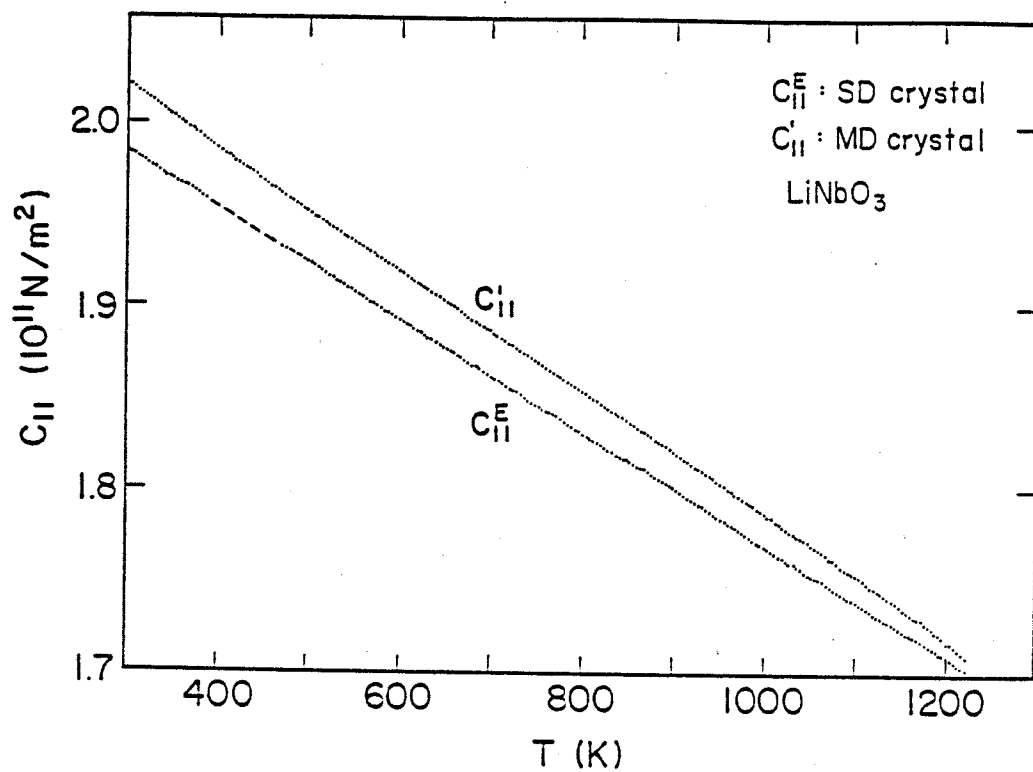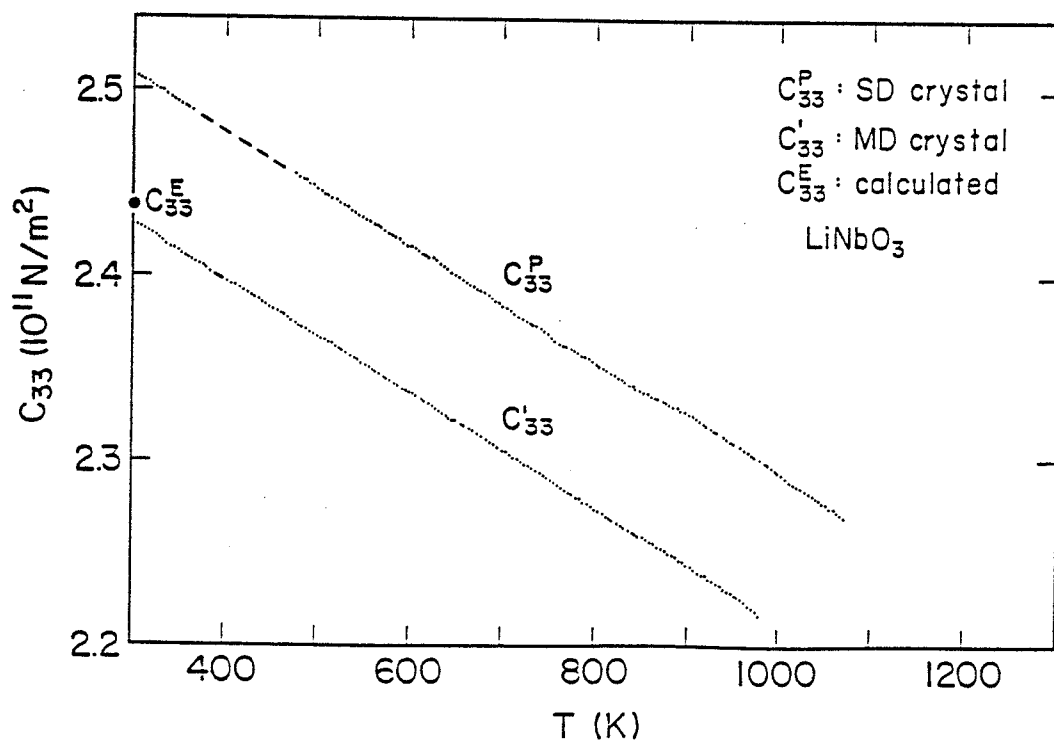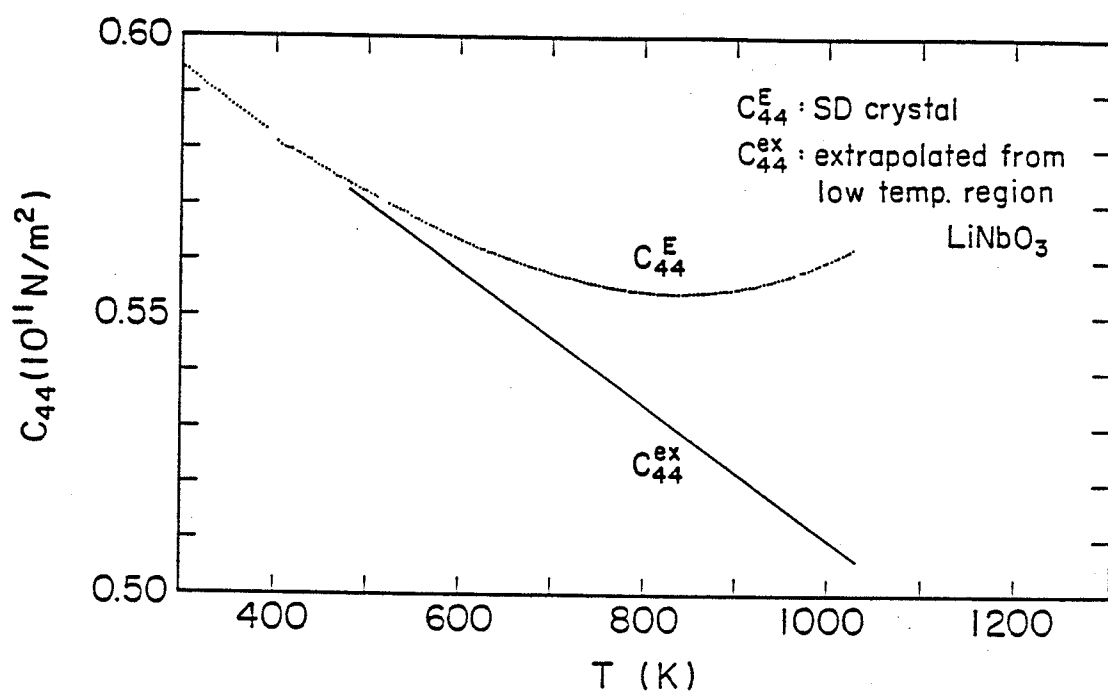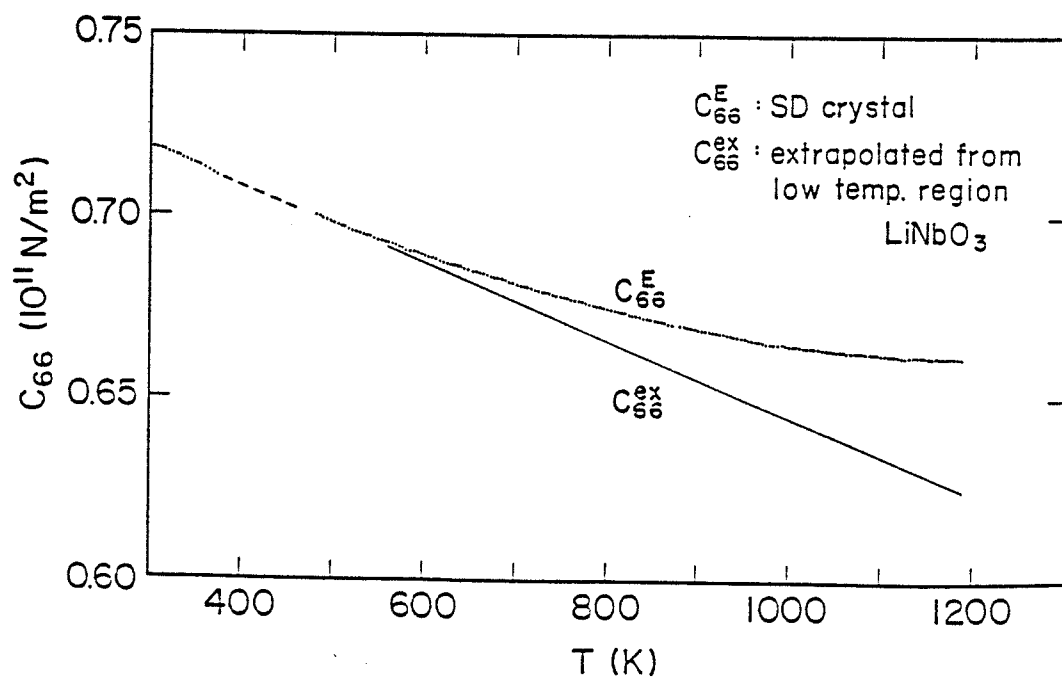
Fig. 5

(c)

(d)

Fig. 5

Fig. 6

(a)

(b)

Fig. 6

(a)

(b)

F i g. 7

(c)

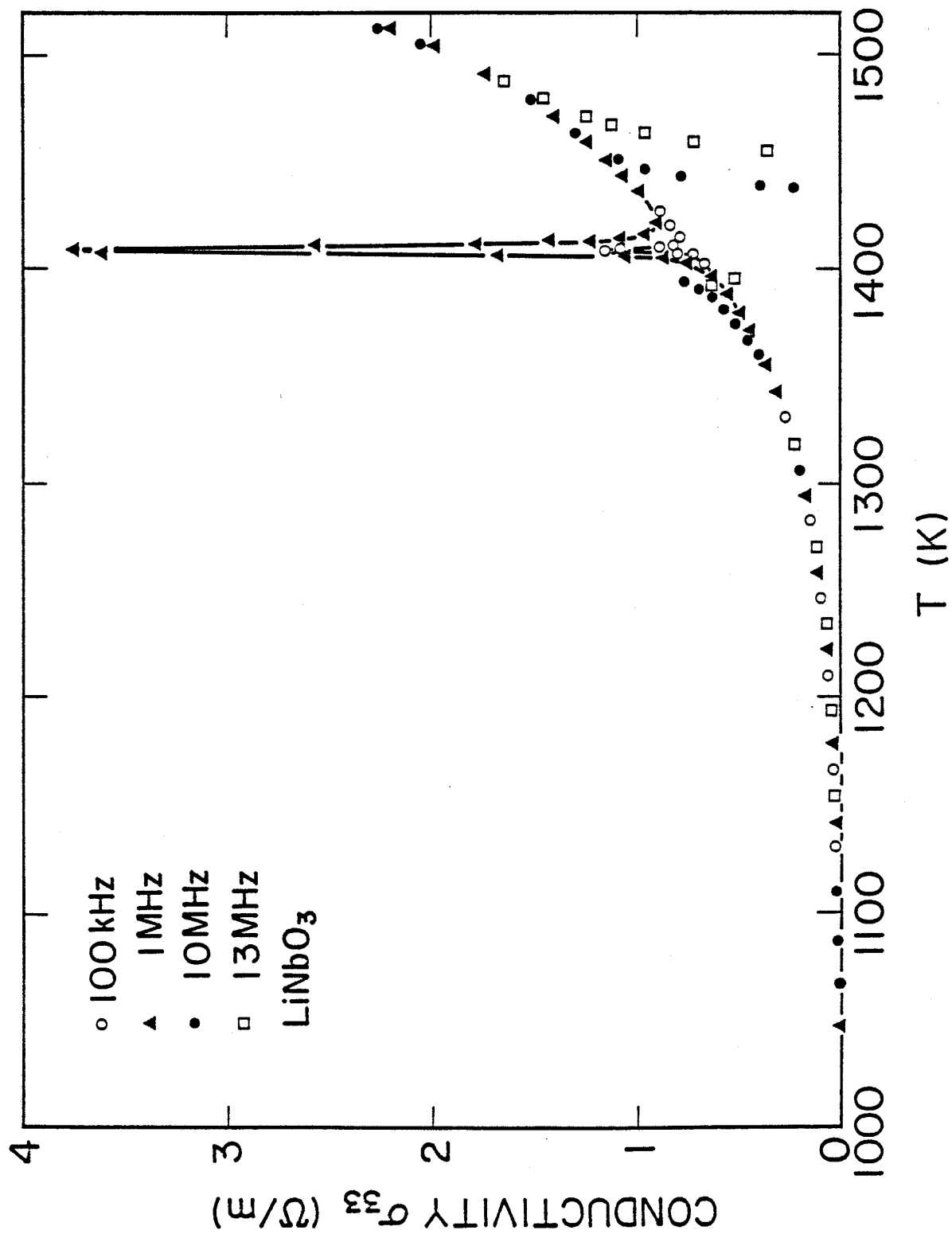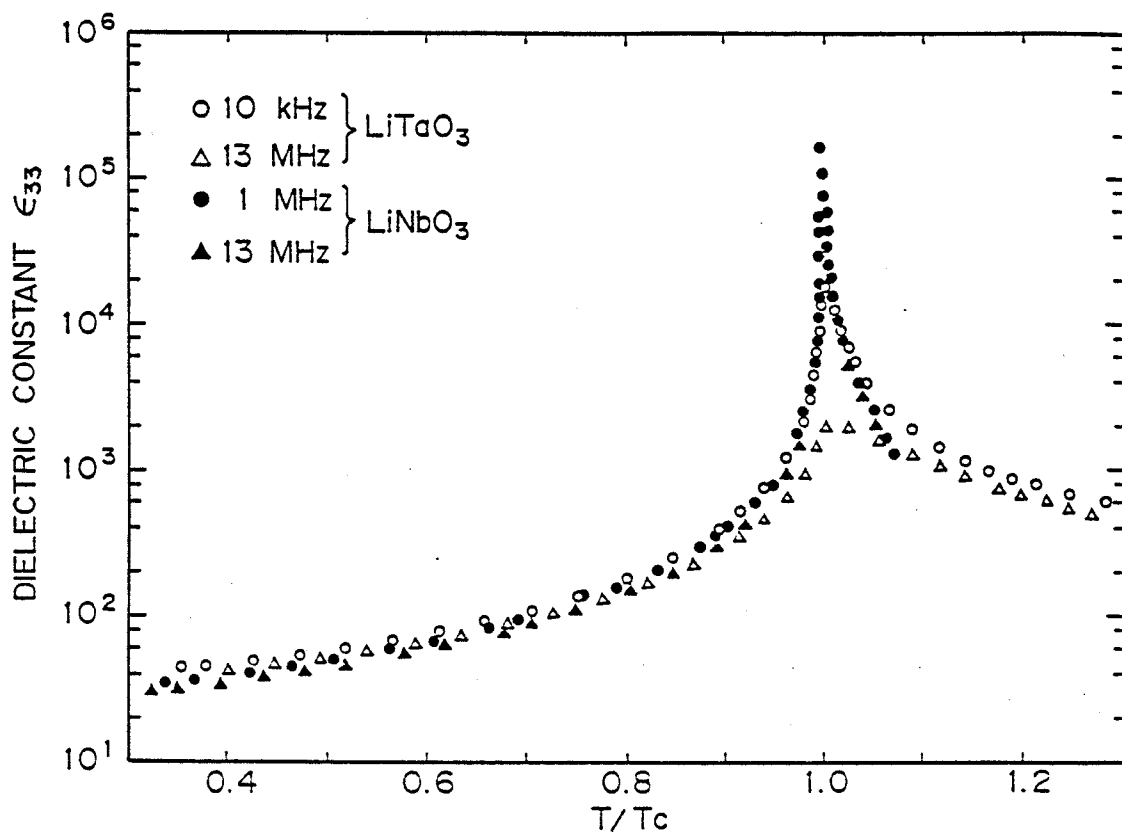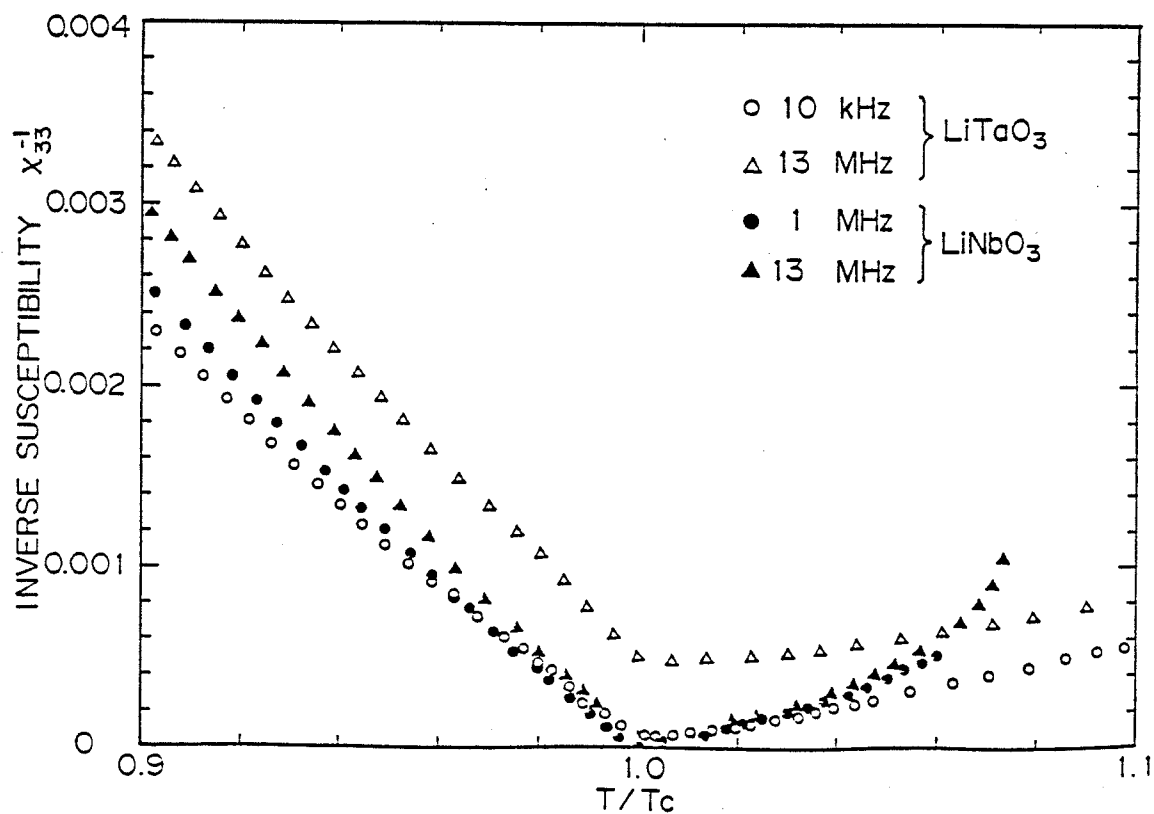

(d)

Fig. 7
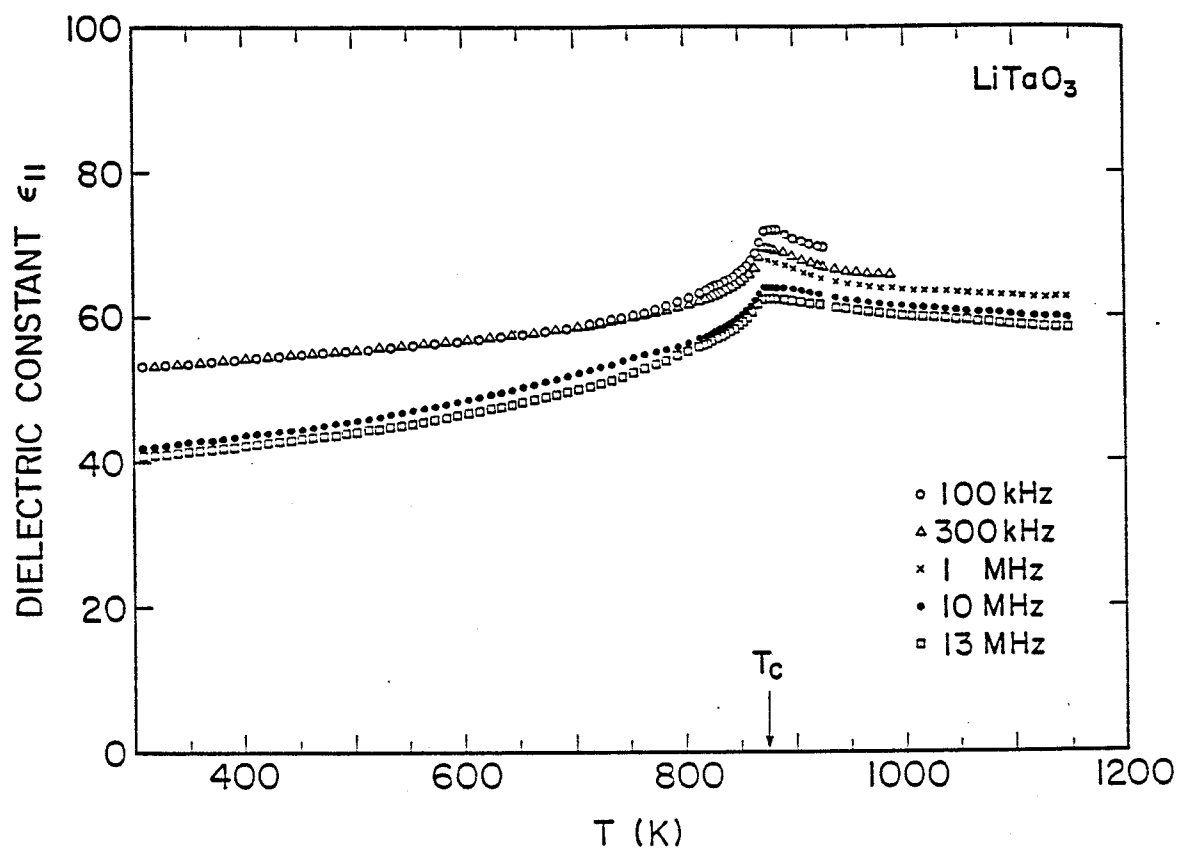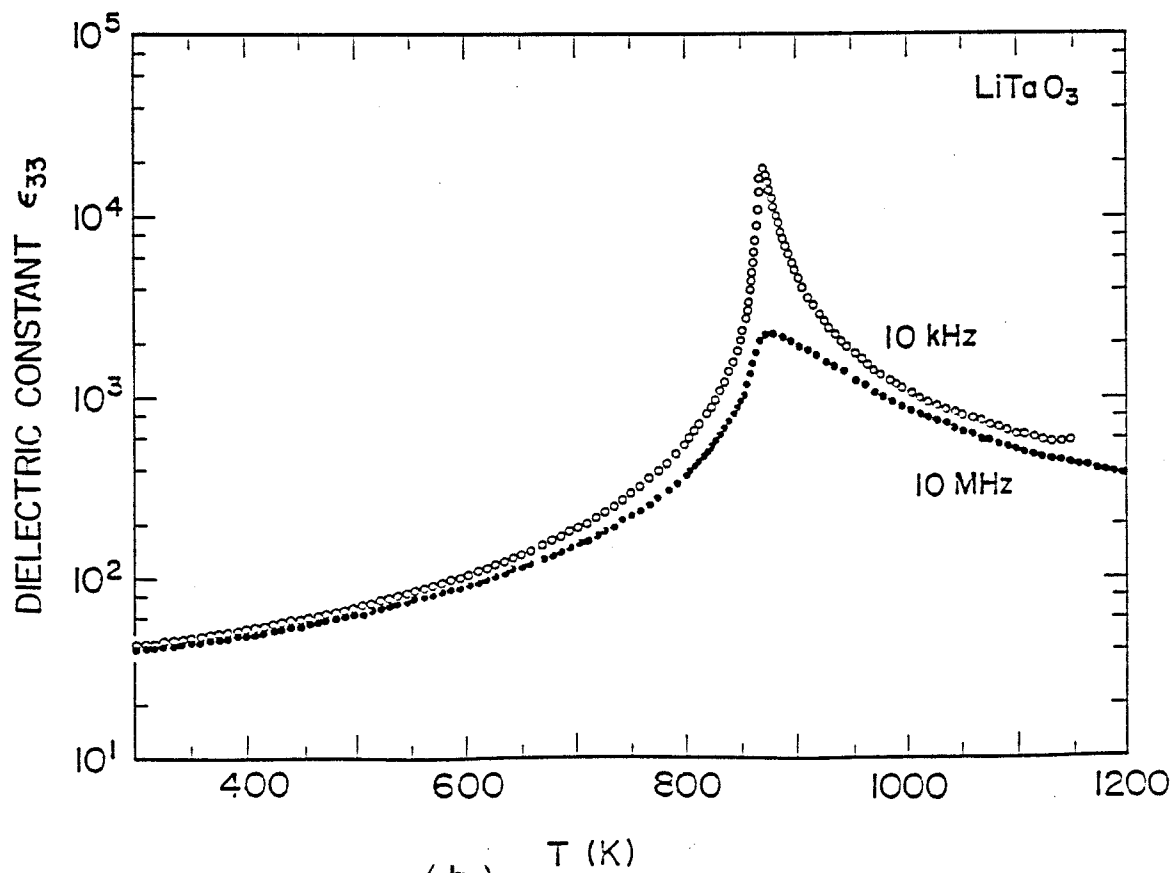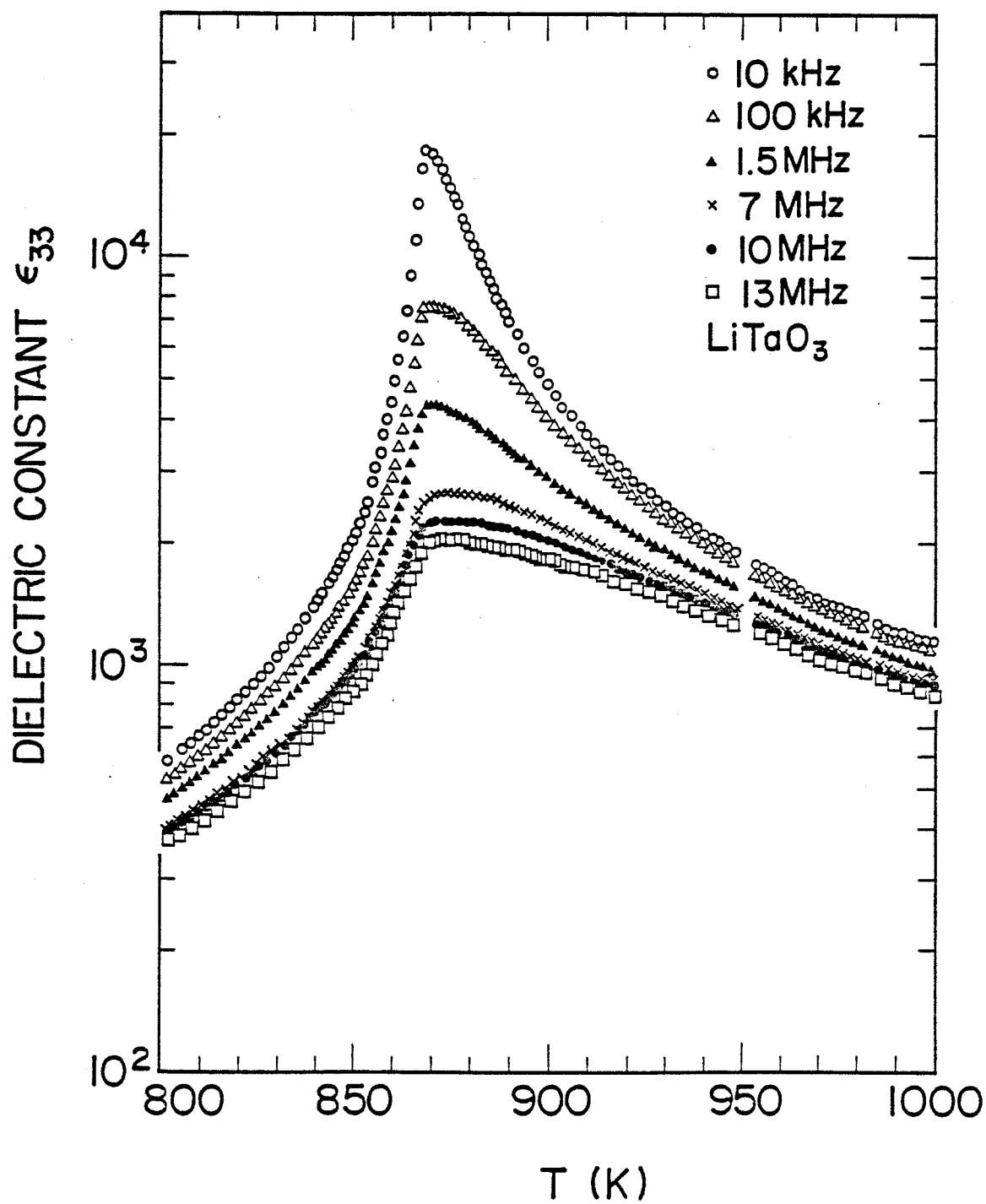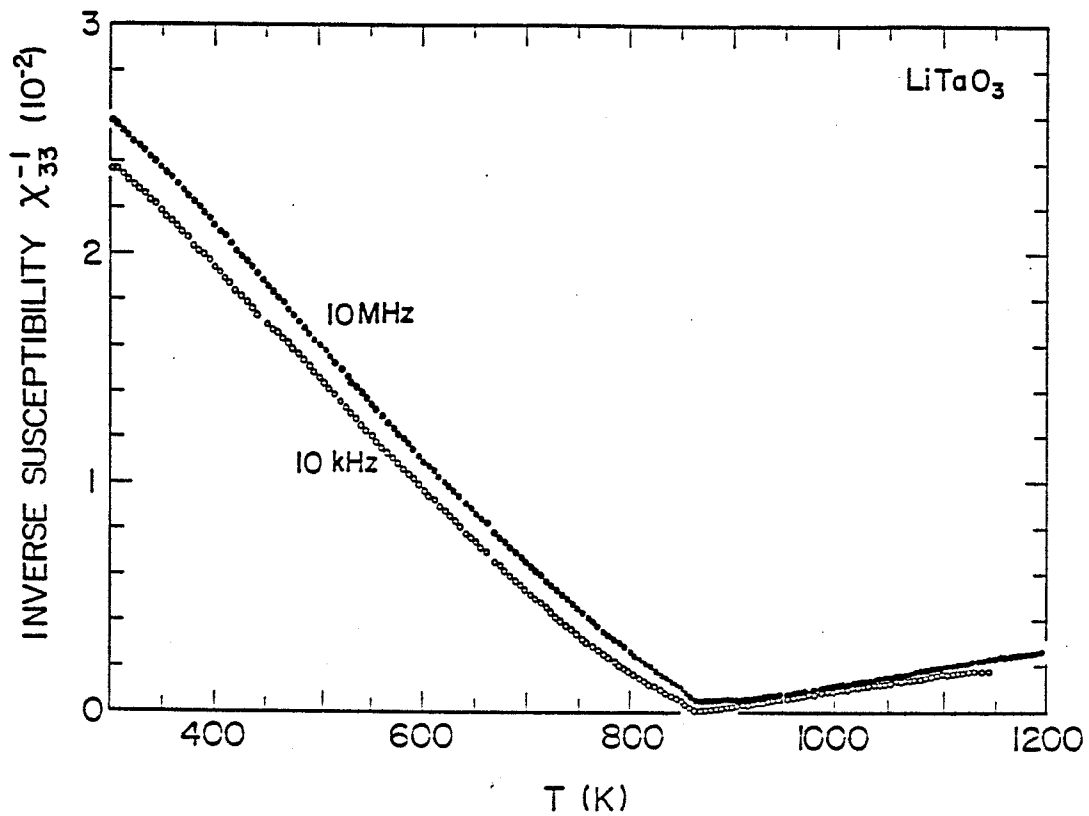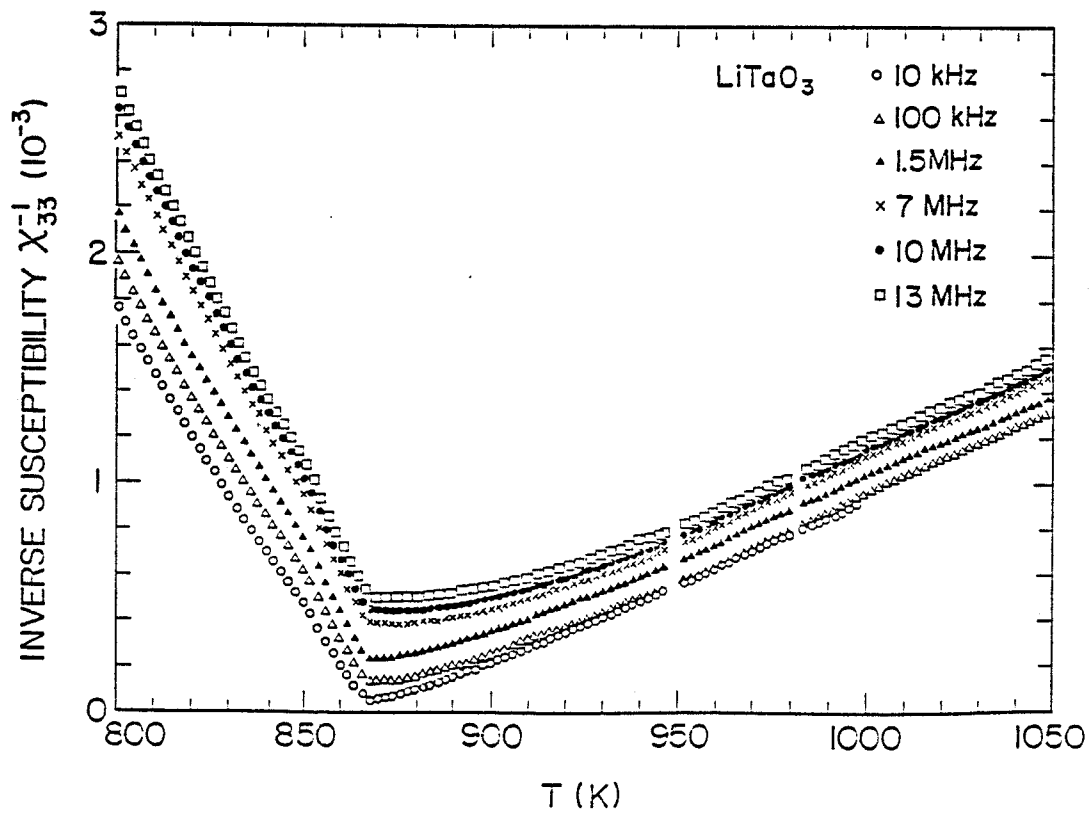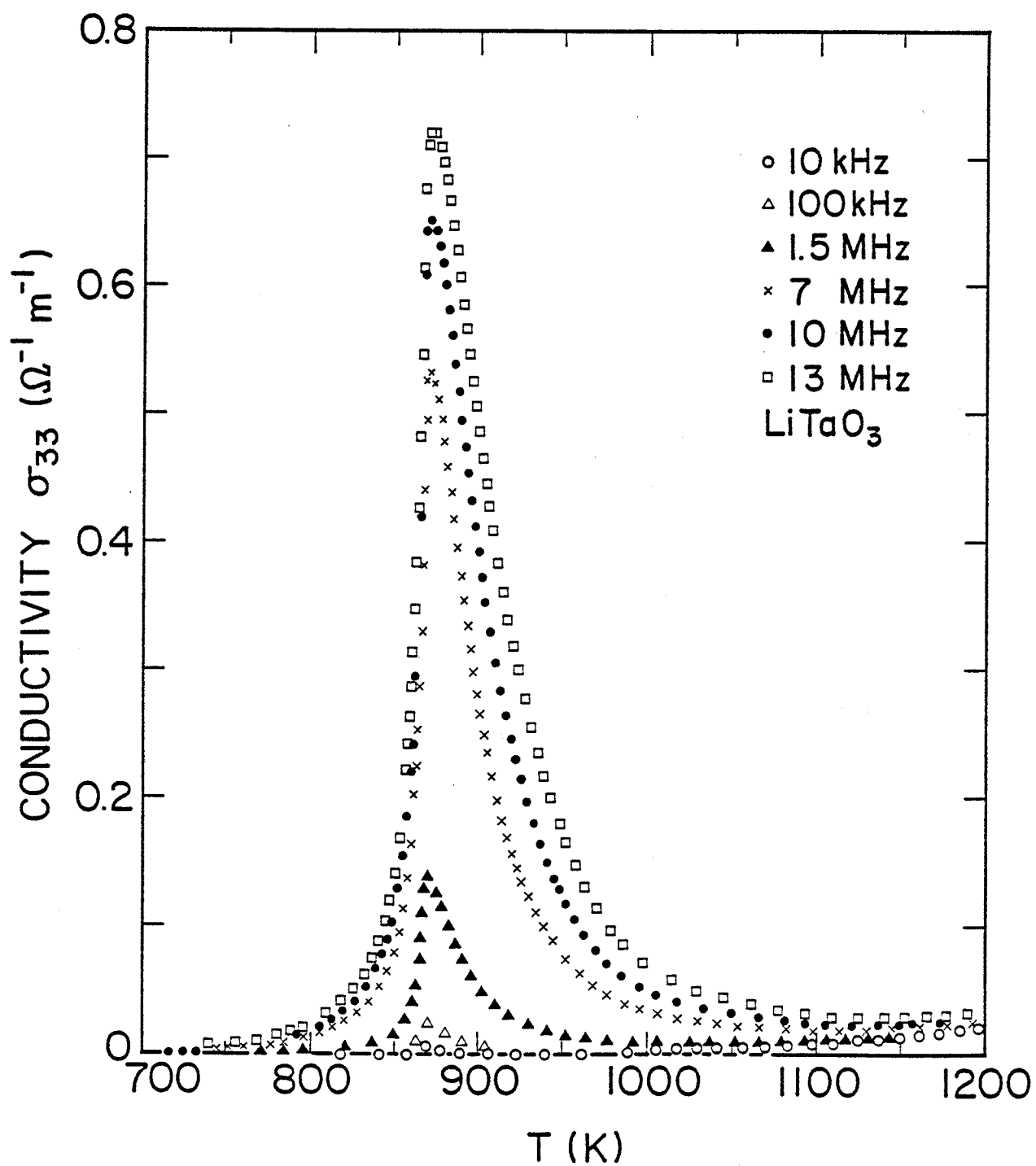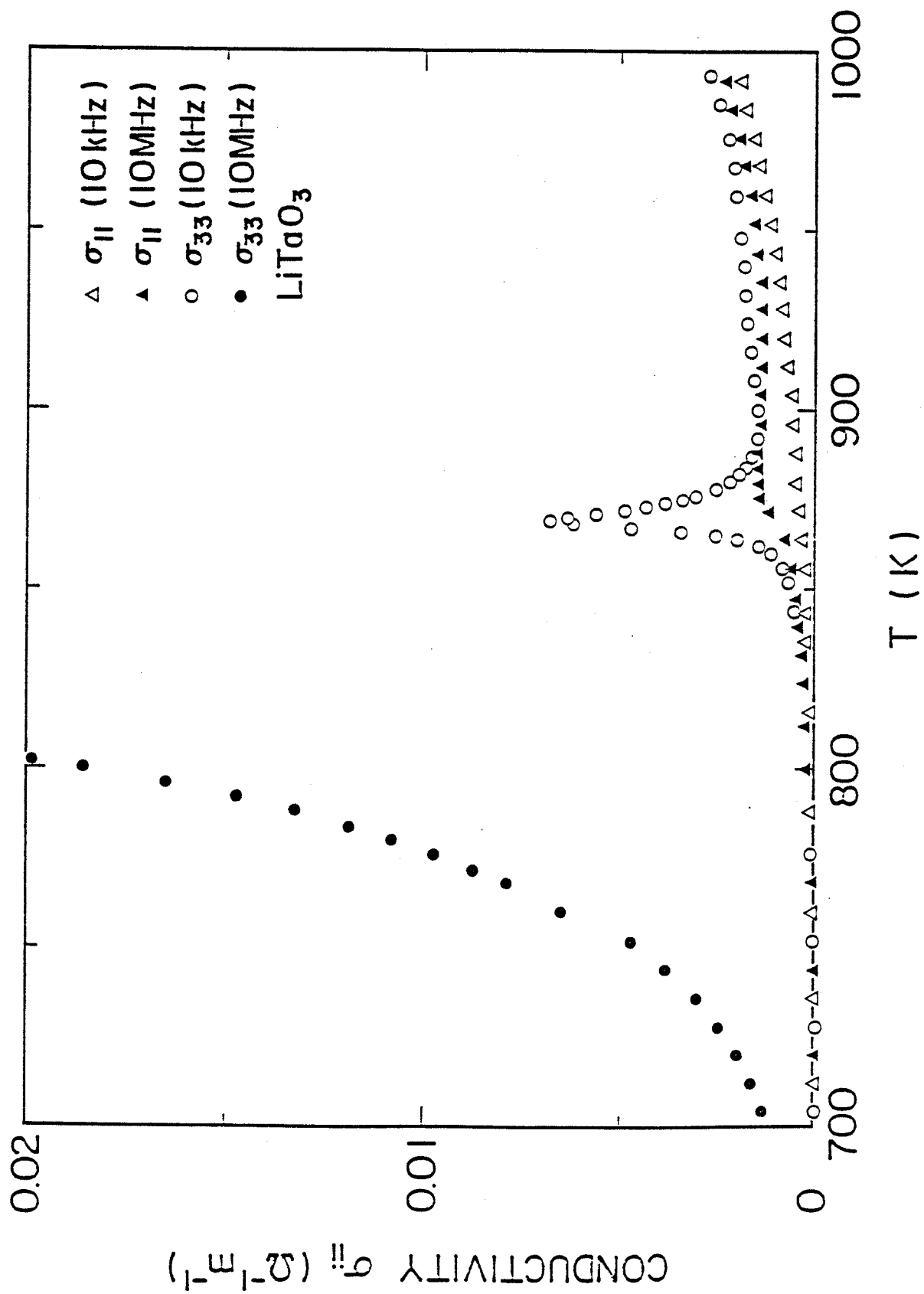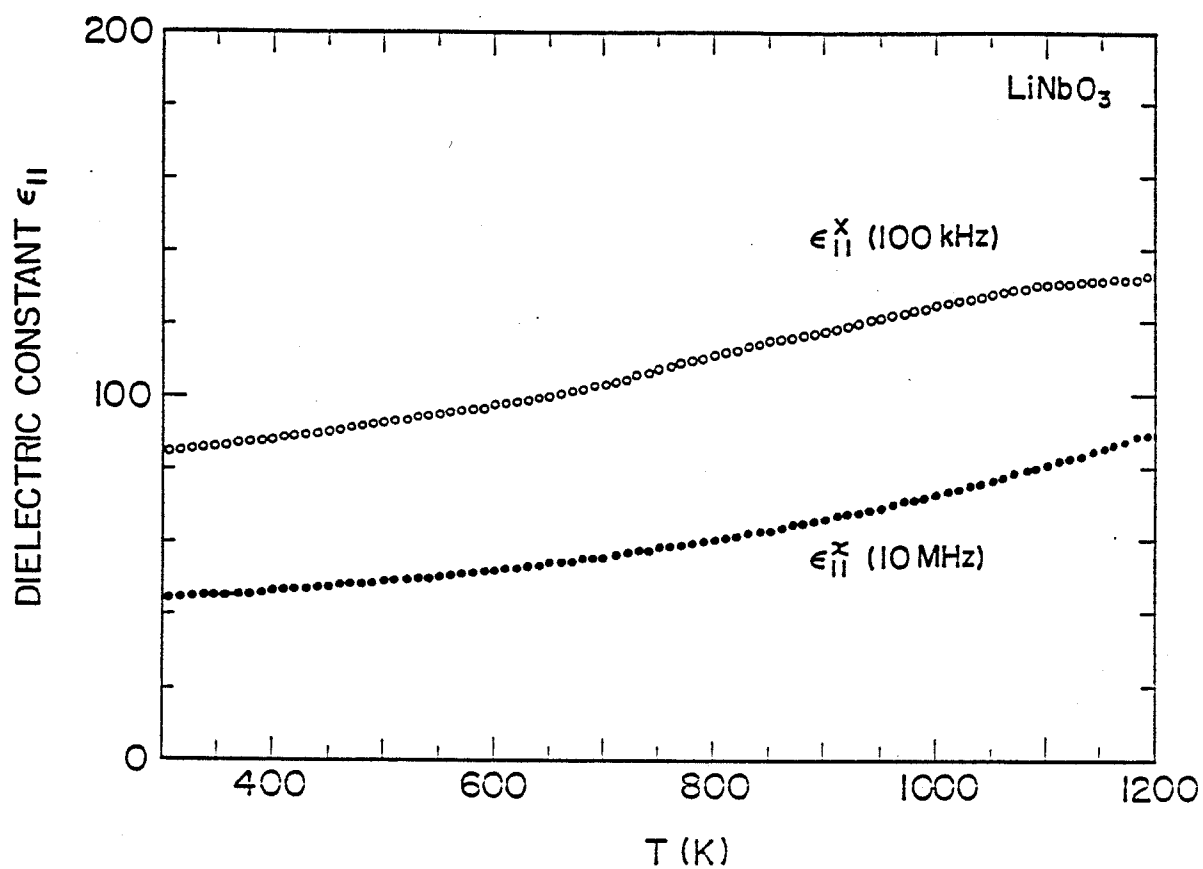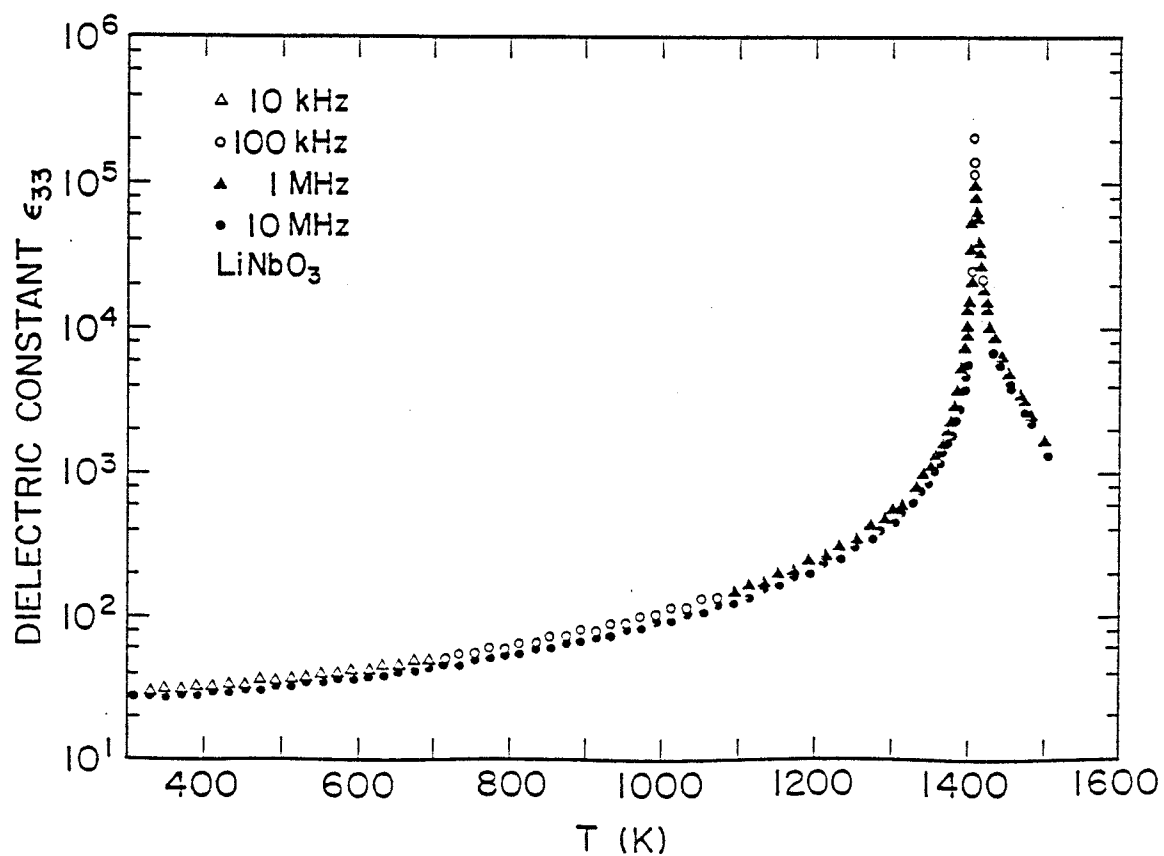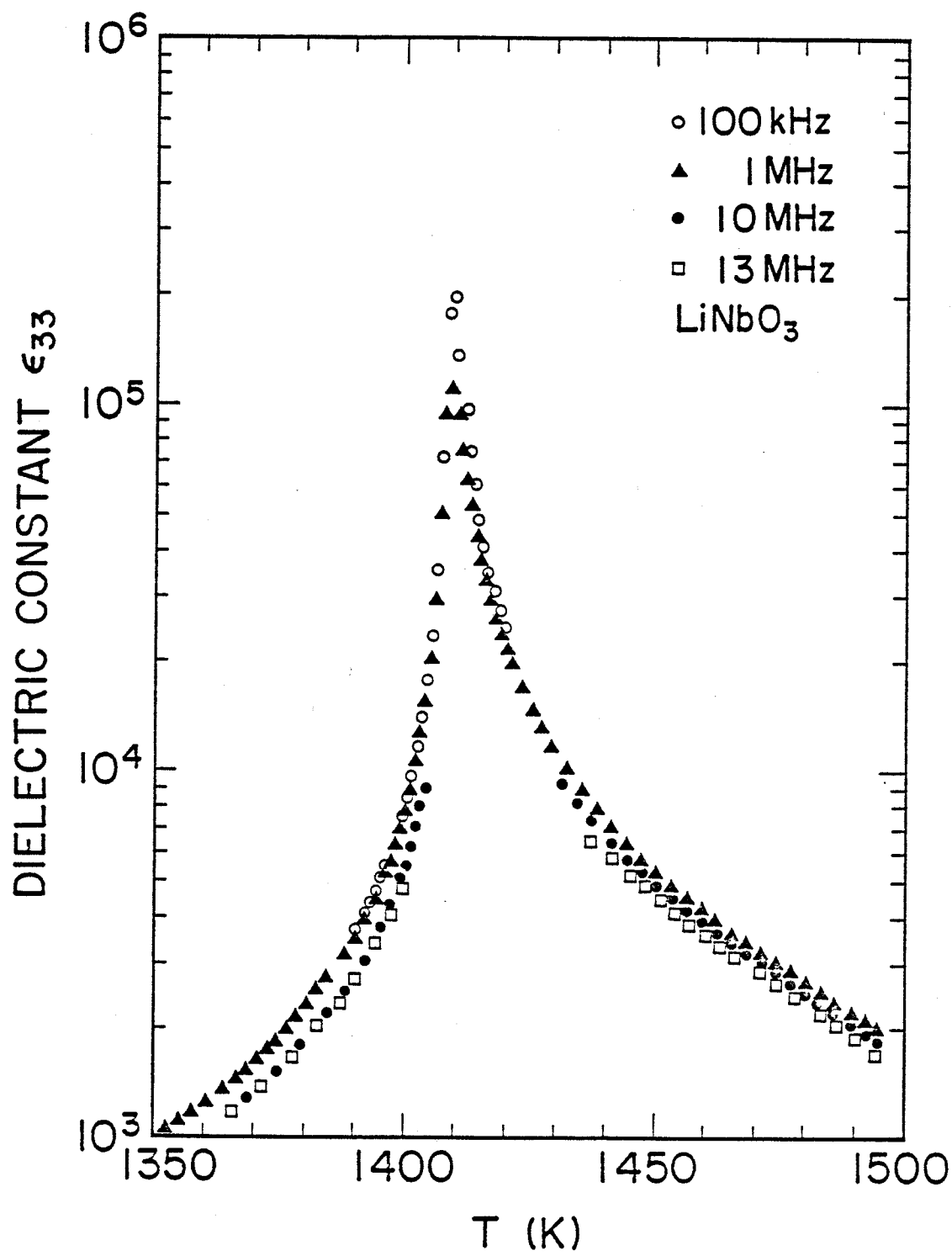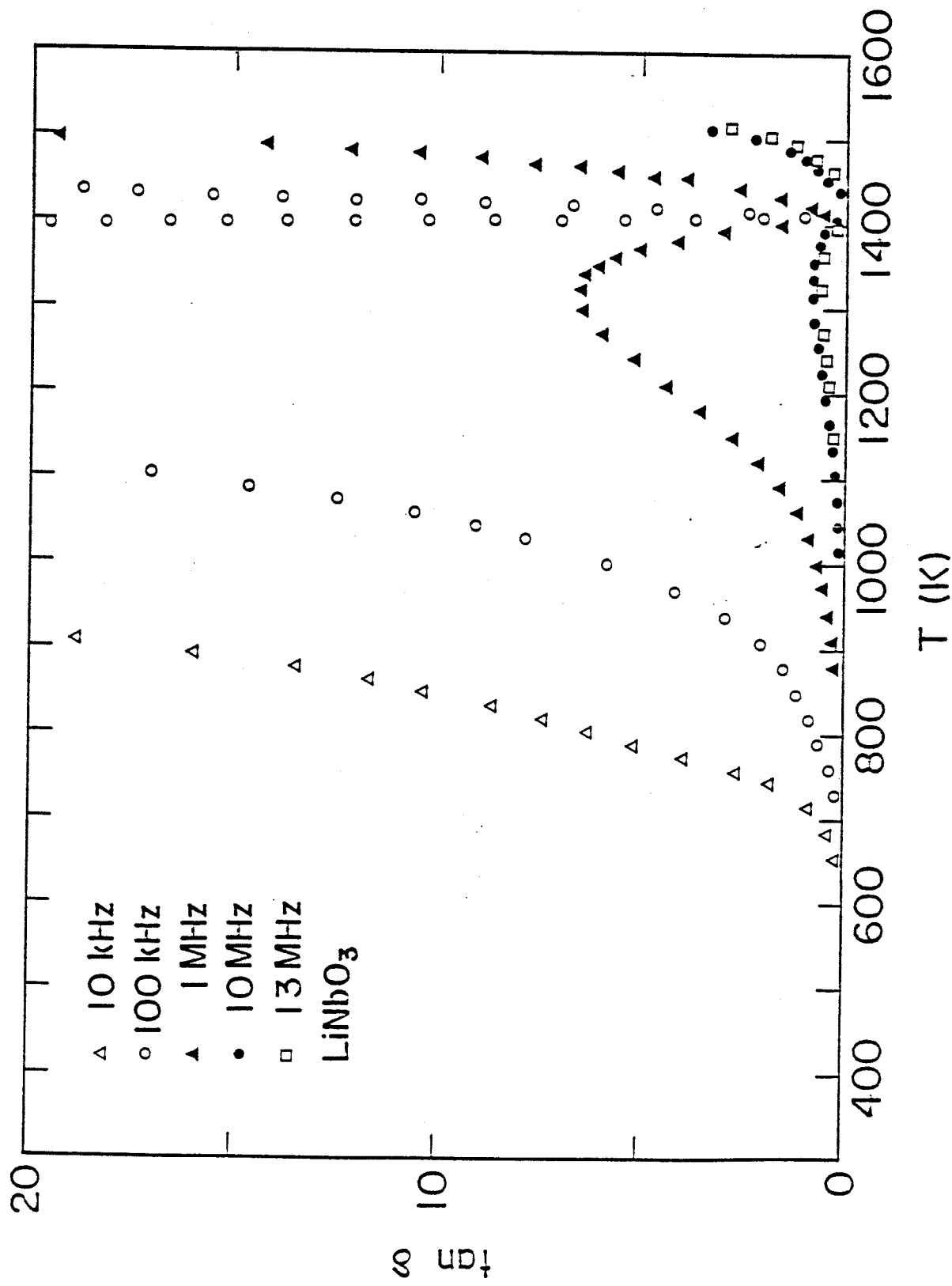
Fig. 8

Fig. 8

(c)

(a)

(b)

Fig. 9

(a)

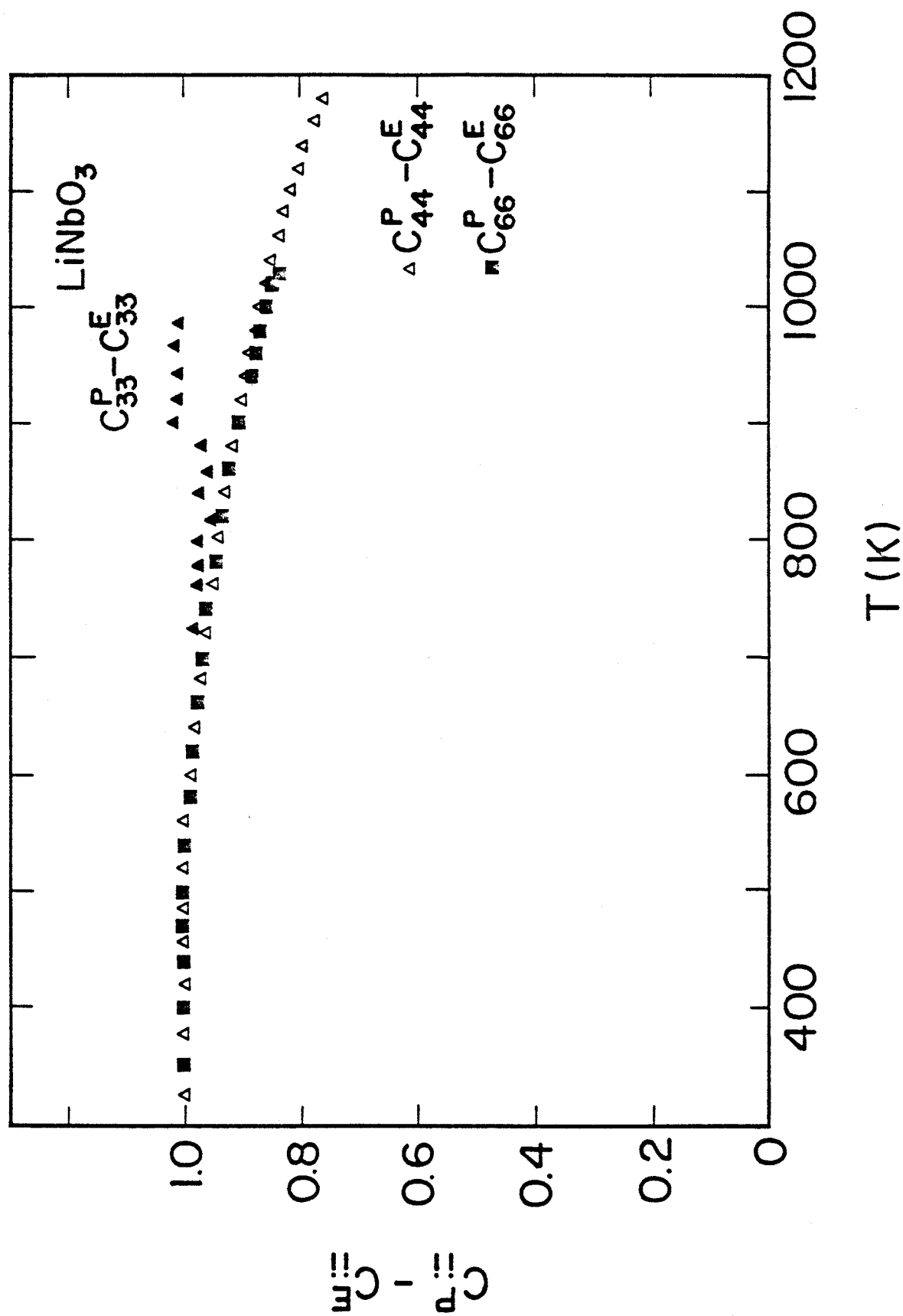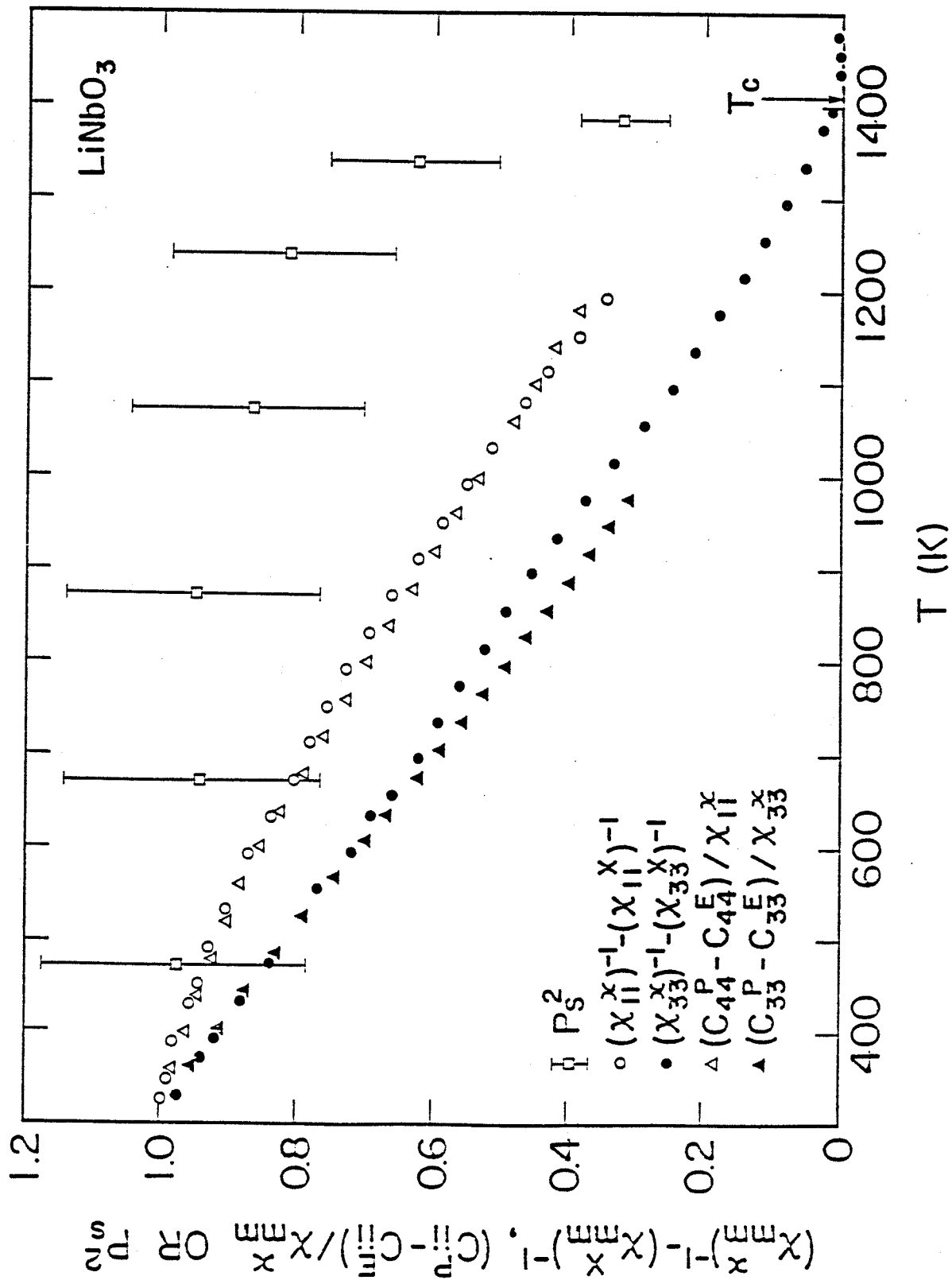Fig. 10

Fig. 10

(b)

Fig. 11

(c)

Fig. 11

Fig. 11

(a)

(b)

Fig. 12

Fig. 13

CONDUCTIVITY σ_{33} (Ω/m)

T (K)

○ 100 kHz
▲ 1 MHz
● 10 MHz
□ 13 MHz

LiNbO$_3$

(a)

(b)

Fig. 14

Fig. 15

LiTaO₃

— extrapolated from high temp. region

$\circ \; C_{11}^E + C_{12}^E$
$\bullet \; C_{11}^i + C_{12}^i$

T_c

T (K)

$C_{11} + C_{12}$ (10¹¹ N/m²)

Fig. 16

Fig. 17

(a)

Fig. 17

LiTaO$_3$

P_S^2

$\square$ $(C_{11}^P - C_{11}^E)/X_{11}^x$

$\triangle$ $(C_{44}^P - C_{44}^E)/X_{11}^x$

$\blacktriangle$ $(C_{33}^P - C_{33}^E)/X_{33}^x$

$\circ$ $(X_{11}^x)^{-1} - (X_{11}^X)^{-1}$

$\bullet$ $(X_{33}^x)^{-1} - (X_{33}^X)^{-1}$

T (K)

$(X_{mm}^x)^{-1} - (X_{mm}^X)^{-1}$, $(C_{ii}^P - C_{ii}^E)/X_{mm}^x$ OR P_S^2

(a)

Fig. 18

(b) $T - T_C$

Fig. 18

The y-axis is labeled $(C_{ii}^P - C_{ii}^E)/\chi_{ii}^x$ OR P_S^2

Legend:
- P_S^2
- $\triangle$ $(C_{44}^P - C_{44}^E)/\chi_{11}^x$
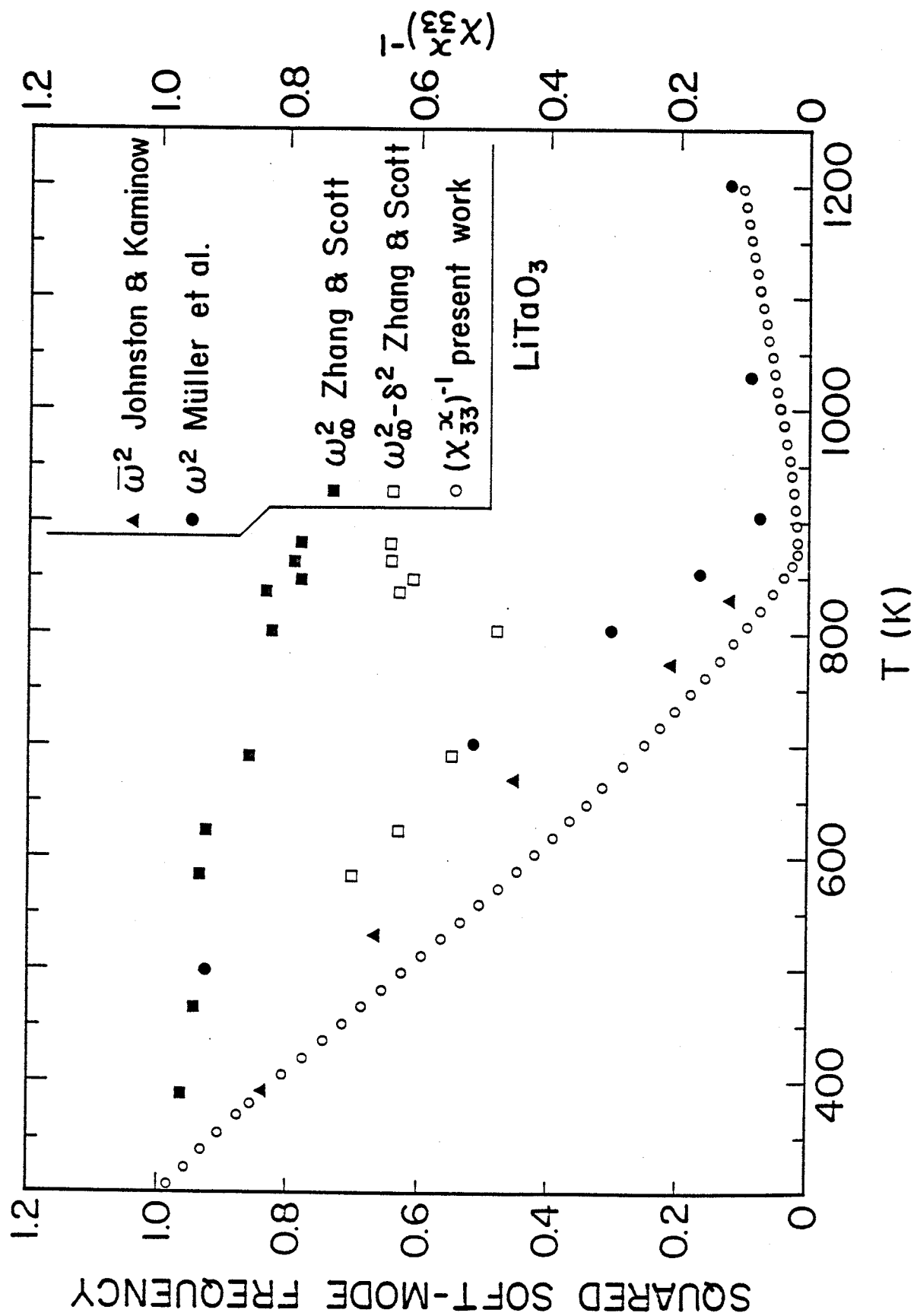- $\blacktriangle$ $(C_{33}^P - C_{33}^E)/\chi_{33}^x$
- $LiTaO_3$
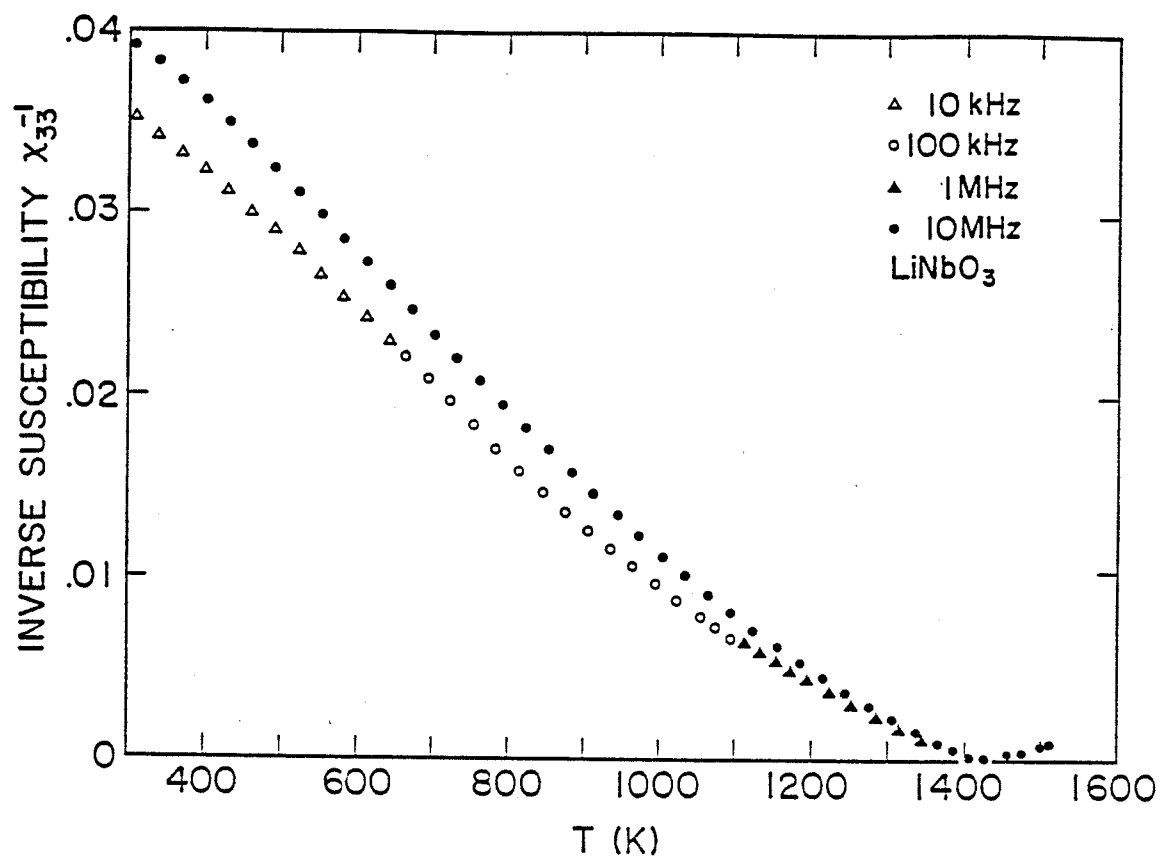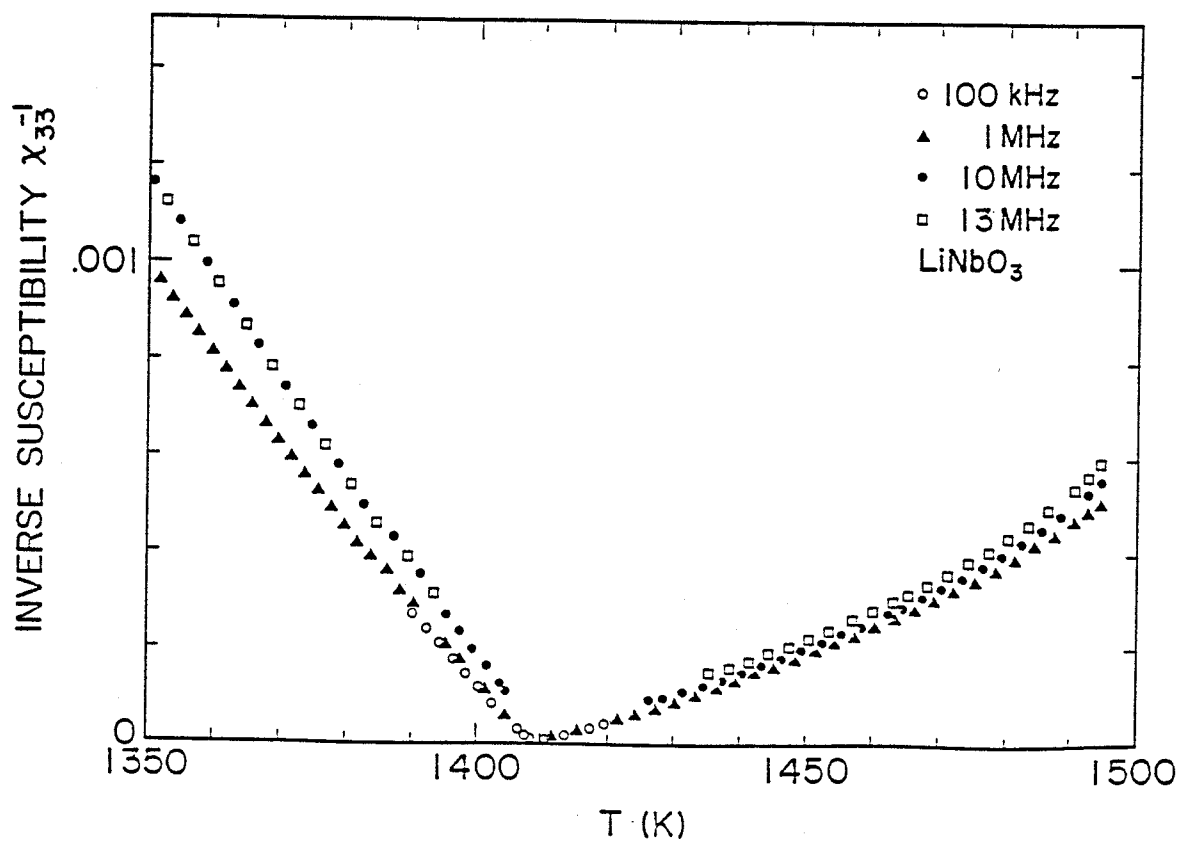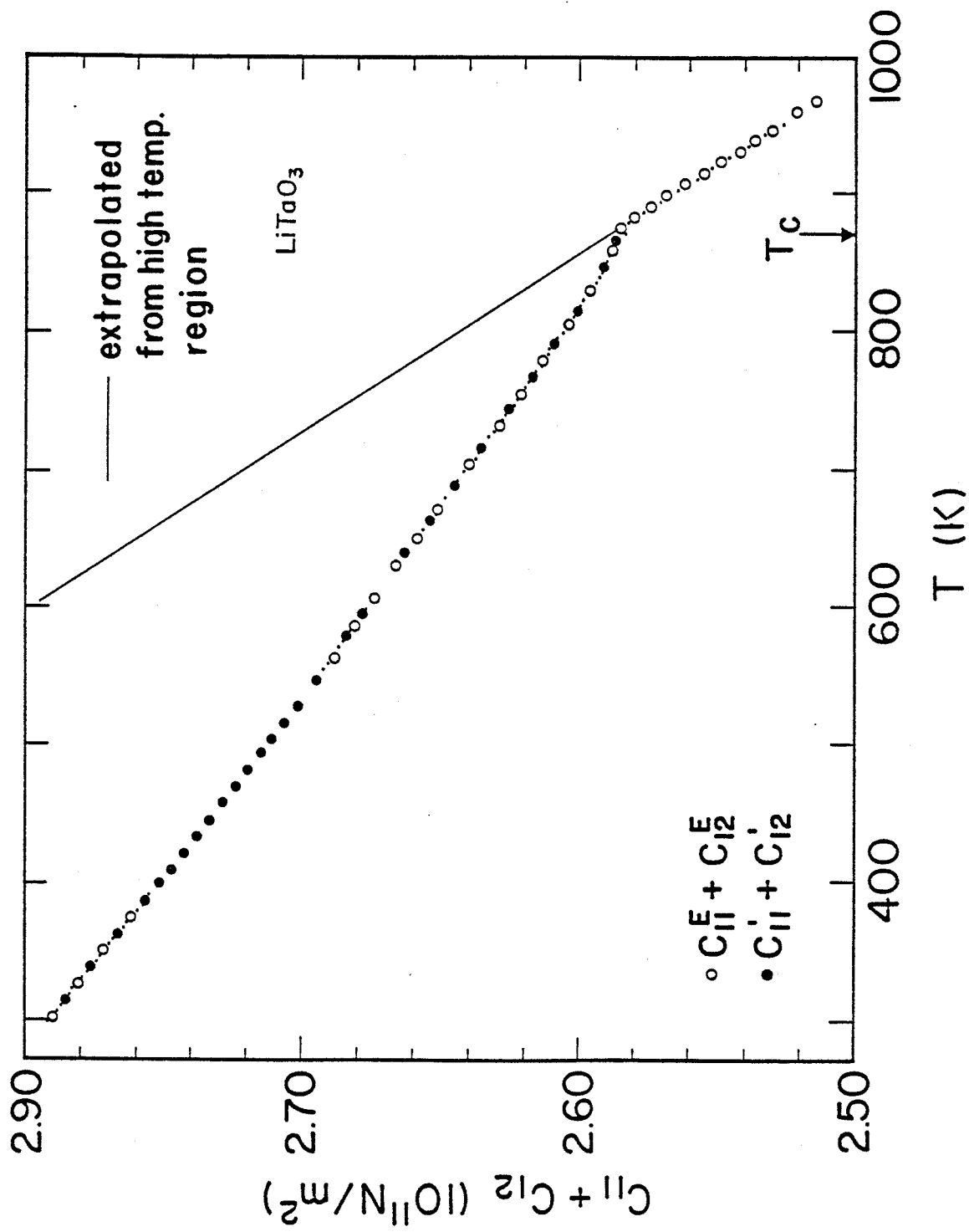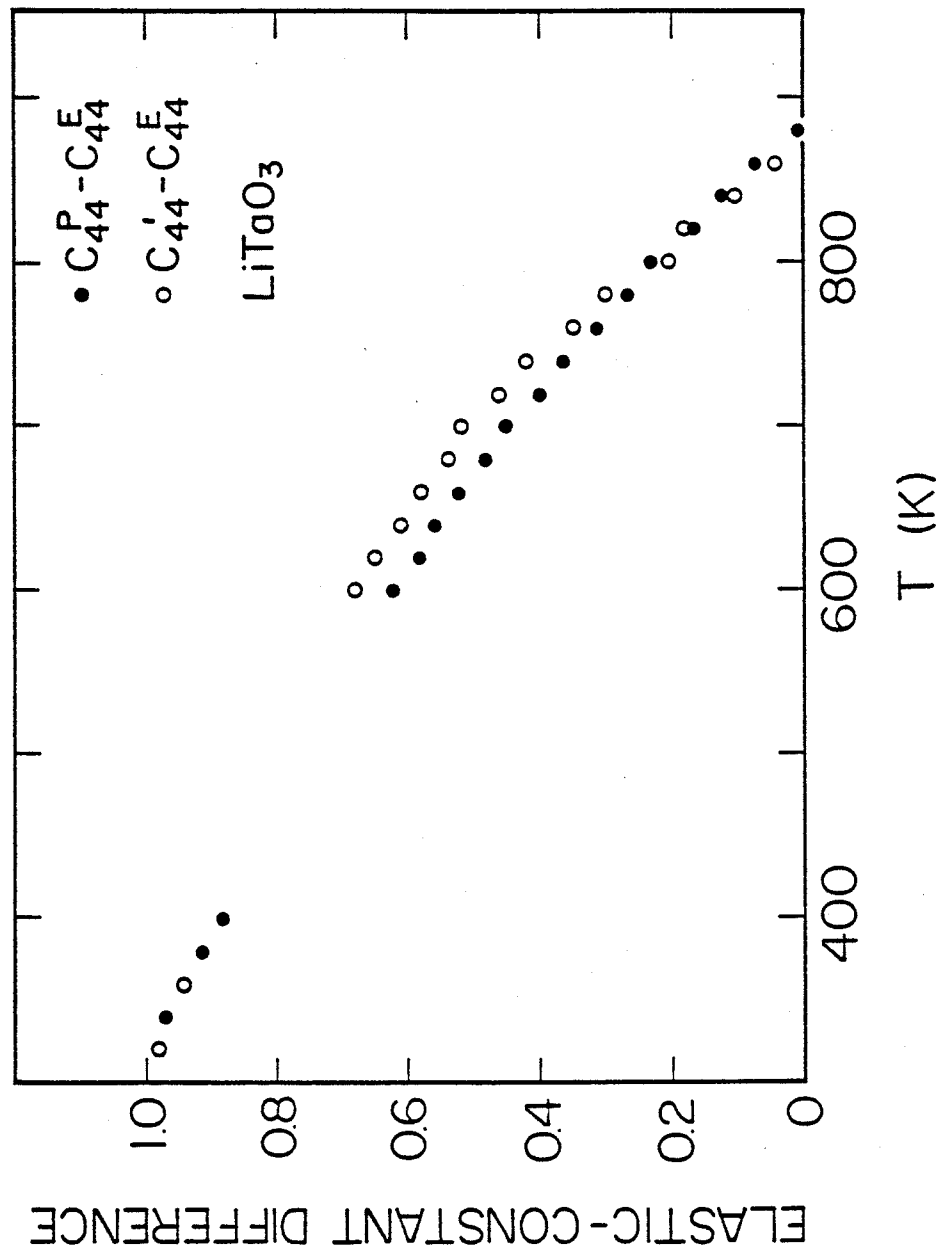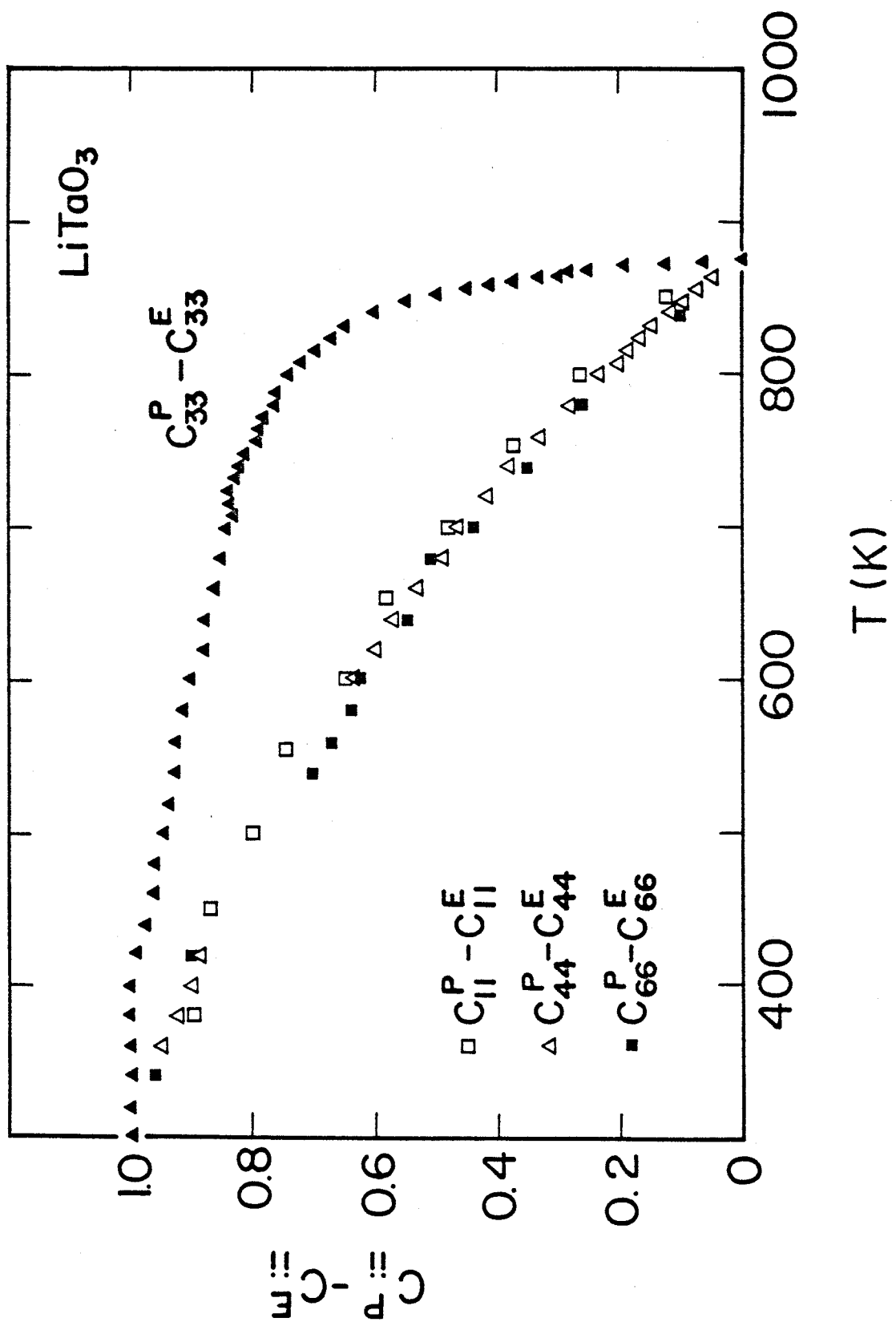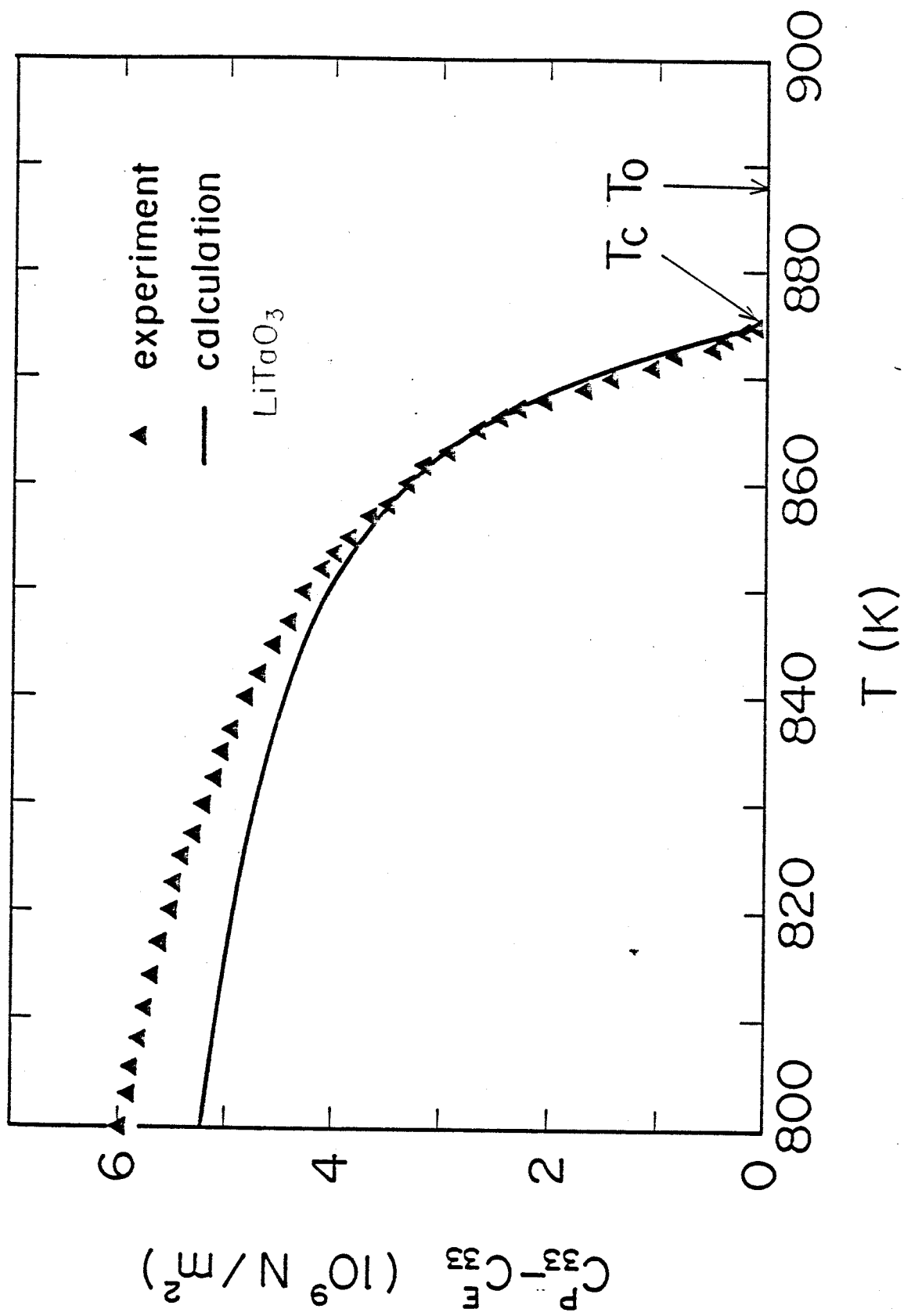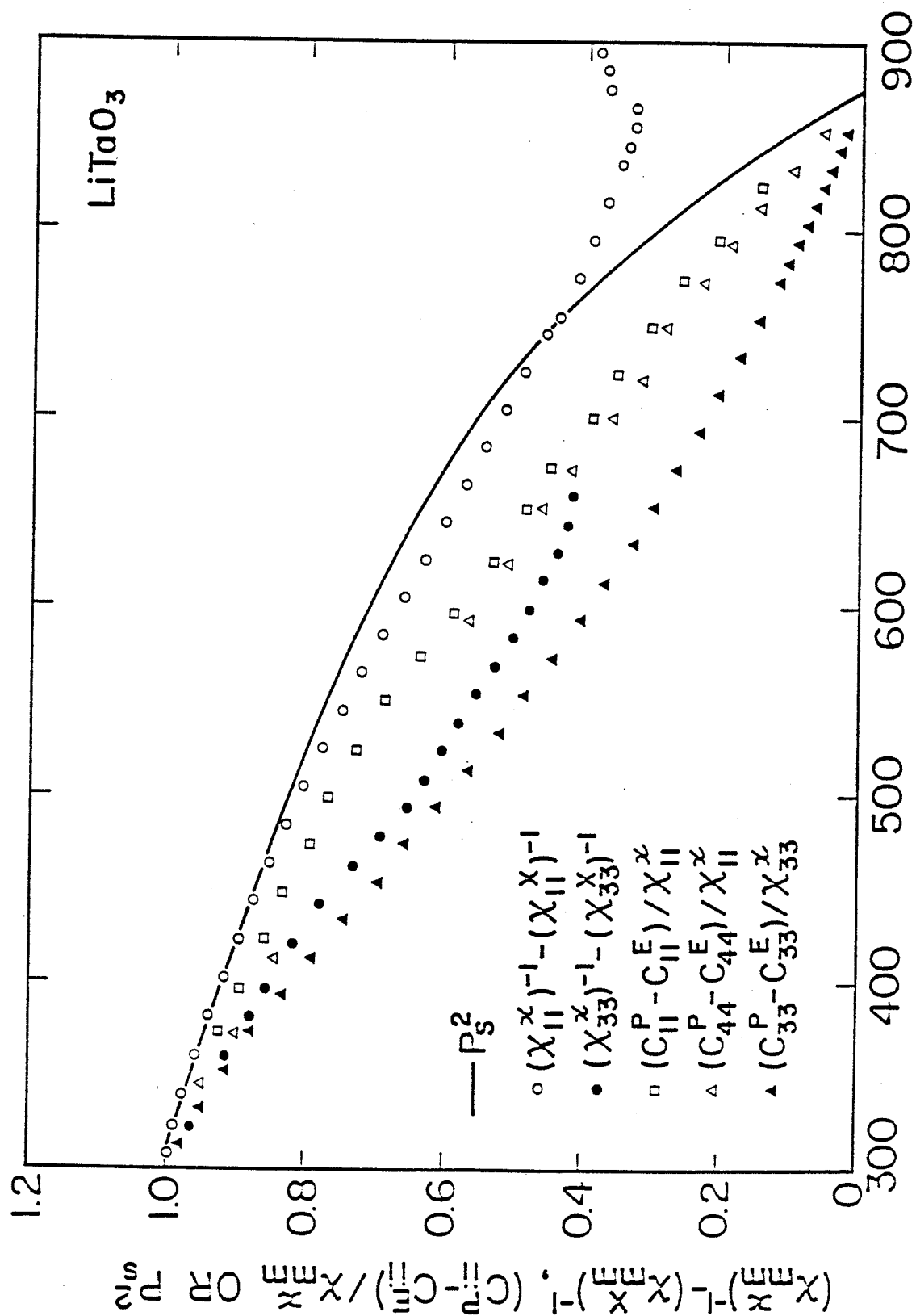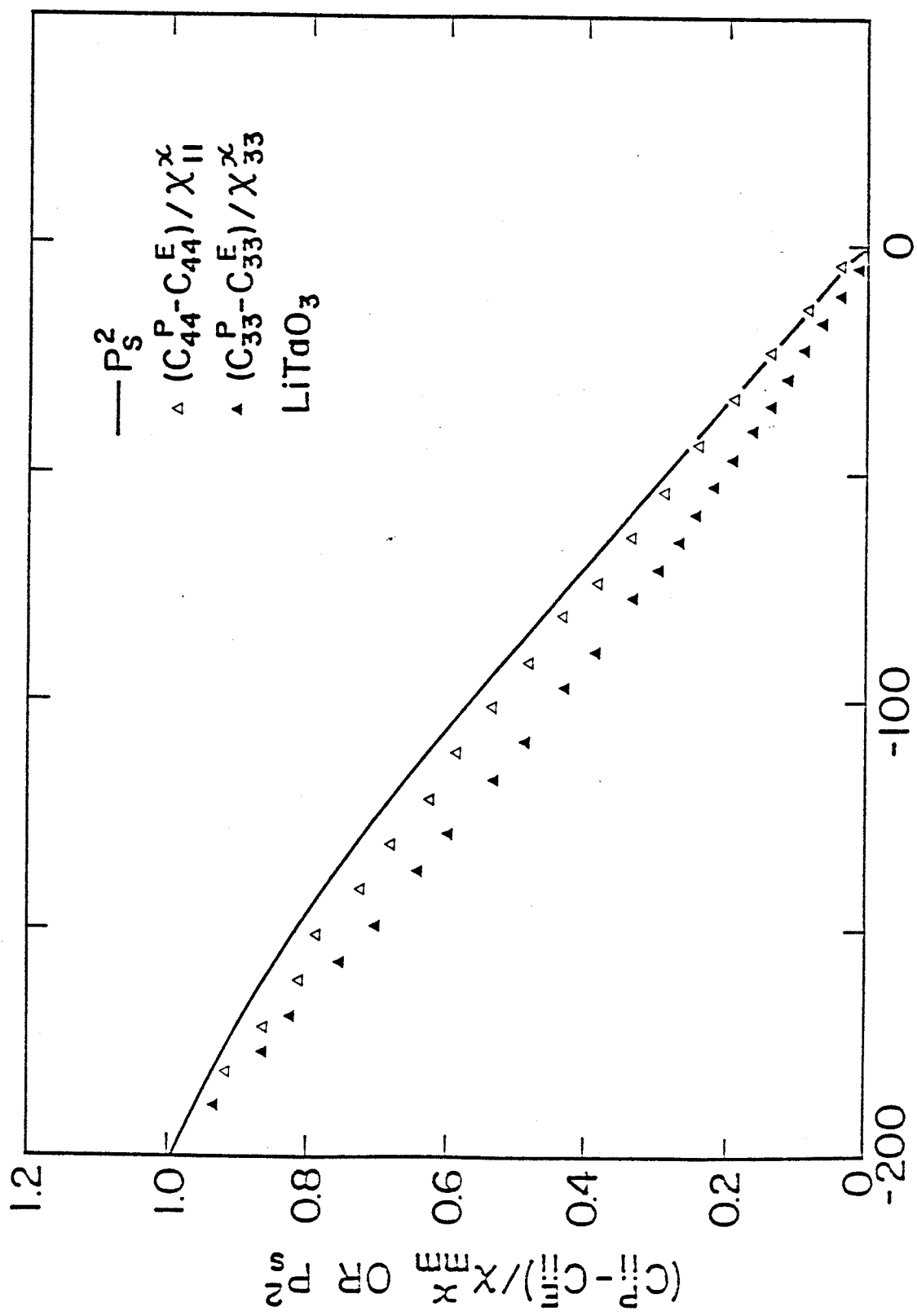
Fig. 19

Fig. 20
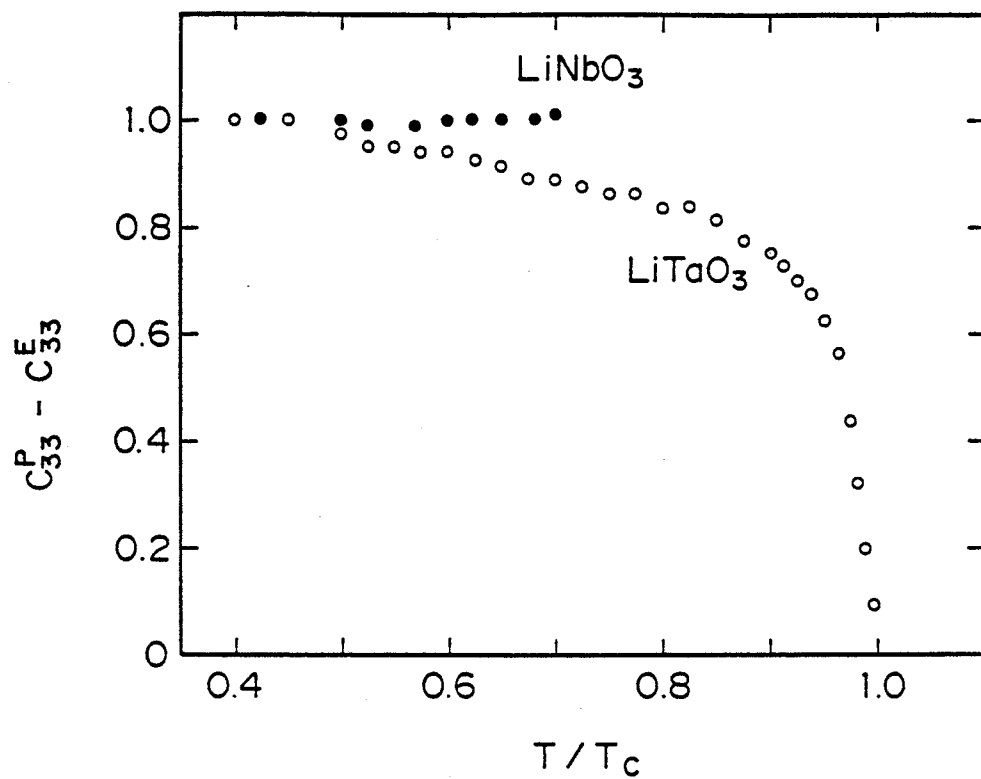
(a)
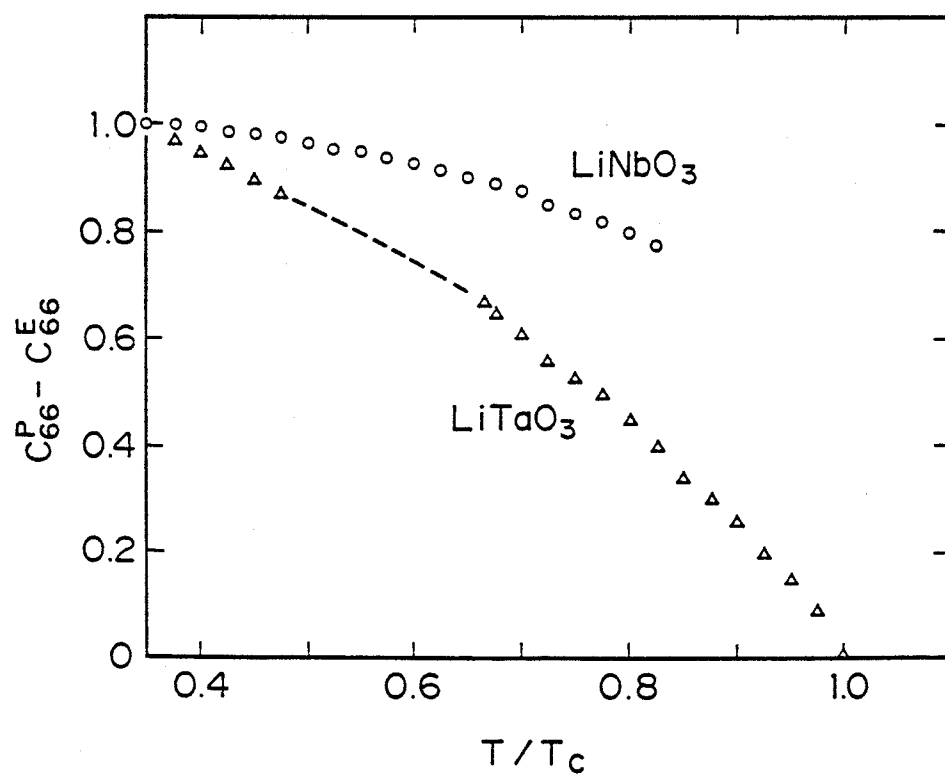
(b)

Fig. 21

Fig. 22

Fig. 23

Fig. 24

DIELECTRIC CONSTANT ϵ''_{33} (10^3)

T (K)

LiTaO$_3$

○—— 10 kHz
△—— 100 kHz
▲—— 1.5 MHz
×—— 7 MHz
●—— 10 MHz
□—— 13 MHz

Fig. 2b